7-21-2008

Models for electromagnetic coupling of lightning onto multiconductor cables in underground cavities

Matthew Higgins

Recommended Citation

Higgins, Matthew. "Models for electromagnetic coupling of lightning onto multiconductor cables in underground cavities." (2008). https://digitalrepository.unm.edu/ece_etds/117

Matthew B Higgins

Candidate

Electrical & Computer Engineering

Department

This dissertation is approved, and it is acceptable in quality and form for publication on microfilm:

Approved by the Dissertation Committee:

Dr. Christos Christodoulou , Chairperson

Accepted:

Dean, Graduate School

Date

MODELS FOR ELECTROMAGNETIC COUPLING OF LIGHTNING ONTO MULTICONDUCTOR CABLES IN UNDERGROUND CAVITIES

BY

MATTHEW BENJAMIN HIGGINS

B.S., Electrical Engineering, The Ohio State University, 1999
M.S., Electrical Engineering, The Ohio State University, 2001

DISSERTATION

Submitted in Partial Fulfillment of the
Requirements for the Degree of

Doctor of Philosophy

Engineering

The University of New Mexico
Albuquerque, New Mexico

May, 2008

DEDICATION

I dedicate this to my loving wife Leigh and my beautiful daughter Nella. I also dedicate this work to the miners and the families of the miners lost in the Sago mine explosion.

ACKNOWLEDGMENTS

I heartily acknowledge Dr. Christos Christodoulou, my advisor and dissertation chair, for all of his support and guidance. I wish to thank Dr. Michele Caldwell, my manager at Sandia National Laboratories, for her guidance and the opportunity to lead the project that led to my dissertation. I also wish to thank Dr. Marvin Morris, my co-author of the original report, for his guidance on the indirect coupling models and many instructive conversations. I thank Dr. Larry Warne for patient conversations on transmission line coupling and models. I thank Dr. Roy Jorgenson for instructing me on how to run simulations on Eiger. I would also like to thank Dr. William Johnson and the rest of the Eiger team for the use of the open-source Eiger code.

Complex work of this type could not have been undertaken without the funding, coordination, and hard work of the MSHA staff that were involved. I wish to thank MSHA staff William Helfrich, Richard Gates, Robert Phillips, Harold Newcomb, Russell Dresch, Dean Skorski, Joseph O'Donnell, and Arthur Wooten for their support of this work. Jurgen Brune and Eric Weiss of NIOSH generously provided their Lake Lynn facility for initial trials of the measurement techniques used at the Sago mine. I thank the ICG staff, Chuck Dunbar, Al Schoonover, Johnny Stemple, Larry Dean, Kermit Melvin, and Brittany Bolyard, for their generous help in arranging access and for providing the services we needed to accomplish the measurement tasks. In spite of our obvious interruptions to their operations as well as extensive demands on their time, they generously provided the services I needed in a timely manner. I am grateful for the

support of Dr. E. Philip Krider and Dr. Martin Uman, who independently reviewed the lightning database information for this document and the previous report. I also wish to thank the consultants, Dr. Tom Novak, Dr. E. Philip Krider, Elio Checca, and Dr. Martin Uman for freely sharing their thoughts on this work. Monte Hieb and John Scott of the State of WV Office of Miners' Health, Safety, and Training provided additional useful information and help to accomplish the work. Finally, I would like to thank the property owners of the land above the sealed area, Mrs. Goldie Gooden, Tim and Chris Leggett, Bill Patterson, and George Roessing, for generously allowing us access to their property in order to drive ground rods, string wires, and operate our equipment despite obvious interruptions to their lives. Most importantly, I would like to thank my measurement team, Dawna R. Charley and Leonard Martinez, for their extraordinary work in the field. Without their hard work and long hours the measurements could not have been completed.

MODELS FOR ELECTROMAGNETIC COUPLING OF LIGHTNING ONTO MULTICONDUCTOR CABLES IN UNDERGROUND CAVITIES

BY

MATTHEW BENJAMIN HIGGINS

ABSTRACT OF DISSERTATION

Submitted in Partial Fulfillment of the
Requirements for the Degree of

Doctor of Philosophy

Engineering

The University of New Mexico
Albuquerque, New Mexico

May, 2008

MODELS FOR ELECTROMAGNETIC COUPLING OF LIGHTNING ONTO MULTICONDUCTOR CABLES IN UNDERGROUND CAVITIES

by

Matthew Benjamin Higgins

B.S., Electrical Engineering, The Ohio State University, 1999

M.S., Electrical Engineering, The Ohio State University, 2001

Ph.D., Engineering, University of New Mexico, 2008

ABSTRACT

This dissertation documents the measurements, analytical modeling, and numerical modeling of electromagnetic transfer functions to quantify the ability of cloud-to-ground lightning strokes (including horizontal arc-channel components) to couple electromagnetic energy onto multiconductor cables in an underground cavity. Measurements were performed at the Sago coal mine located near Buckhannon, WV. These transfer functions, coupled with mathematical representations of lightning strokes, are then used to predict electric fields within the mine and induced voltages on a cable that was left abandoned in the sealed area of the Sago mine. If voltages reached high enough levels, electrical arcing could have occurred from the abandoned cable. Electrical arcing is known to be an effective ignition source for explosive gas mixtures.

Two coupling mechanisms were measured: direct and indirect drive. Direct coupling results from the injection or induction of lightning current onto metallic conductors such as the conveyors, rails, trolley communications cable, and AC power shields that connect from the outside of the mine to locations deep within the mine. Indirect coupling results from electromagnetic field propagation through the earth as a result of a cloud-to-ground lightning stroke or a long, low-altitude horizontal current channel from a cloud-to-ground stroke. Unlike direct coupling, indirect coupling does not require metallic conductors in a continuous path from the surface to areas internal to the mine.

Results from the *indirect* coupling measurements and analysis are of great concern. The field measurements, modeling, and analysis indicate that significant energy can be coupled directly into the sealed area of the mine. Due to the relatively low frequency content of lightning (< 100 kHz), electromagnetic energy can readily propagate through hundreds of feet of earth. Indirect transfer function measurements compare extremely well with analytical and computational models developed for the Sago site which take into account measured soil properties.

TABLE OF CONTENTS

LIST OF FIGURES

LIST OF TABLES

ABBREVIATIONS, ACRONYMS AND INITIALIZATIONS

CW	Continuous Wave
dB	deciBel
DOE	Department of Energy
FFT	Fast Fourier Transform
IFFT	Inverse Fast Fourier Transform
NLDN	National Lightning Detection Network
USPLN	United States Precision Lightning Network

Chapter 1 Introduction

On January 2, 2006, an explosion was initiated in a methane-air mixture within a sealed area at the Sago underground coal mine near Buckhannon, WV that resulted in the deaths of twelve miners. The approximate location of the initiation of the explosion is shown in Figure 1-1.

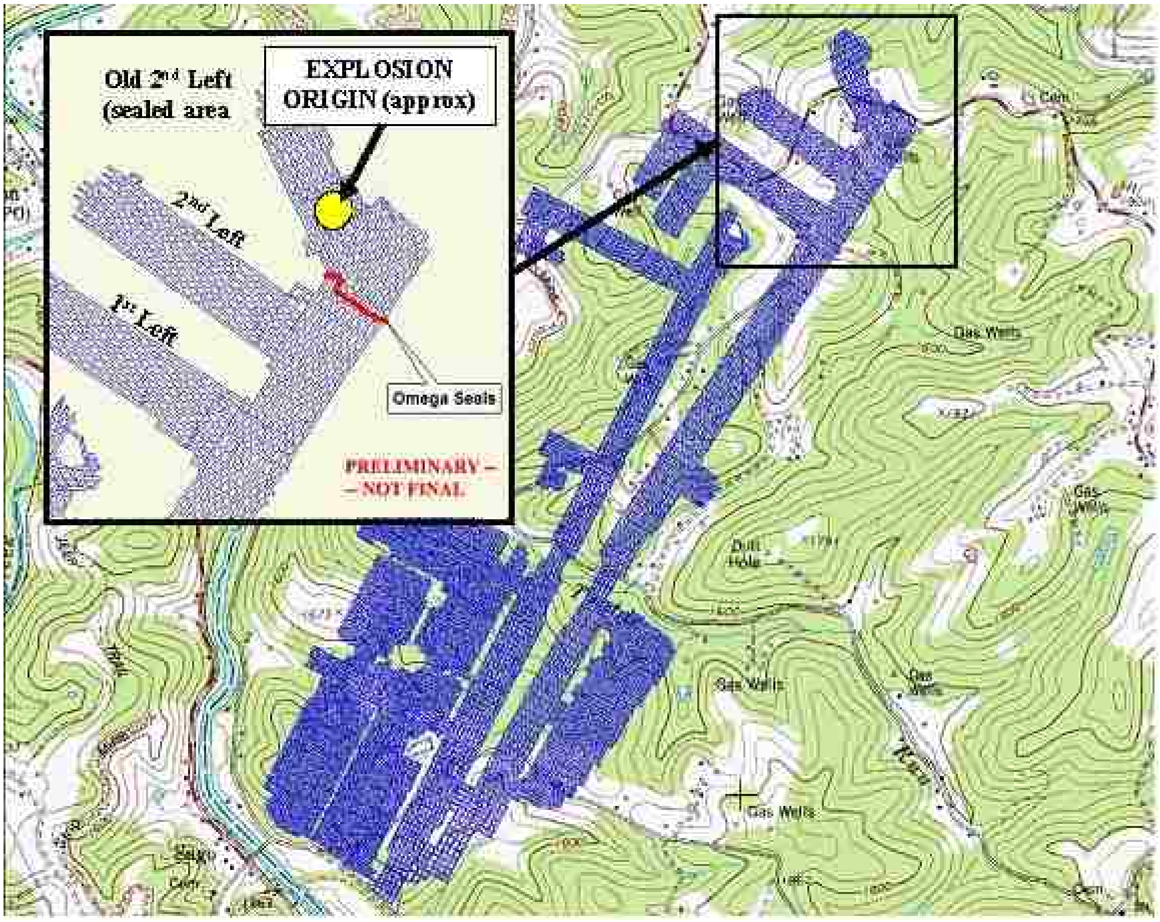

Figure 1-1 Approximate location of initiation of explosion in sealed area of Sago Mine.

Because of the fraction of a second simultaneity of the explosion and nearby lightning strokes recorded by the National Lightning Detection Network (NLDN) and the United States Precision Lightning Network (USPLN), lightning is strongly suspected to have caused the explosion. Additional eyewitness reports of other lightning not recorded by NLDN and USPLN further these suspicions [1]. If the timing of the recorded lightning strokes and the underground mine explosion are considered independent statistical events, then the probability that such a combined event would occur at random in a given year is extremely low. When this highly improbable event is coupled with the fact that at least eleven underground coal mine explosions have occurred since 1990 (see Appendix D) in which lightning is suspected of being the cause, it further supports the need to understand the potential role of lightning in the Sago disaster [2-5]. The coupling mechanisms that may have brought lightning energy into the sealed area at Sago were unclear and complicated by the fact that there were no known metallic penetrations into the sealed area of the Sago mine, unlike other sealed area explosions. Prior to 1990, lightning location and timing data was unavailable, leaving the possibility that many earlier mine explosions could also be correlated to lightning events.

The goal of this work was to perform field measurements at the Sago site and to develop analytical models to quantify potential lightning coupling mechanisms that are capable of delivering significant energy into the sealed area of the Sago mine.

1.1 Motivation for Research and Measurements

Over the last decade research labs, such as Sandia National Laboratories, have developed unique capabilities to characterize and mitigate lightning effects on high value assets within the Department of Energy (DOE) and other agencies as part of a national security mission in nuclear weapons stockpile stewardship. Additionally, the history of potential lightning induced mine explosions suggested that using modern electromagnetic measurement techniques and analysis could be valuable during the investigation at the Sago mine. These modern lightning coupling measurement techniques were developed by DOE/NNSA specifically for the evaluation of the performance of lightning protection systems on buried, explosive storage structures, nuclear weapons assembly and dismantlement facilities, and at tunneling systems at the DOE Nevada Test Site. Some of the national labs' developed techniques have been compared and validated using rocket-triggered lightning measurements [6-8] and have undergone significant technical review within the DOE and by the Defense Nuclear Facility Safety Board, an independent federal agency established by Congress in 1988. These direct injection measurement techniques are supplemented with novel indirect measurement techniques developed specifically for this work.

The author is not only a Ph.D. candidate at the University of New Mexico, but also a Senior Member of Technical Staff at Sandia National Laboratories. This dissertation is an extension of the initial investigation of lightning coupling into the Sago coal mine led by the author. The author's work for the initial investigation used in this dissertation includes the development of novel experimental measurement techniques, data collection and analysis, and coupling measured data with analytical models and lightning data to produce estimations of voltages on cables in the sealed area of the mine. The work done solely for this dissertation includes investigation and development of analytical and numerical coupling models to validate the measurement techniques and extend the usefulness of the direct coupling results.

1.2 Objectives of Measurements

The principal objectives of this work were to identify, characterize, and quantify the electromagnetic paths of lightning electrical energy into the sealed area of the Sago underground coal mine. These paths include direct coupling through metallic penetrations into the operating area of the mine and indirect coupling through the earth overburden to conductors in the sealed area. Measurement results were compared with basic analytical models to confirm the validity of proposed lightning coupling mechanisms. The measured transfer functions were then used to predict the voltages generated on a cable left abandoned within the sealed area from the lightning stroke locations and amplitudes determined by the NLDN and the USPLN.

1.3 Measurement Method and Analysis

The coupling mechanisms of lightning energy into the Sago mine have been divided into (1) direct coupling via metallic penetrations from the outside of the mine that are terminated immediately outside the sealed area, and (2) indirect coupling through the soil and rock overburden above the sealed area. The metallic penetrations analyzed, modeled, and measured were the AC power shields, the coal conveyer system, the transportation rail system, and the mine trolley communication cable. The primary focus of this study was to determine electric fields within the mine and the resulting induced voltage on a cable within the sealed area due to both the direct and indirect coupling mechanisms. Electrical arcing is known to be an effective ignition source for explosive gas mixtures, and corona discharge has been postulated to be so as well. However, given the timescale of lightning (~100 μs) it is unlikely that corona would develop before an electrical arc. Corona is due to ionization of surrounding air and usually a precursor to arcing, given sufficient voltage.

Lightning coupling mechanisms were characterized by driving potential pathways with low-level, continuous sinusoidal signals and measuring the resultant signals at distant locations. The resultant data, when divided by the input signal, produces a transfer function that can be coupled with a mathematical representation of lightning strokes to calculate a resultant signal at points inside the mine. The advantages of using this technique are as follows:

- Measurements can be made without waiting for a natural or triggered lightning in the vicinity.
- Safety is not compromised due to use of low-level signals and interference with ongoing mine operations is minimized.
- The frequency content of the low-level drive signal can be tailored to that of natural lightning.
- Many data points can be taken with this method which enhances the precision of the transfer functions.

The disadvantage is that the nonlinear effects of high-voltage arcing cannot be taken into account.

1.3.1 Direct Coupling Transfer Function Measurements and Analysis

Because all metallic conductors into the Sago mine were terminated outside the sealed area of the mine, current cannot be injected from outside the sealed area directly into the sealed area. However, currents flowing on conductors inside the mine, but outside of the sealed area, may be able to induce voltage on a cable inside the sealed area through electromagnetic coupling. To determine the amplitude of these currents, attenuation on each conductor entering the mine was measured using transfer function techniques. Low-level direct coupling transfer function measurements were made by injecting current onto metallic penetrations at the entrance to the mine and then measuring the voltage and current levels on these penetrations at various points within the mine, up to immediately outside the sealed area. The voltage induced on conductors inside the sealed area could then be calculated based on the projected current level on conductors outside the sealed area and an analytical estimate of the electromagnetic coupling between this current and the conductors inside the sealed area. The measurements were made over a frequency range from 10 Hz to 100 kHz, corresponding to wavelengths in air of 3×10^7 meters to 3000 meters respectively. We are able to use very small signals because our instrumentation is very sensitive and has a large dynamic range. We demonstrated that we could measure induced currents at a very large distance from the source even with significant attenuation. The metallic penetrations were also modeled as canonical transmission lines to better understand their responses.

Because the direct-drive measurements are taken as a function of frequency, the mathematical representation of a lightning stroke is transformed as a function of frequency. To use the data, the direct-drive transfer functions were multiplied by the frequency representation of a lightning stroke. The product was inverse Fourier transformed to represent the resultant signals inside the mine from a lightning event outside the mine, as a function of time. To represent the worst-case scenario input for the purpose of these calculations, an assumption was made that the lightning stroke attached to the metallic penetrations at the entrance of the mine.

1.3.2 Indirect Coupling Transfer Function Measurements and Analysis

The large currents in a lightning stroke have an associated magnetic field. When a lightning stroke attaches to the earth, this creates a magnetic field tangential to the ground. For a fully developed lightning stroke, it is reasonable to approximate this magnetic field as

$$H(r) = \frac{I}{2\pi r}$$

over a distance of 30 m – 1000 m, where I = lightning current and r = distance from stroke attachment. For distances within 30 m of the attachment, magnetic field calculations are more complex and this approximation is incomplete. To a first order of approximation and as a bound, the magnetic field is calculated above a perfectly conducting ground plane, as above. This approximate tangential magnetic field is used as a drive to generate current in the finitely conducting earth. The calculations in this dissertation do not deal with magnetic fields generated in the immediate vicinity of lightning strokes; therefore, these interactions will not be evaluated here. For distances greater than 1000 m from the attachment, the approximation for the magnetic field at the surface may be an overestimation, but can be considered a reasonable upper bound.

When lightning attaches to the ground, the magnetic field tangential to the ground creates currents not only on the surface, but deeper in the earth as well. It is a fundamental principle of electromagnetics that magnetic fields on the surface of a conductor can generate currents within the conductor of some depth. For frequencies sufficiently low that displacement currents can be neglected, this is called the *skin effect* and is dependent upon the resistivity of the conductor. When displacement currents are neglected, the electromagnetic coupling phenomena are called *diffusion coupling* or, equivalently, *eddy current coupling*. The skin depth characterizes the exponential decay of these currents in planar geometries. Resistivity measurements have shown the soil in the vicinity of the sealed area of the Sago mine to be a fairly good conductor; therefore, it is reasonable to assume that some electromagnetic energy can propagate from the surface of the earth into the sealed area of the mine. This effect is similar to propagating radio waves through seawater, also a fairly good conductor, and communicating with submarines.

The methodology used to measure the electromagnetic coupling through the earth is to simulate magnetic fields in the earth by connecting a frequency variable voltage source via straight wires on the surface between ground rods at either end of the wires. The ground rods are placed a significant distance from each other, approximately 100 m on either side of the region where the electric fields are measured, or where voltage is induced on an insulated wire. The electric field and the voltage on a cable are measured over a frequency range from 10 Hz to 100 kHz. At this point we have the electric field and voltage response on the pump cable in the sealed area from a known linear current distribution on the surface. A great deal of effort was put into validating these novel measurement techniques using analytical and numerical models.

Two steps are involved in calculating the response of a lightning stroke attachment at a distance from the sealed area. The first step involves estimating the magnetic field (or surface current) above the sealed area from a lightning attachment to the ground at a distance from the sealed area. The second step involves calculating the electric field in the sealed area of the mine due to the uniform magnetic field (or surface current) on the surface using the parameters determined from the coupling measurements. Once these connections are made with data in the frequency domain, then the Fourier transform of the lightning stroke can be multiplied by the transfer function. The inverse Fourier transform of the product can be taken to determine the peak electric field and peak voltages that would be caused by a lightning attachment of a given amplitude at a given location with respect to the sealed area. If the peak induced voltages are significant, arcing between conductors could occur. A few tenths of a milliJoule of energy in the arc would be a sufficient ignition source for a combustible methane-air mixture [9]. This amount of energy is readily available from almost any arcing process envisioned in a lightning induced event. Bulk air breakdown in small gaps (several millimeters) occurs at average electric field values of approximately 10 kV/cm with standard lightning waveforms [10]. Surface arcing can occur at electric field values in the 5 kV/cm range.

1.4 Soil and Rock Site Data

The soil and rock resistivity play a major role in determining the amplitude and frequency dependence of indirect coupling into the sealed mine area. Several studies provide resistivities measured with different techniques and equipment. The resistivities determined by the different measurements appear to be somewhat inconsistent. However, resistivities in [11] match the numbers that give us the best results for our analysis of electromagnetic coupling through the ground. The resistivities in [11], using a best fit to electromagnetic sounding data, are 100 Ω-m from 0 to 40 feet, 10 Ω-m from 40 to 120 feet, and 100 Ω-m from 120 to 350 feet deep, yielding an average of 77.3 Ω-m above the sealed area at the borehole. In this study an average resistivity of 80 Ω-m is used to characterize the soil and rock overburden atop the sealed area of the Sago mine.

1.5 Lightning Event Information

Three positive polarity lightning strokes were identified by the NLDN and the USPLN that were coincident with the Sago underground coal mine sealed area explosion. Their location, polarity, and amplitude are shown in Figure 1-2.

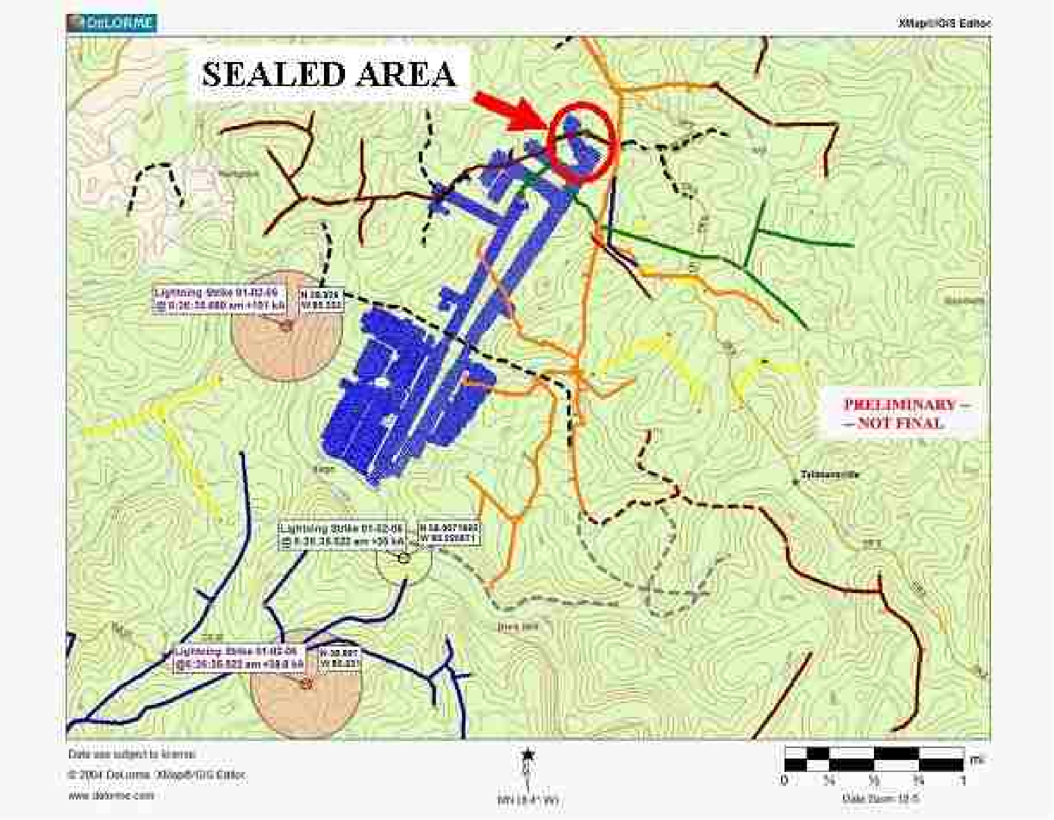

Figure 1-2 Location of lightning strokes at Sago Mine near simultaneous with sealed area explosion.

Table 1-1 gives the location, polarity, and amplitude of the identified strokes. Also provided in the table are the distances from the stroke locations to the sealed area, and the angle that a line between the stroke location and the borehole above the sealed area makes with the pump cable in the sealed area. It should be noted that physical evidence of only stroke number 3 was found after several searches of each attachment area. An analysis of the USPLN and NLDN data strongly suggest that stroke number 1 and 2 in Table 1-1 represent a single stroke, and not two separate events [1,12].

Table 1-1 Lightning detection network data, January 2, 2006

Stroke No.	**Time**	**Longitude/ Latitude**	**Polarity**	**Amplitude** (kA)	**Distance to Borehole** (km)	**Angle with Cable** (Degrees)	**Detection System**
1	6:26:35.522am	N38.897/ W80.231	Positive	38.8	5.44	52.8	NLDN
2	6:26:35.522am	N38.9071693/ W80.2201	Positive	35	4.02	49.3	USPLN
3	6:26:35.680am	N38.926/ W80.233	Positive	101	2.91	85.5	NLDN

The accuracy of the NLDN is shown in general by the confidence ellipses drawn around the most probable locations. The ellipses give the probability that the lightning is actually inside the ellipse. The estimated 99% location uncertainty for both strokes detected by NLDN was better than 1.1 km (0.7 miles). The fact that the tree was found damaged approximately 197 feet (59 m) from the most probable location of the 101 kA stroke further demonstrates the NLDN location accuracy near the Sago mine [1,12,13]. Recent validation experiments on the NLDN have shown stroke detection efficiencies between 70 – 85% and flash detection efficiencies of 90 – 95% [14]. (Lightning flashes are typically comprised of multiple strokes.) It is believed that the two strokes (1 and 3 from Table 1-1) at Sago were part of the same flash [13].

Several other possibilities exist that were not, or could not, be confirmed by the lightning detection network data. Although quite reliable and accurate, the possibility exists of strokes not being detected. Simultaneous thunder and flash were reported by residents living on top of or nearby the sealed area [1]. In addition, the lightning detection networks are designed to locate the ground strike points of cloud-to-ground strokes and do not provide information about the channel geometry above those points, such as if a stroke had a long, low horizontal component that could be important in radiating fields into the mine. Also, upward discharges that are initiated by tall vertical structures will not be detected by the systems unless the initial continuous current phase is followed by at least one leader-return stroke sequence [12,13]. There were several tall communication towers (the tallest being ~ 200 ft.) within a mile of the sealed area, the closest being approximately 0.5 miles.

1.6 Other Site Information

Measurements discussed in this dissertation were made on the most likely coupling paths into the sealed area. Other potential conduits of lightning energy are mentioned in this section, but were not characterized due to the limited budget and schedule of this work. While they are mentioned here for completeness, the lack of measured data on them does not change the conclusions.

All vertical pipes in the vicinity of the sealed area are shown in Figure 1-3. The vertical pipe closest to the sealed area of the mine is the gas well pointed out in Figure 1-3. It is unlikely that any field enhancements due to the vertical pipes would induce a significant amount of voltage onto the pump cable in the sealed area because the cable is orthogonal to the pipes. However, as potential conduits for lightning energy, they are mentioned here for completeness. Computational simulations calculating the fields induced by estimated current on the closest vertical gas well are shown in Section 3.4.

The horizontal gas pipes that are in the vicinity of the sealed area are also shown in Figure 1-3. These pipes are in general buried at a depth of 2 feet from the surface. The response on the pump cable, or electric fields in the sealed area, due to the current drive of the horizontal gas pipes was not characterized because it was not planned for and was not characterized because of liability issues. The gas pipes, if driven locally to the sealed area, would have similar coupling characteristics to the pump cable as that of the indirect drive experimental setup. If the gas pipes were driven remotely, the amount of attenuation from one point on the pipes to another point is mostly dependent upon the resistivity of the soil surrounding the pipes. If the soil surrounding the pipes has low resistivity, a majority of current injected onto the pipes would attenuate in a short distance. However, if the pipes are either not in contact with the soil or the resistivity of the soil is large, then the pipes would act as insulated conductors. Attenuation on the pipes in this case would be much less.

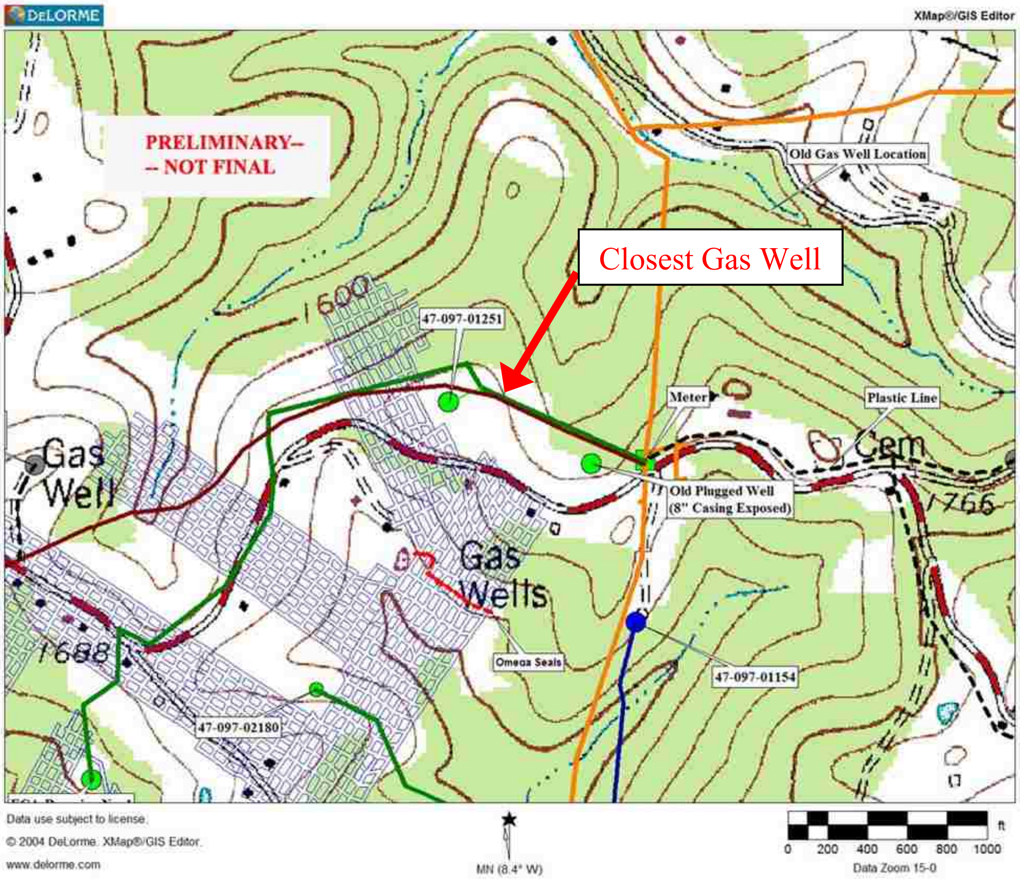

Figure 1-3 Vertical pipes in vicinity of sealed area of Sago Mine.

Both telephone wires and AC power lines were in the vicinity of the 101 kA positive stroke and could have provided metallic conduction paths into the Sago mine AC power system, or the telephone communication system, or to other metallic penetrations into the mine. The location and routing of this wiring with respect to the stroke are shown in Figure 1-4. The direct-drive measurements discussed in Section 2.1 lead to the conclusion that even if the power and telephone lines were conduits of the lightning energy, they would not be a plausible source of energy to cause high voltage in the sealed area.

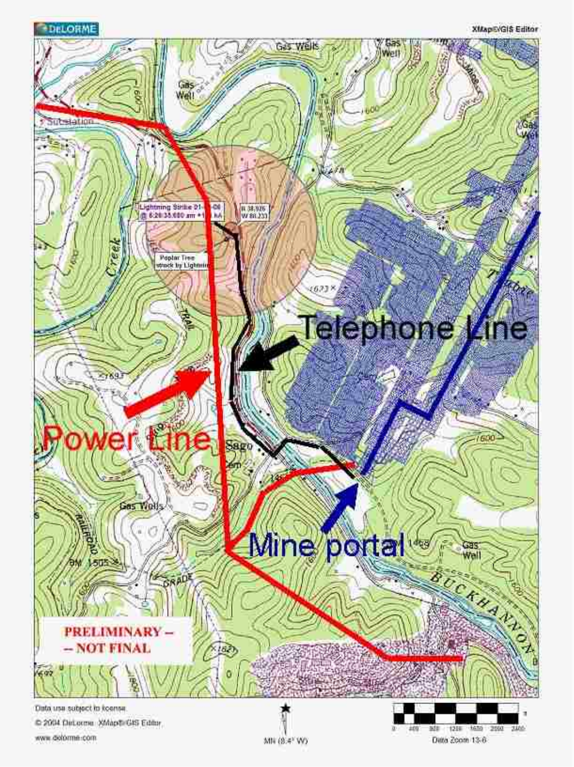

Figure 1-4 AC power distribution lines and telephone lines near positive 101 kA stroke.

The presence of metallic roof mesh and pump cabling and its relationship to the approximate location of initiation of the explosion are shown in Figure 1-5. The pump cable is shown as the red line and the green shaded area depicts the metallic mesh. The pump cable is noted because indirect coupling measurements are made on it. With these measurements, the voltages induced on the pump cable due to lightning strokes on the surface are calculated in this dissertation.

The metallic mesh is noted because it is used in some of the measurements for grounding purposes. It was not considered a plausible receiver or antenna of the electromagnetic energy that propagates underground because it appears to be well grounded at regular intervals to the roof of the sealed area, and, therefore, would not support a large voltage potential.

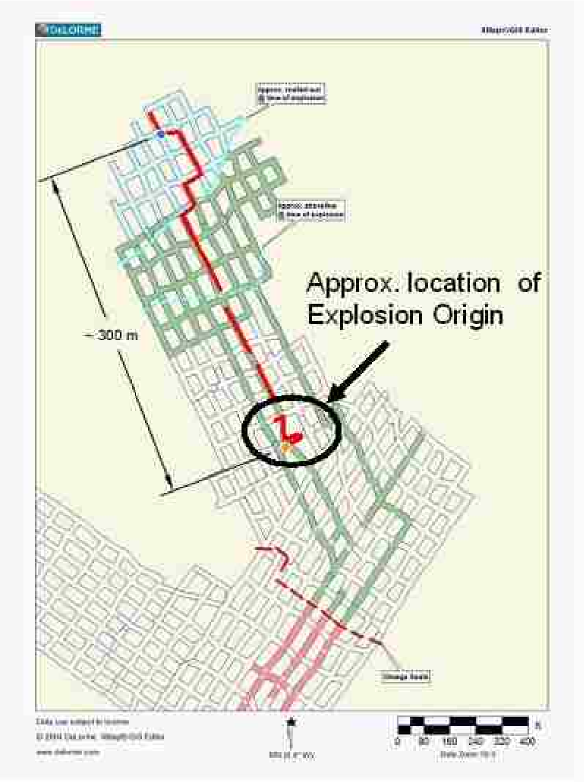

Figure 1-5 Roof mesh and cable in sealed area where explosion was initiated. The red line represents a cable from a water pump located at the top of the figure. The green lines represent metallic roof mesh.

1.7 Previous Work on Lightning Induced Mine Explosions

Recent previous works by Novak and others [15,16] have utilized commercial, numerical electromagnetic codes to calculate the voltages on metal-cased boreholes connecting the surface with the sealed areas in mines. They have postulated corona discharge as an initiating mechanism based on experimental work by combustion researchers [17,18]. Berger, Geldenhuys, Golledge, Zeh, and others have analyzed the specific situation of lightning-caused explosions in shallow South African underground coal mines [19-23].

The Australian, German, and Chinese literature on lightning initiated underground coal mine explosions has not been thoroughly explored for this dissertation.

1.8 Fidelity Issues of Study

To have confidence in the measured results, several fidelity issues were addressed to ensure that the measurements could be used to calculate a realistic natural lightning response.

1.8.1 Applicability of the Indirect-drive Test Setup

Nonlinearities at the lightning attachment point often cause arcing either on the surface of the soil or into the soil that are not duplicated by the low-level drive current measurement method. Because these arcs are limited to the attachment area, they do not affect the overall current flow at large distances to a significant degree. Therefore the stroke attachment region is not considered here.

However, good correlation between the measured results and the homogeneous earth models suggest these deviations are negligible for this particular work. Ground rods were needed to establish a return current path for the measurements. This is a deviation from the current flow of natural lightning.

Chapter 2 Measurement Methods

2.1 Direct Drive

The goal of direct drive measurements is to characterize the attenuation or decrease in signal from the entrance of the mine to various distances into the mine. This is accomplished by directly injecting a current on various conductive lines going into the mine and measuring the current at points further in the mine.

Ideally, the transfer functions of each conductive line going into the mine would be measured in the same configuration as it was during the time of the explosion. However, the grounding at the entrance of the mine was changed following the explosion. Changing back to the old grounding state required the power to the mine be removed, thus stopping all mining operations. A small set of measurements were made while power was disconnected. It was not possible to conduct all measurements in the one day when the power was disconnected, and stopping mine operations for three days was not feasible. Therefore, the rail, trolley communication line, and conveyor belt structure were measured at six locations at a later time, with the mine grounding system in its current state. The transfer function of the shield on the power cables could not be measured while power was energized.

The main differences between the current and previous state of the grounding system are which conductors are grounded together and lightning arrestors installed. The previous state of the grounding system had all four conductive penetrations grounded together at the mine entrance with no lightning arrestors in place. The current state of the grounding system has only the rail, trolley communication line, and the shield of the power cables grounded together. The conveyor belt structure is grounded separately and both systems have lightning arrestors installed. Since lightning arrestors only are activated when there is a voltage with sufficient amplitude to arc across a spark gap, there is no effect to the measurements due to their introduction into the grounding system. The effect of separate grounding of the conveyor structure is very minimal, due to the conveyor structure being contained in a separate tunnel and having a separation from the other conductors of ~ 70 feet. The largest difference that will be noticeable in the data between the measurements of the previous and current configuration is that the electrical AC power was disconnected on the first measurement day. The measurements taken while AC power was not present have much less 60 Hz (and harmonics of 60 Hz) clutter visible in the transfer functions and are thus much cleaner. The measurements taken with the AC power present (even though all instrumentation was isolated and powered from batteries) show significant clutter contamination at 60 Hz and the harmonics of 60 Hz.

2.1.1 The Differences and Similarities between Conductive Penetrations

The four conductive penetrations going into the entrance of the mine that were measured were 1) the shield on the power cable, 2) the rail, 3) the trolley communication line, and 4) the metallic structure of the belt conveyor. The conveyor structure and the rail both appeared to be grounded frequently (the rail by surface contact with the ground and periodic bolts), and the conveyor structure by periodic legs bolted to the ground. The shield on the power conductor appeared to be grounded at each power center. The trolley communication cable was an isolated wire running the length of the mine and was only grounded at the entrance. Because of this, at low frequencies the attenuation on the trolley communication line is quite small.

2.1.2 Setup/Equipment Layout with Photos

The principal measurement method used to characterize the coupling through metallic penetrations into the mine is shown in Figure 2-1. This is a novel new technique that utilizes the dynamic range and speed of a network analyzer over a distance of > 2 miles. Current is driven onto the metallic penetration with an audio amplifier and is returned through either a local ground or a "fence" ground. The local ground consisted of three 18-inch long conductive ground rods driven into the top soil. Each rod was approximately five feet from the other rods and 20 feet away from the driving point. The "fence" ground was long wire attached to the chain link fence that runs along the hillside above the entrance of the mine, as shown in Figure 2-2.

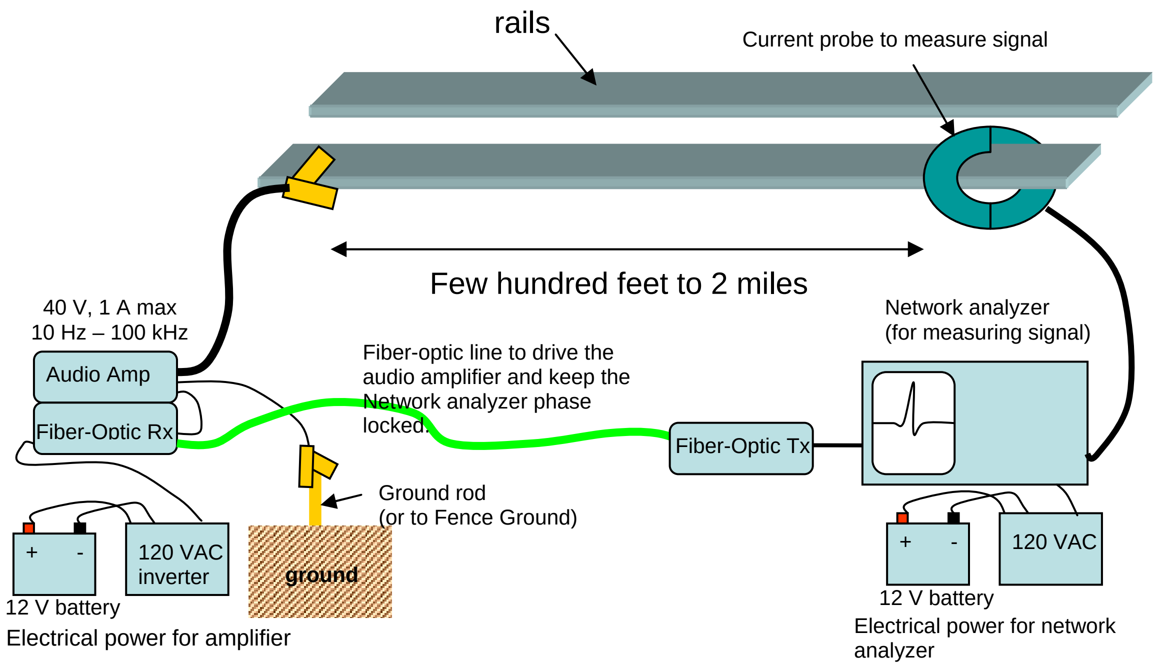

Figure 2-1 Direct drive conceptual drawing.

Figure 2-2 Sago Mine with fence ground example.

The reasoning for the two grounding techniques was to help show the difference between a local point source drive and a distributed current source drive. A lightning stroke drive could be considered a distributed current source. The fence drive provided a distributed source for at least several hundred meters. The fence ground also provided a lower ground resistance, which in turn allowed more current to be driven on the lines. By driving more current on the line, the dynamic range of the measurement system was increased. The resistance of the local ground with respect to the rail was 90.2 Ω and the resistance of the fence ground with respect to the rail was 3.68 Ω. It is easy to see from this DC measurement that 20 to 30 times the amount of current could be driven on the fence ground than the local ground. The resistance of the local ground with respect to the conveyor structure was 97.5 Ω, and the resistance of the fence ground with respect to the conveyor structure was 10.08 Ω. All DC ground measurements were made with a Megger DET 5/2 Earth Tester.

The direct-drive system is broken into two parts, the drive end and the measurement end. The drive end consists of a 12 V marine battery and a 120 VAC inverter to provide isolated power for the measurement equipment, a fiber optic receiver, an audio amplifier driven by a network analyzer, connecting wires to the conductor being driven, and wires to a ground (local or fence). The drive signal produced by the network analyzer is optically coupled to the audio amplifier allowing the signals to be phase-locked to increase the sensitivity of the measurements and allow for phase measurements. The technique of phase-locked detection allows measurement of voltages as low as tens of nanoVolts. The measurement end consists of a 12 V battery and a 120 VAC inverter for isolated power for the measurement equipment, a fiber optic transmitter, a network analyzer, and current and voltage measurement probes. The voltage measurements on the rail, power, and conveyor were made with respect to the roof mesh. Voltage measurements were not made on the trolley communication line because it was isolated without an exposed conductor.

Previous methods used to measure voltage and current transfer functions of large metallic structures over a large distance have been developed at Sandia [7]. The method utilized a function generator on the drive side and a spectrum analyzer on the measurement side. The frequency and amplitude were set by hand and then the drive operator would contact the measurement operator by radio (or mine communication phone) to set the frequency of the spectrum analyzer and record the amplitude by hand. Each frequency for each conductor at a given location could take between 1 to 3 minutes. This method only provided an amplitude transfer function with very sparse frequency spacing.

The method developed in this dissertation utilizes the dynamic range and frequency sweep speed of a network analyzer. In addition, the transfer function has both amplitude and phase information, which is important to ensure causality in an inverse Fourier transform. The key to this method is the use of a fiber optic transmitter/receiver pair with an operational frequency band from DC to ~10 MHz. By placing the fiber optics on the drive signal of the network analyzer, instead of the measure side, there is no degradation to the dynamic range of the measurement. Being able to take an S21 measurement over a distance of 2 miles, without line of sight, is truly unique. Also, the data acquisition for the entire system was automated using the LabView programming language. With the automation, the transfer function of a conductor at 201 frequencies can be measured in approximately the same amount of time as a single frequency was measured using the previous technique, a 200 times improvement in speed. Also, the inclusion of a car audio amplifier allowed for an increase in the current driven on the conductors, increasing the overall dynamic range. The audio amplifier served two purposes, it increased the drive signal and it transformed the output impedance to 4 ohms (which was much closer to the input impedance of the various conductors with the fence ground). The audio amplifier did limit the measurements in terms of frequency response. The amplifier was only useable up to ~100 kHz, where it would have been instructive to have measurements up to 1 MHz in frequency.

The measurements were conducted at seven locations along the left rail, trolley communication line, and the conveyor belt structure as they proceeded into the mine. The first three locations correspond to the first three power centers in the mine, where there would be access to the shield of the power cables. The last two locations correspond to the branching of the rails to the 1st and 2nd left switch (major branches of the mine). Also the last location is the closest point to the entrance to the sealed area, where the explosion occurred. The 4th and 5th locations were chosen for the convenience of the man-trip (or trolley) being able to be moved off of the main tracks and allow workers to pass the measurement operation. Hence, the 1st and 2nd right spurs were chosen. The total number of measurement points chosen was somewhat random, but the purpose of covering the major features of the entire mine was accomplished.

Measurements were conducted at the first three locations for the power cable shield. The power cable shield measurements were completed while the power was turned off. The power cable shield was not measured during regular mine operation due to safety concerns. Table 2-1 lists mine features at each measurement location, the approximate distance to the entrance (drive location), and the conductors measured. The measurement locations are also shown on the map of the mine in Figure 2-3.

Table 2-1 Direct drive measurement locations

				Conductors Measured: Voltage (V) & Current (I)	
Location	**Mine Feature**	**Break Number**	**Approximate Distance from Entrance**	**Grounding System in Configuration 1**[1]	**Grounding System in Configuration 2**[2]
1	#1 Power Center	Belt 1, Break 1	30 m (98 ft.)	Power Cable Shield (V&I)	Trolley Comm Line (I) Rail (V&I) Conveyor (V&I)
2	#2 Power Center	Belt 2, Break 1	459 m (1506 ft.)	Power Cable Shield (V&I) Trolley Comm Line (I) Rail (V&I)	Trolley Comm Line (I) Rail (V&I) Conveyor (V&I)
3	#3 Power Center	Belt 3, Break 1	669 m (2195 ft.)	Power Cable (V&I) Trolley Comm Line (I) Rail (V&I)	Trolley Comm Line (I) Rail (V&I) Conveyor (V&I)
4	1st Right Spur	Belt 3, Break 16	1076 m (3530 ft.)		Trolley Comm Line (I) Rail (V&I) Conveyor (V&I)
5	2nd Right Spur	Belt 4, Break 11	2178 m (1.35 miles)		Trolley Comm Line (I) Rail (V&I) Conveyor (V&I)
6	1st Left Switch	Belt 4, Break 50	3255 m (2.02 miles)		Trolley Comm Line (I) Rail (V&I) Conveyor (V&I)
7	2nd Left Switch	Belt 4, Break 59	3491 m (2.17 miles)		Trolley Comm Line (I) Rail (V&I) Conveyor (V&I)

---

[1] Mine grounding system similar to the grounding scheme in place during explosion.
[2] Mine grounding system in current state.

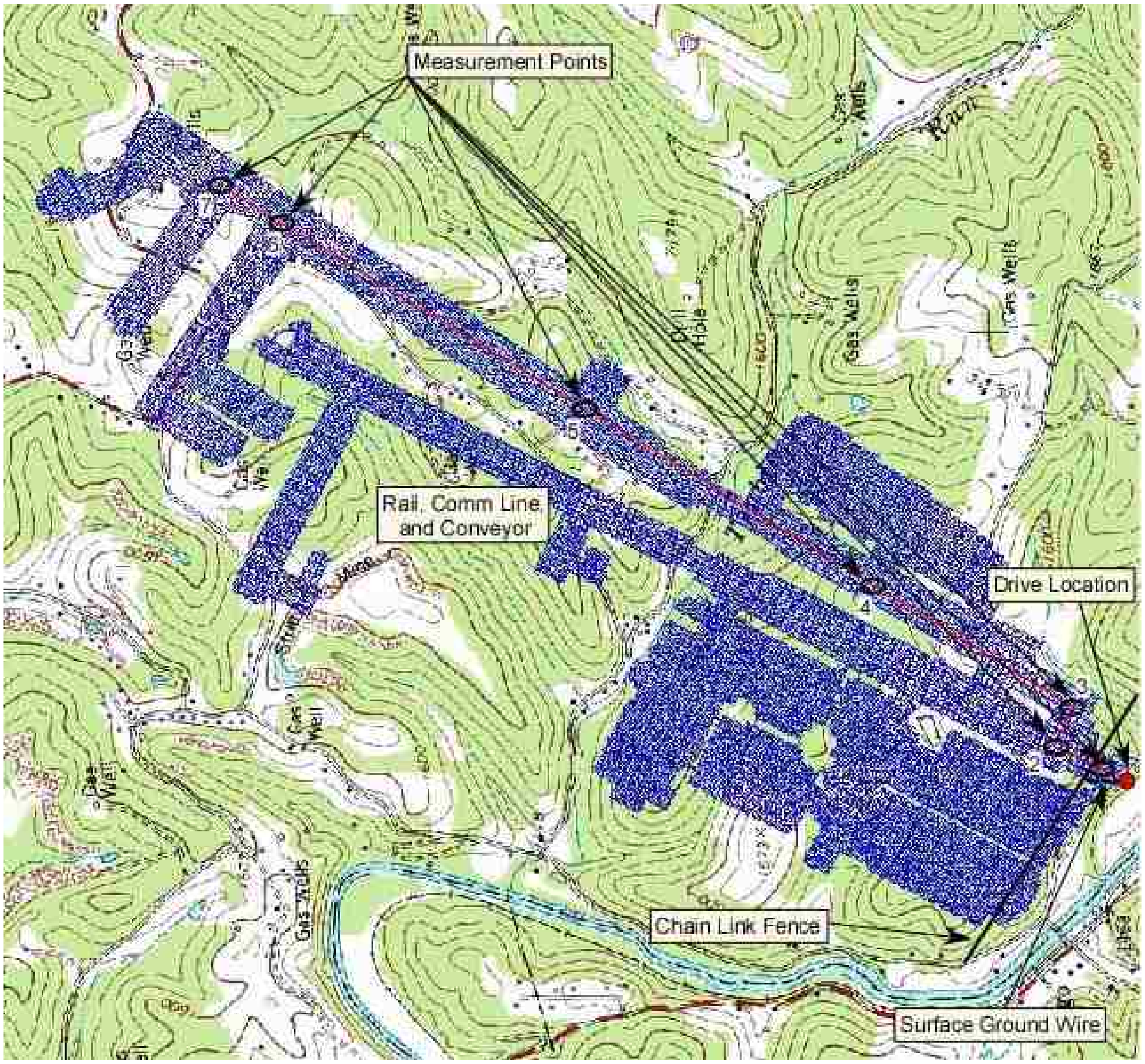

Figure 2-3 Direct drive measurement locations.

Three current probes were used for the various measurements: a Pearson model 110A; a Pearson model 4688; and a LEM-flex model RR3035 current probe. The voltage was measured with a high-impedance voltage probe model P601 made by Nanofast. The current and voltage probes are shown on the various conductive penetrations in Figure 2-4.The calibration curves for each probe versus frequency are located in Appendix A.

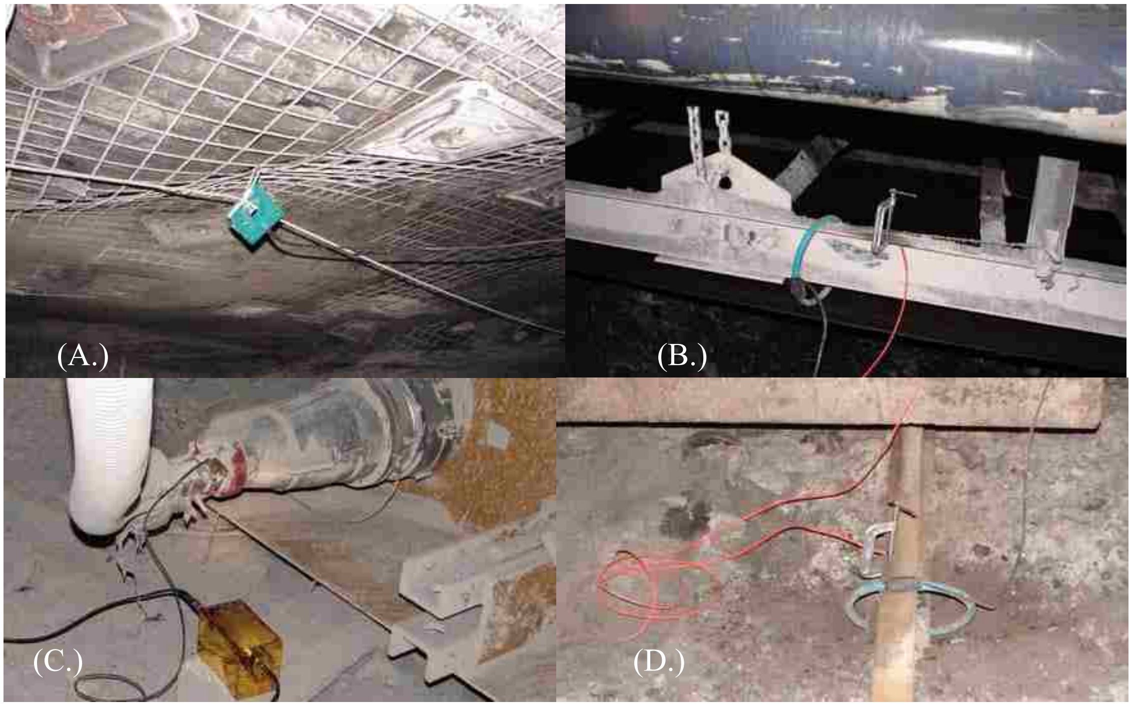

Figure 2-4 (A.) Current probe on trolley communication cable. (B.) Current probe and voltage connection on conveyor belt structure. (C.) Voltage probe on power cable. (D.) Current probe and voltage connection on rail.

2.1.3 Results

The results from the direct drive measurements were consistent with expectations. All of the processed spectral, or frequency-domain, voltage, and current transfer functions for each conductive penetration at each location can be found in Appendix B. For clarity, only a summary of the results is shown here. The summary tables show the attenuation of the peak amplitude of a positive and negative lightning-like pulse attached at the entrance of the mine. This quantity is calculated by multiplying the spectral representation of the current of a positive/negative lightning pulse by the current transfer function measured of a given conductor at a given location (that was measured in the mine). The spectral representation of the lightning pulses was calculated by transforming the temporal pulse using a 2^{20} point fast Fourier transform (FFT) in Matlab. Additions were made to the built-in FFT routine, such as creating a frequency array, automatically determining the number of points, and corrections in scaling.

The measured S_{21} data from each position was read into Matlab along with the calibration data for the various current probes, voltage probes, fiber optics, and attenuators. The S_{21} data at position X was compensated as shown in Figure 2-5.

Since the measured transfer functions had only 201 points, interpolation was needed to match the frequencies of the spectral representation of the lightning pulse. The magnitude of the transfer function was, in general, slowly varying with frequency; therefore a linear interpolation method was used in Matlab.

The product of the spectral lightning and current transfer function was then transformed to the time-domain by a 2^{21} point inverse fast Fourier transform (IFFT). The attenuation listed in the tables is then simply the peak output divided by the peak input.

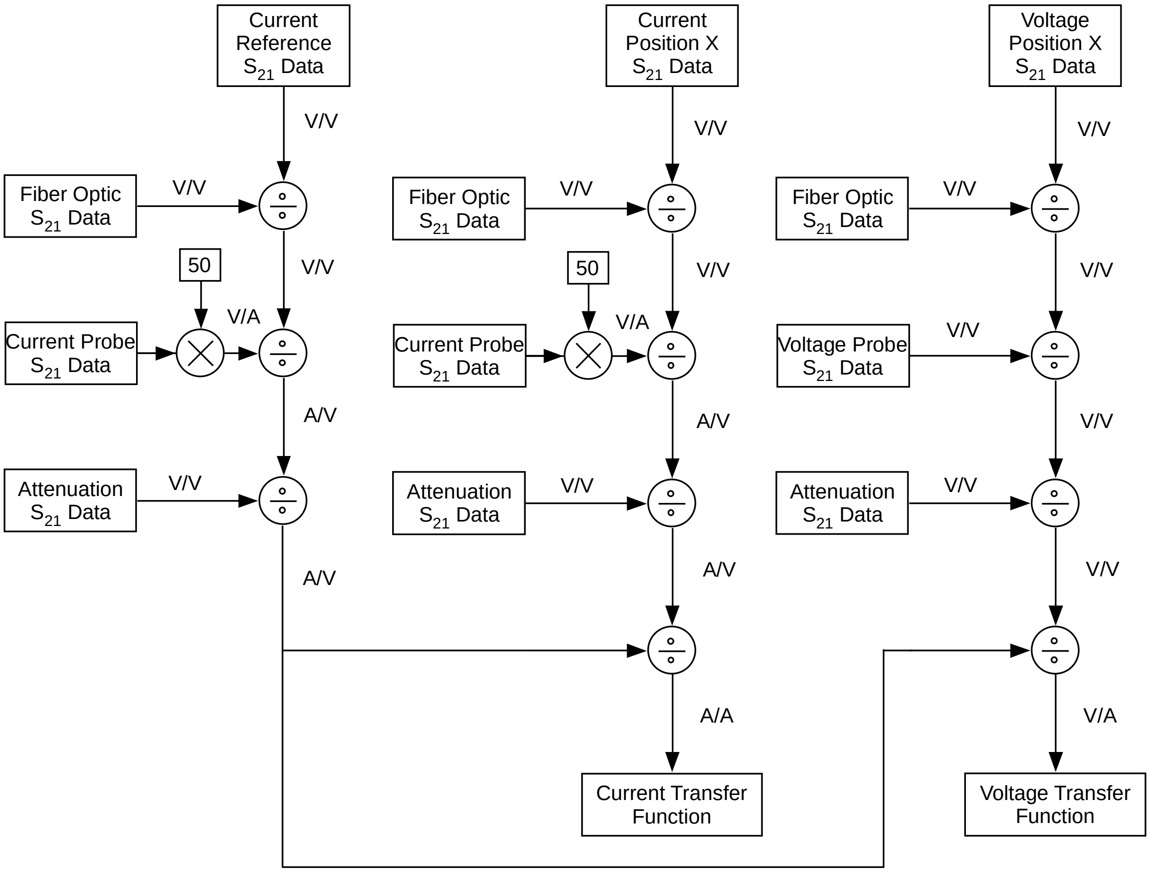

Figure 2-5 Flow graph of transfer function data processing.

The peak current output to peak current input attenuation, for the various conductors at the measured locations, given a positive lightning waveform, are shown in Table 2-2 and Table 2-3 and, given a negative lightning waveform, are shown in Table 2-4 and Table 2-5. Table 2-2 and Table 2-4 show the attenuation with the mine grounding system in its current state, while Table 2-3 and Table 2-5 show the attenuation with the mine grounding system like it was during the explosion. The darkened cells of the tables indicate no measurements were recorded in the given locations.

Table 2-2 Summary of current transfer functions, using positive lightning waveform, for conductive penetrations with current mine grounding

	Trolley Comm Line		Conveyor		Rail		Power Cable Shield	
Location	Local Gnd	Fence Gnd	Local Gnd	Fence Gnd	Local Gnd	Fence Gnd	Local Gnd	Fence Gnd
1	1.7x10^{-3}	2.9x10^{-3}	2.2x10^{-2}	2.9x10^{-2}	8.9x10^{-2}	1.4x10^{-1}	■	■
2	■	■	■	■	■	■	■	■
3	1.8x10^{-3}	2.8x10^{-3}	3.2x10^{-3}	4.9x10^{-3}	3.6x10^{-4}	9.2x10^{-5}	■	■
4	1.7x10^{-3}	2.8x10^{-3}	5.6x10^{-4}	1.1x10^{-4}	3.8x10^{-4}	9.4x10^{-5}	■	■
5	1.4x10^{-3}	2.2x10^{-3}	7.2x10^{-4}	2.7x10^{-4}	3.9x10^{-4}	3.0x10^{-4}	■	■
6	1.2x10^{-3}	1.9x10^{-3}	4.0x10^{-4}	1.1x10^{-4}	5.5x10^{-4}	4.2x10^{-4}	■	■
7	1.2x10^{-3}	2.0x10^{-3}	3.0x10^{-4}	9.3x10^{-5}	2.3x10^{-4}	3.5x10^{-4}	■	■

Table 2-3 Summary of current transfer functions, using positive lightning waveform, for conductive penetrations with former mine grounding

	Trolley Comm Line		Conveyor		Rail		Power Cable Shield	
Location	Local Gnd	Fence Gnd	Local Gnd	Fence Gnd	Local Gnd	Fence Gnd	Local Gnd	Fence Gnd
1	■	■	■	■	■	■	4.6x10^{-2}	6.2x10^{-2}
2	1.3x10^{-3}	1.6x10^{-3}	■	■	2.6x10^{-4}	3.7x10^{-4}	1.8x10^{-2}	2.8x10^{-2}
3	1.3x10^{-3}	1.5x10^{-3}	■	■	1.4x10^{-4}	1.7x10^{-4}	1.6x10^{-2}	2.5x10^{-2}
4	■	■	■	■	■	■	■	■
5	■	■	■	■	■	■	■	■
6	■	■	■	■	■	■	■	■
7	■	■	■	■	■	■	■	■

Table 2-4 Summary of current transfer functions, using negative lightning waveform, for conductive penetrations with current mine grounding

	Trolley Comm Line		Conveyor		Rail		Power Cable Shield	
Location	Local Gnd	Fence Gnd	Local Gnd	Fence Gnd	Local Gnd	Fence Gnd	Local Gnd	Fence Gnd
1	2.4x10^{-3}	4.3x10^{-3}	2.2x10^{-2}	2.9x10^{-2}	8.4x10^{-2}	1.4x10^{-1}	■	■
2	■	■	■	■	■	■	■	■
3	2.7x10^{-3}	4.7x10^{-3}	3.7x10^{-3}	5.2x10^{-3}	3.2x10^{-4}	1.3x10^{-4}	■	■
4	2.4x10^{-3}	4.2x10^{-3}	5.7x10^{-4}	1.4x10^{-4}	3.1x10^{-4}	1.7x10^{-4}	■	■
5	2.0x10^{-3}	3.4x10^{-3}	8.1x10^{-4}	3.1x10^{-4}	4.3x10^{-4}	3.4x10^{-4}	■	■
6	1.8x10^{-3}	3.2x10^{-3}	4.4x10^{-4}	2.9x10^{-4}	5.3x10^{-4}	5.4x10^{-4}	■	■
7	1.7x10^{-3}	3.0x10^{-3}	2.9x10^{-4}	8.7x10^{-5}	2.6x10^{-4}	1.9x10^{-4}	■	■

Table 2-5 Summary of current transfer functions, using negative lightning waveform, for conductive penetrations with former mine grounding

	Trolley Comm Line		Conveyor		Rail		Power Cable Shield	
Location	Local Gnd	Fence Gnd	Local Gnd	Fence Gnd	Local Gnd	Fence Gnd	Local Gnd	Fence Gnd
1							$4.7x10^{-2}$	$6.2x10^{-2}$
2	$2.2x10^{-3}$	$3.0x10^{-3}$			$4.0x10^{-4}$	$6.0x10^{-4}$	$1.8x10^{-2}$	$2.7x10^{-2}$
3	$2.2x10^{-3}$	$2.8x10^{-3}$			$1.6x10^{-4}$	$2.2x10^{-4}$	$1.6x10^{-2}$	$2.4x10^{-2}$
4								
5								
6								
7								

2.2 Indirect Drive

2.2.1 Setup/Equipment Layout with Photos

The method used to characterize indirect electromagnetic coupling into the sealed area is shown in Figure 2-6 and Figure 2-7. This is also novel new technique that utilizes the dynamic range and speed of a network analyzer to simulate a very basic phenomenon of a line current source at a ground interface. The current from the audio amplifier (which is driven by the output from the network analyzer) is driven on to a long wire above the ground which is terminated at each end with ground rods. The ground rods are placed so as to produce a current distribution in the ground that simulates a linear current drive.

In order to account for all angles of current source orientation, two orthogonal cable configurations were needed for the indirect drive measurements. One configuration was through ground rods placed so as to drive the current parallel to the sealed area of the mine and over the area where the explosion occurred as shown in Figure 2-7A. The surface drive wire was approximately 500 m long. A second configuration was through ground rods placed so as to drive the current perpendicular to the sealed area of the mine and over the area where the explosion occurred as shown in Figure 2-7B. In this case the surface drive wire was only 200 m long. Using the results from these two configurations the fields due to an arbitrarily oriented current source drive above the sealed area can be calculated using trigonometric functions.

There were no previous methods to measure this situation, but a function generator and spectrum analyzer would have been the logical pair. The method developed in this dissertation again utilizes the dynamic range and frequency sweep speed of a network analyzer and captures the amplitude and phase information needed for accurate inverse Fourier transforms. This time the fiber optic units were used to bring the measured signals to the surface through a non-conductive bore hole. It would increase the dynamic range of the measurement system to place the fiber optics on the drive side, however the logistics of transporting the network analyzer deep into the previously seal area made the choice clear. So a reduction in dynamic range was traded for speed of equipment setup and a reduction in the risk of expensive equipment damage. The audio amplifier with an output impedance to 4 ohms matched the impedance of the two grounded wire drive very well and allowed a fair amount of current to be driven. Communication with the team positioned in the previously sealed area of the mine was accomplished using a fiber optic Ethernet link with a voice over IP program on two laptops.

Two types of measurements were made to characterize the indirect coupling into the sealed area. The more time consuming of the two was the electric field mapping measurements made in the vicinity of the explosion ignition area, where the core hole is located. The other measurement was the induced voltage on a spliced intact pump cable going from the back of the sealed area to the location of the core hole. The pump cable was spliced with 12-gauge wire to recreate the length of pump cable believed to have been there during the explosion[3]. The end of the pump cable at the back of the mine was originally attached to the pump which was submerged underwater and chained to the ceiling mesh. For the measurements, the pump cable was connected with 12-gauge wire to the ceiling mesh and the exposed conductors were placed under water approximately four crosscuts from the back of the sealed area[4]. The approximate total length of the recreated cable was 300 m (984 ft).

The electric field at various locations in the sealed area of the mine was measured with an active dipole antenna connected to a receiver via fiber optics. The fiber-optic receiver is connected to the network analyzer measurement port so that the signals are phase-locked in order to measure very small signals in the microVolt/meter range. The three polarizations of the electric field were measured at a total of 15 locations for both the parallel and perpendicular wire current drives. The three polarizations measured were the vertical, P-directed (parallel to the length of the sealed area), and X-directed (transverse to the length of the sealed area). A photo of the dipole antenna in horizontal and vertical polarization is shown in Figure 2-9. The exact locations of the measured electric field are shown in Figure 2-8 where the distance between locations was approximately 10 m. The figure shows 17 total locations; however, positions P1 and P9 were not measured due to water hazards. Because of the amount of data taken and the spacing between measurement points, the lack of these two points does not impact the results.

---

[3] As a note, there is some disagreement as to the length and positioning of the pump cable at the time of the explosion. The test team used information provided at the time of the measurements, which was that the pump cable was intact and the cable shield was grounded to the submerged pump.

[4] Test team was unable to reach the back of the sealed area where the pump would have been (it was removed after the explosion) due to water.

The induced voltage measurements were taken on the pump cable with both a parallel and perpendicular surface wire drive. These measurements were also conducted using the instrumentation system shown in Figure 2-6. The induced cable voltage was measured with a Nanofast high-impedance probe in the vicinity of the core hole, and transmitted to the surface with fiber optics.

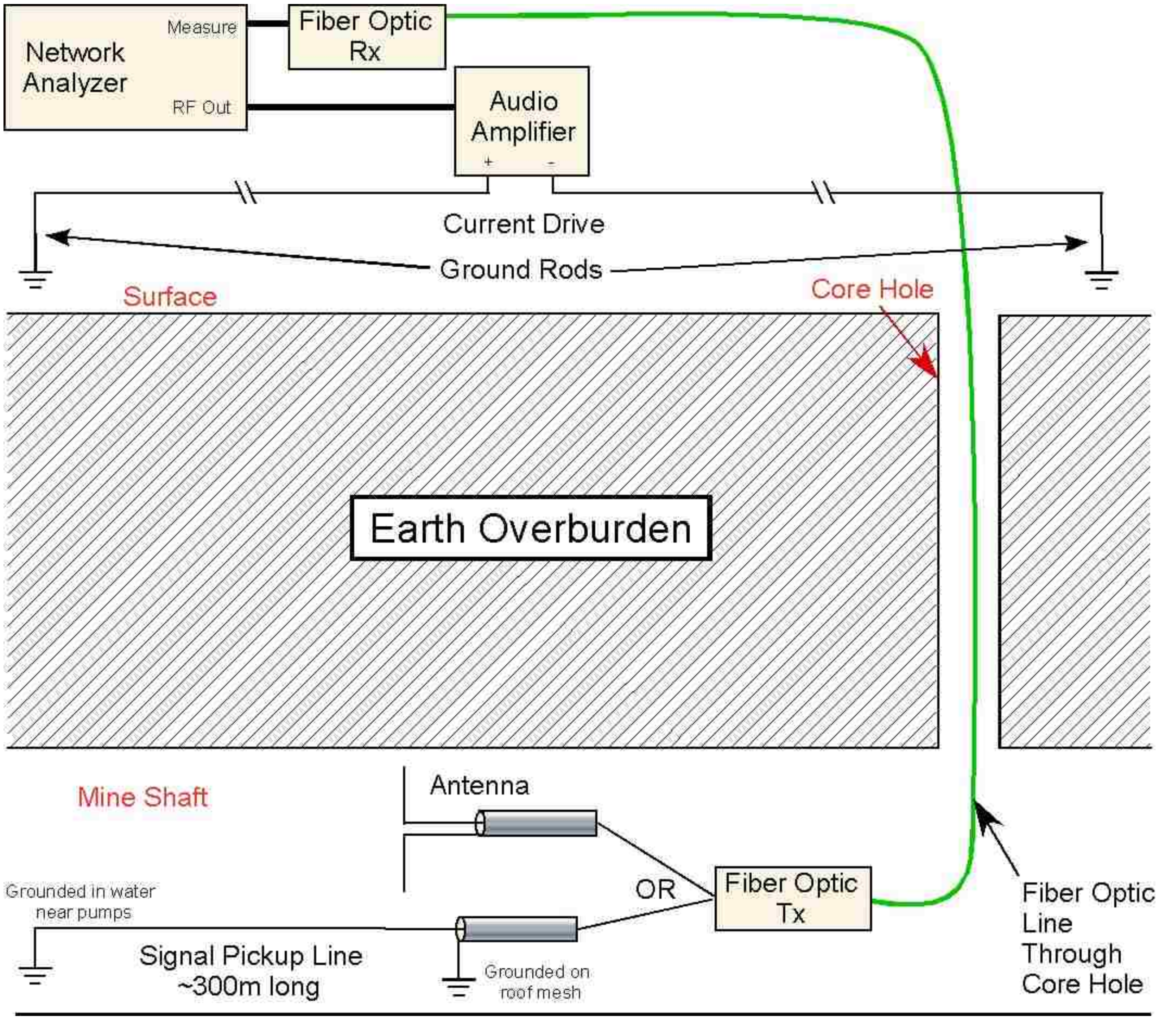

Figure 2-6 Indirect drive conceptual drawing.

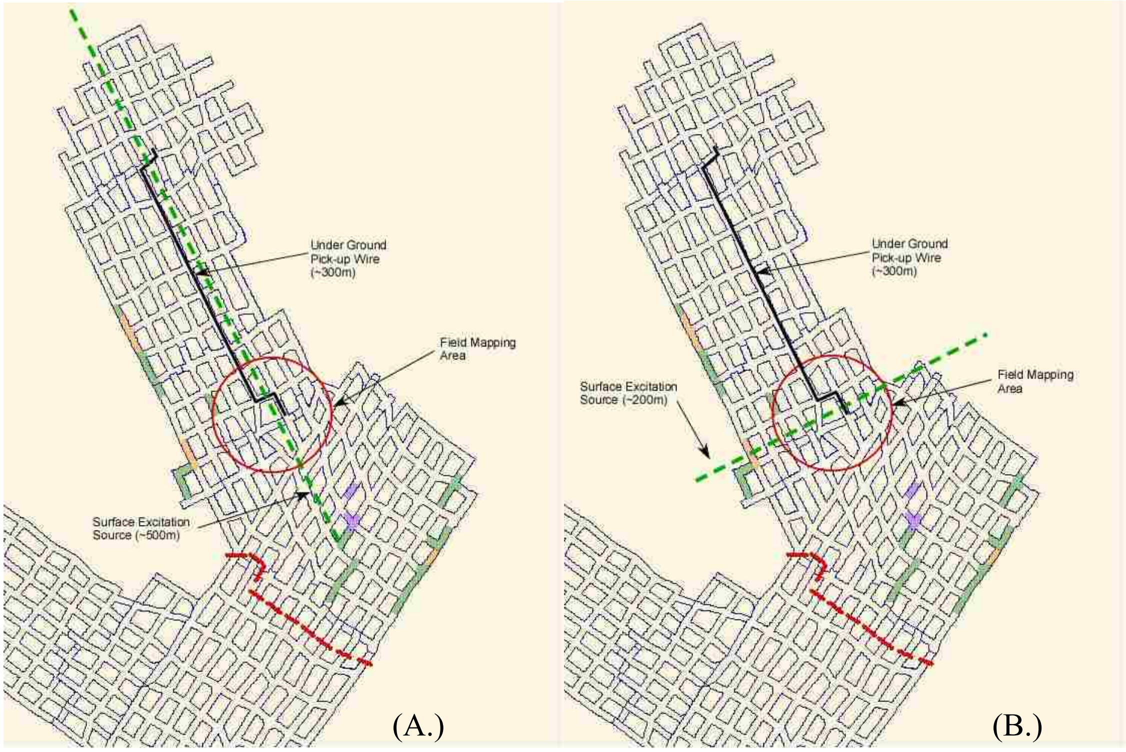

Figure 2-7 Parallel (A.) and perpendicular (B.) surface current drive for indirect drive measurements.

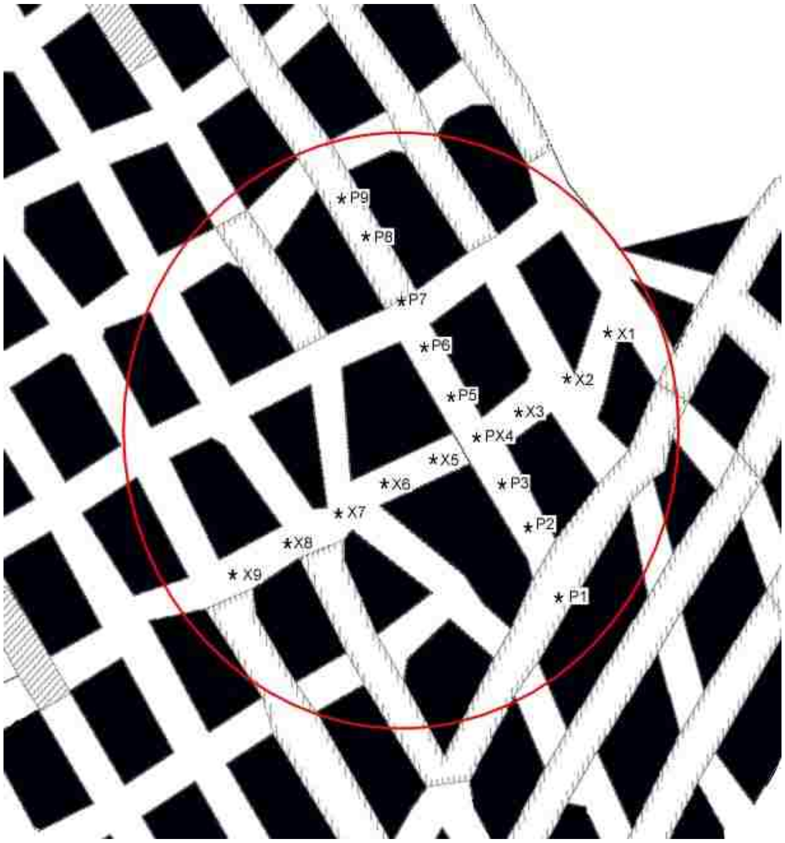

Figure 2-8 Electric field measurement locations.

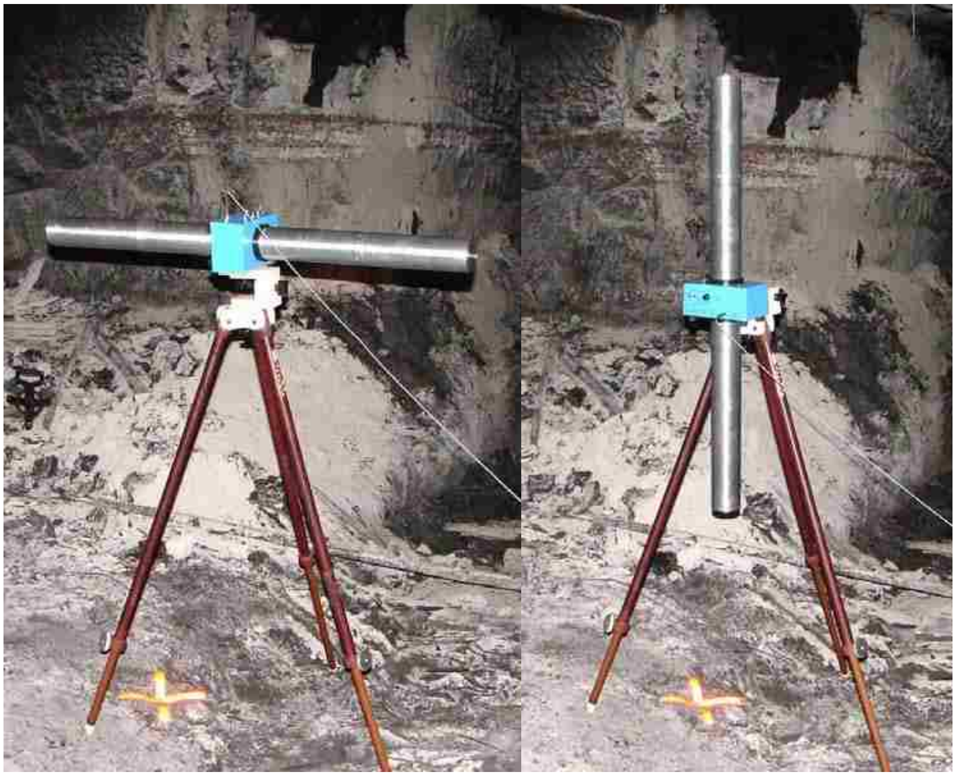

Figure 2-9 Active dipole antenna in horizontal and vertical polarizations inside previously sealed area.

2.2.2 Results

The purpose of the electric field mapping of the explosion area was to first look for any field inhomogeneities due to geological features, and second to compare to the analytical model. An added benefit was the ability to verify the induced voltage on the pump cable by integrating the parallel component of the electric field across it. The electric field measurements are shown first and then the induced cable voltage is plotted. The electric field results did show an enhanced electric field at the P5 and the X7 locations (this is noted for general interest,) but do not impact the cable results. The cable integrates or averages the fields over the cable length to build-up a potential difference or voltage.

The data collected for the indirect drive tests from the dipole antenna was only usable above 100 Hz. This was due to a very large 60 Hz clutter signal from surrounding power lines and the high noise level from the network analyzer below 40 Hz. Both of these factors were overcome for the long wire voltage measurement by reducing the IF bandwidth of the network analyzer from 10 Hz to 2 Hz. The reduction of the IF bandwidth lowered the noise floor considerably and reduced the sensitivity of the transfer function to the 60 Hz clutter; however, the time for a single swept measurement increased from ~1.5 minutes to ~10 minutes. With the large number of measurements desired for characterizing the electric field in the sealed area, the higher IF bandwidth was used for the majority of the data collected. As a result, only data from frequencies above 100 Hz are plotted for the dipole measurements in the body of this dissertation. The full spectrum of the data collected can be found in Appendix B.

The normalized composite electric fields from the dipole antenna at various locations are plotted in this section. The composite electric field is simply the root-sum-square or amplitude of the electric field vector. The measured electric field is normalized by the current in the drive wire on the surface, so that the units are V/m/A.

The normalized electric fields due to the wire current drive parallel to the P-direction, measured at locations P2 through P8 and X1 through X9, are shown in Figure 2-10 and Figure 2-11, respectively. Similarly, the fields due to the wire current drive perpendicular to the P-direction, measured at locations P2 through P8 and X1 through

X9, are shown in Figure 2-12 and Figure 2-13, respectively. This information is summarized in Table 2-6.

Table 2-6 Summary of figures for drive configurations

Drive Configuration	Electric Field at P locations	Electric Field at X locations
P-directed Current Drive (Parallel)	Figure 2-10	Figure 2-11
X-directed Current Drive (Perpendicular)	Figure 2-12	Figure 2-13

Referring to Figure 2-10, note that the composite electric fields measured in a path parallel to and immediately below the drive are about the same amplitude. The presence of metal objects near the antenna affects the local fields somewhat. The measurement at P5 was made in the area between unconnected sections of roof mesh. The slight resonance at about 60 kHz in the P5 measurement was probably caused by a resonance of the cable that was attached for the voltage measurements. This cable was not removed for the electric field measurements, and high electric fields may have been induced on the disconnected end of the cable at resonance.

Referring to Figure 2-11, note that the low-frequency amplitude tended to decrease as the electric field antennas were moved away from the center line immediately below the drive line.

Referring to Figure 2-12, the composite electric fields measured in a path perpendicular to the drive cable are reduced significantly from the field due to a parallel drive cable. Again, a slight resonance was seen at P5.

Referring to Figure 2-13, the fields measured parallel to and below the perpendicular drive are comparable in amplitude to those shown in Figure 2-10. Because of the closer spacing of the ground rods on the surface, more variation was shown in the individual measurements.

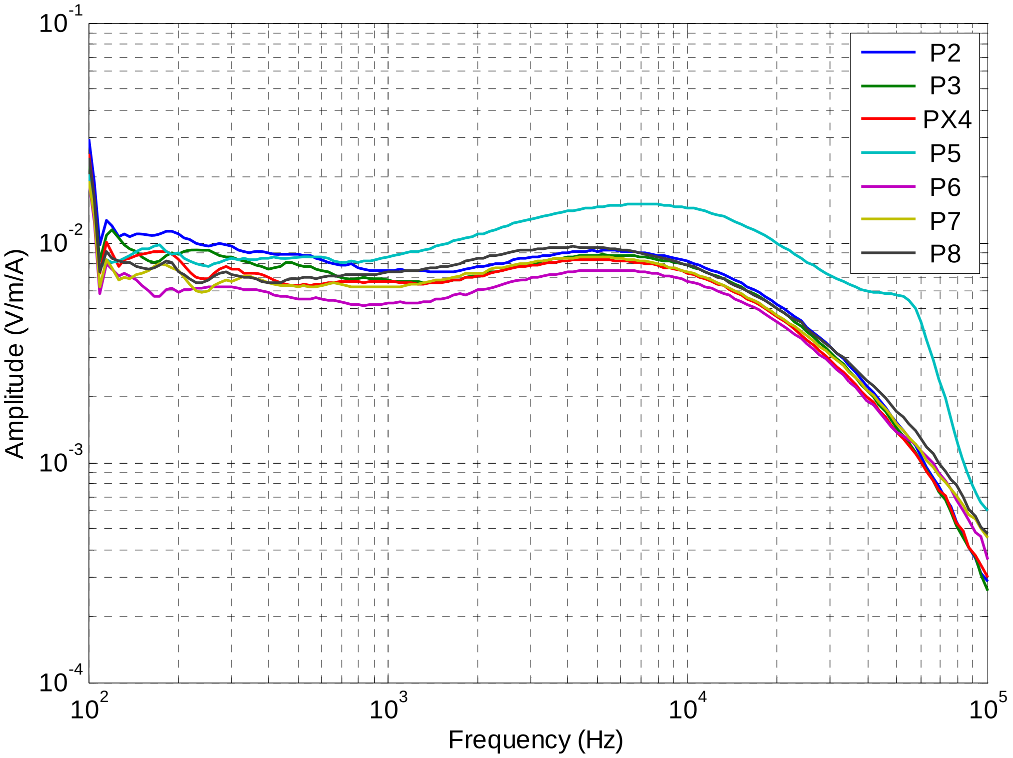

Figure 2-10 Composite electric field along P-direction with parallel line drive on surface.

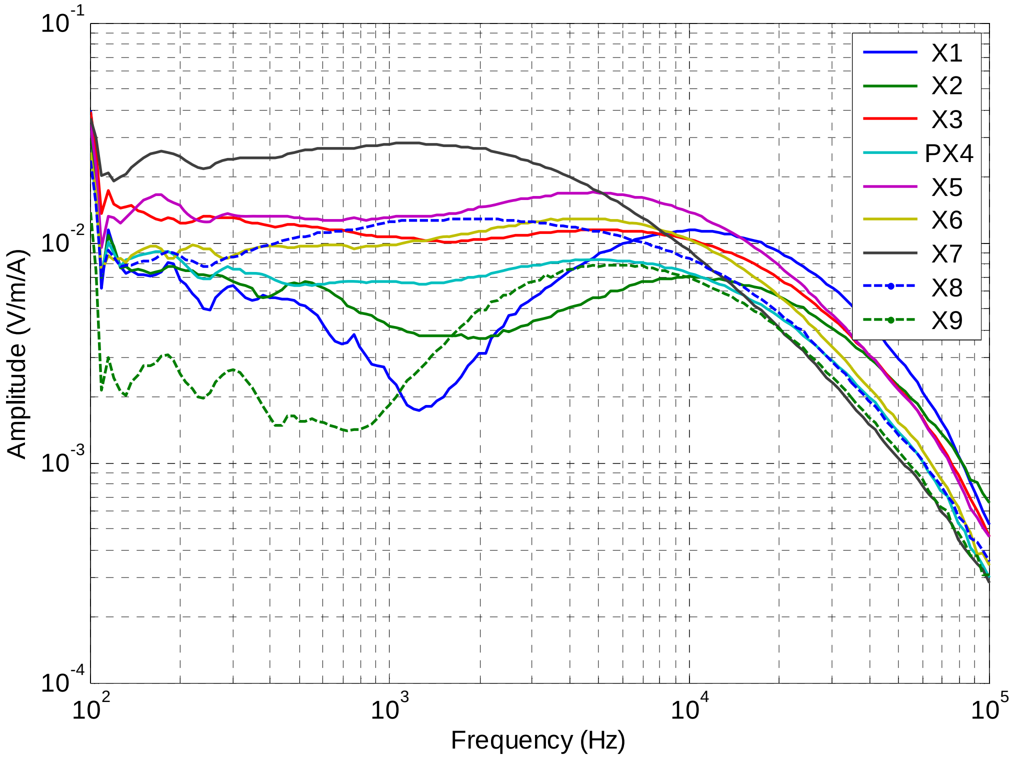

Figure 2-11 Composite electric field along X-direction with parallel line drive on surface.

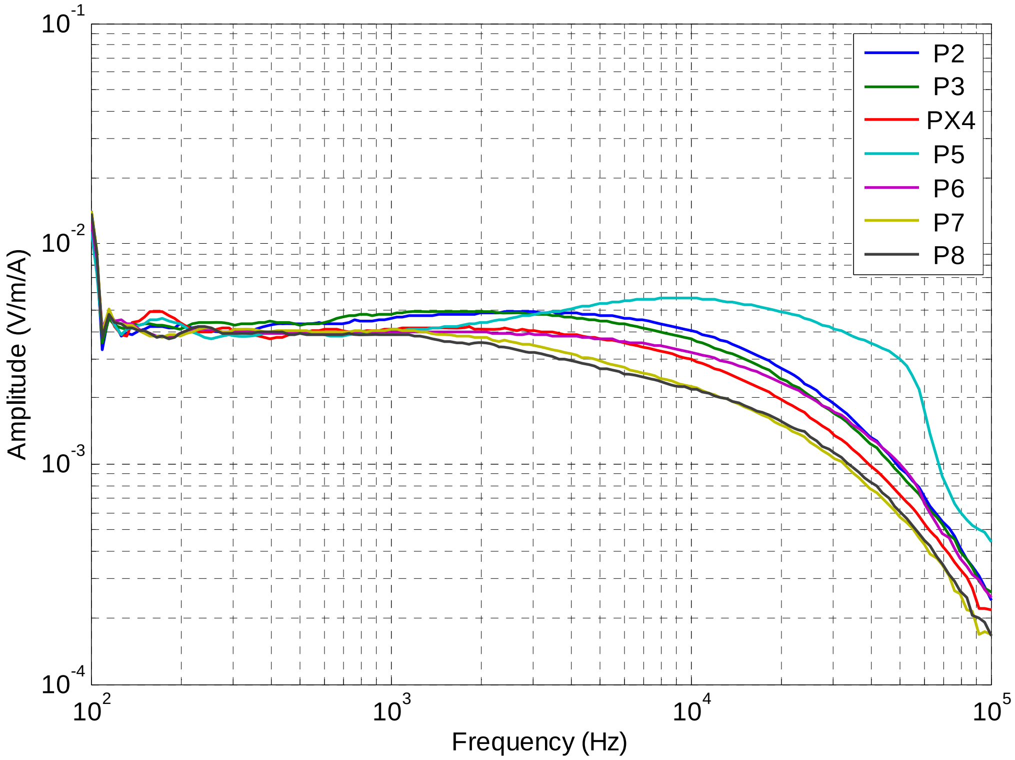

Figure 2-12 Composite electric field along P-direction with perpendicular line drive on surface.

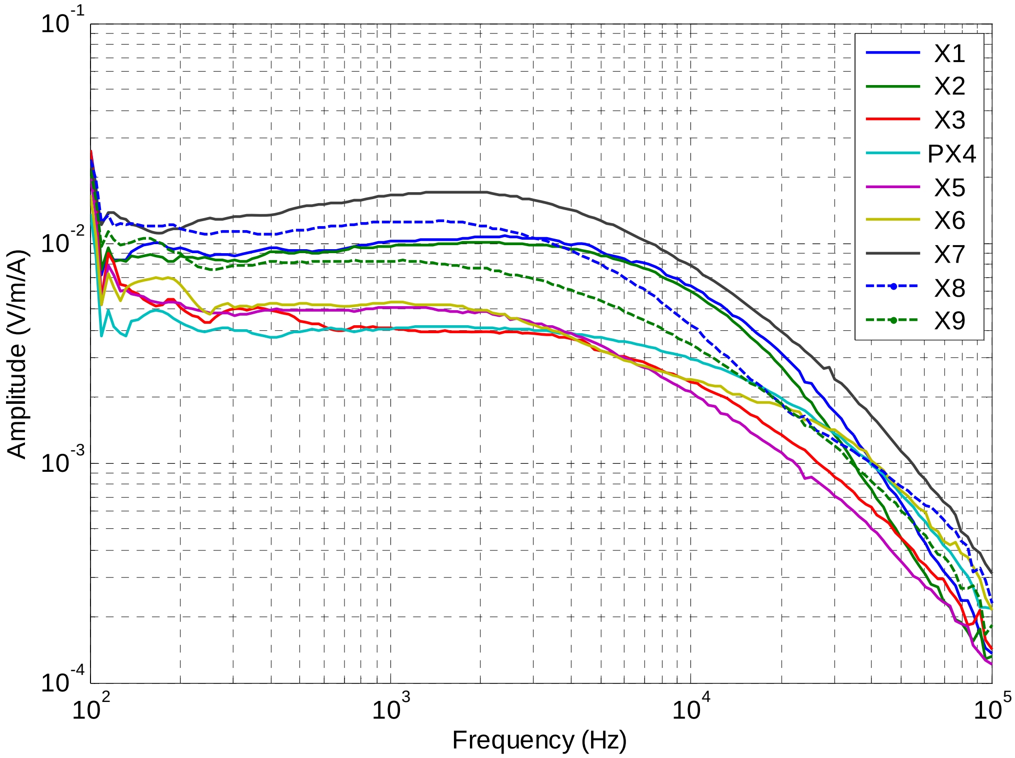

Figure 2-13 Composite electric field along X-direction with perpendicular line drive on surface.

The voltage on the pump cable was measured with a high-impedance voltage probe and the network analyzer set to a 2 Hz IF bandwidth. The normalized results of the voltage amplitude plotted relative to the drive current on the surface wire, with units of Volts per Amp (V/A), are shown in Figure 2-14. There is a spike at 60 Hz due to stray signals from power lines. The data is skewed by noise only below 20 Hz.

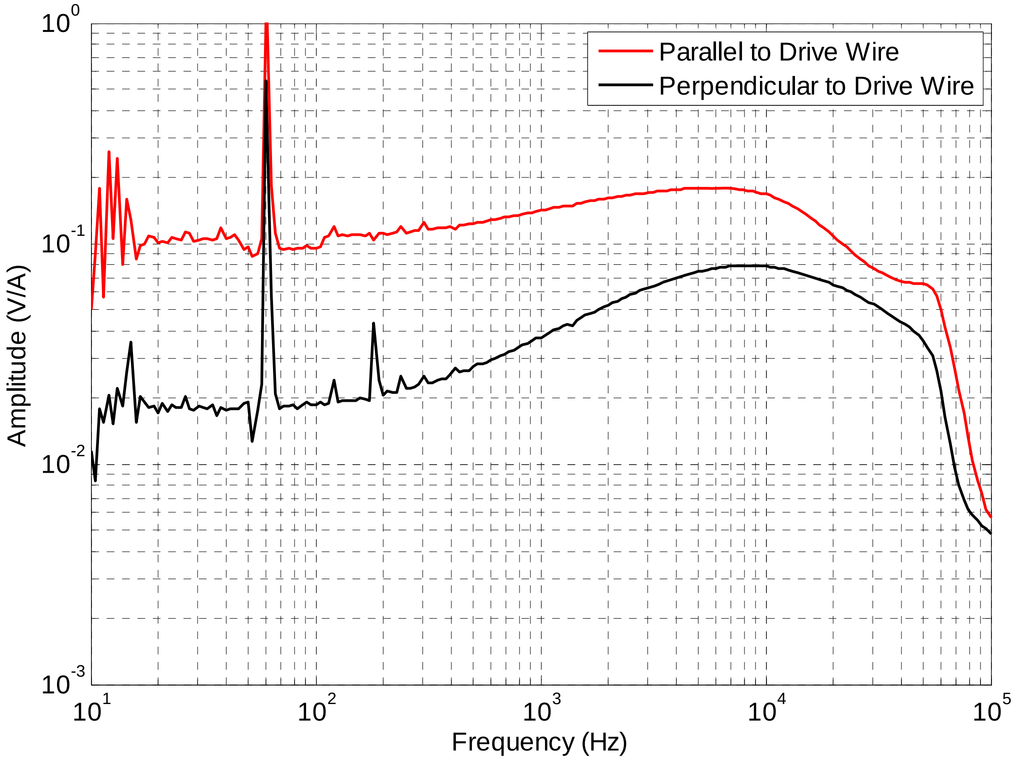

Figure 2-14 Induced voltage on pump cable (~300 m or 984 ft. long) due to wire current drives on surface.

To compare the induced voltage measured on the pump cable with the field measurements, we will look only at the parallel surface drive induced fields from P2 to P8. Furthermore, we will only look at the horizontal polarization directed along the P-axis, parallel to the direction of the drift. The horizontal polarized electric fields are shown in Figure 2-15. The normalized electric fields are in units of Volts per meter per Amp (V/m/A) while the normalized induced voltage on the pump cable are in units of Volts per Amp (V/A). If we integrate the electric fields over the length of the pump cable, we should obtain the induced voltage from Figure 2-14. Assuming a simple uniform distribution we can simply multiply the electric field by a length. The effective length of cable (similar to the effective area of an antenna) needed to match the electric fields measured with the induced voltage measured was found to be approximately 120 m

(394 ft). With a uniform field distribution, this would mean that only the 120 m (394 ft) closest to the measurement end of the cable contribute to the induced voltage. However, a uniform field distribution from the current drive is unrealistic, as discussed in the following chapter. The comparison between the measured induced voltage and the electric field multiplied by the effective length of 120 m (394 ft) is shown in Figure 2-16.

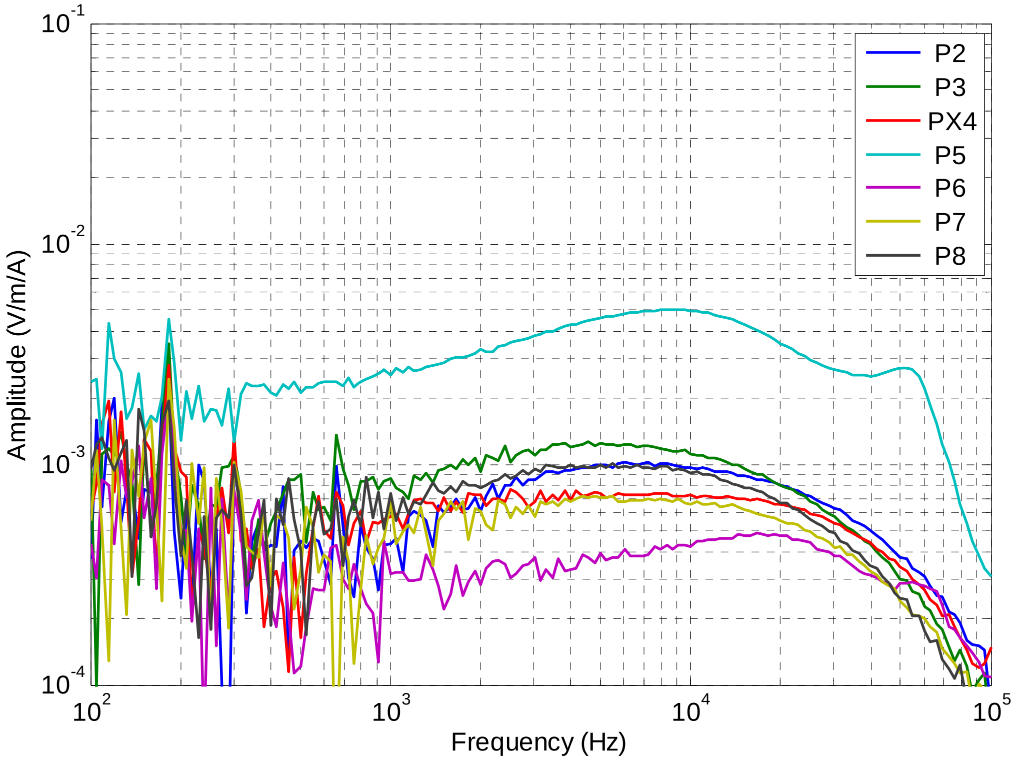

Figure 2-15 P-directed electric field along P-direction with parallel line drive on surface.

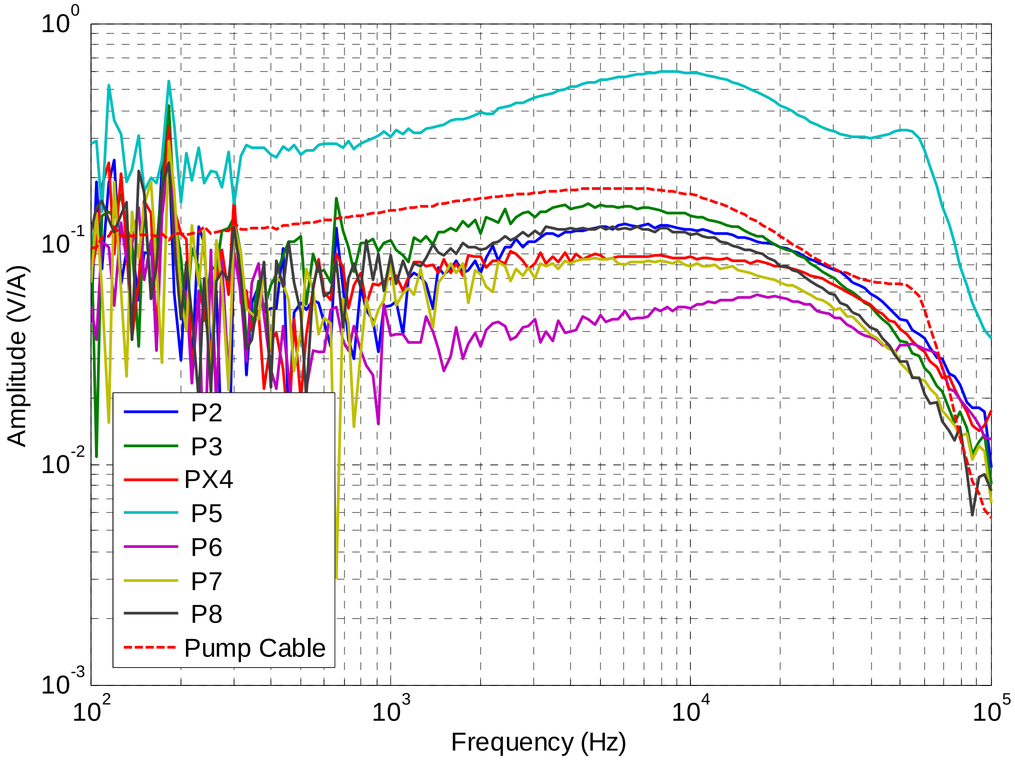

Figure 2-16 P-directed electric fields multiplied by an effective cable length of 120 m (394 ft) compared with the induced voltage on the pump cable.

Chapter 3 Analysis of Electromagnetic Coupling Phenomenology Models

Modeling is an integral part of analyzing and predicting electromagnetic coupling effects. Just as computational models need analytic models and careful measurements to perform validation and verification, so too do experimental measurements need analytic and computational models for validation. The modeling allows much of the real world clutter to be removed and focus on the first order factors of importance. Thus modeling was included in this dissertation to compare the measurements with theoretical calculations. One of the main purposes of the indirect modeling is to show that simple propagation models from surface to underground are sufficient for these lightning propagation calculations.

In this chapter transmission line models will be presented for geometries similar to those found in the tunnels of a coal mine. These models will be compared with experimental results collected at the Sago coal mine. Then coupling models for the indirect transmission of energy underground will be developed and presented. The indirect coupling models will also be compared with experimental results from the Sago coal mine.

3.1 Direct Coupling via Metallic Penetrations into Mine

There were four main metallic penetrations considered in the measurement section. Each penetration shall be considered for analysis using transmission line theory, starting with the trolley communication line. One reason to use transmission line theory is that the electrical behavior of the penetration can be predicted over a broad band of frequencies. Transmission line theory is applicable for the frequencies of interest (10 Hz to 100 kHz) because the length scale of the lines in the mine are on the order of ten kilometers and because for the two conductor models the dominant TEM mode has no low frequency cutoff. The transmission line equations for these two conductor models collapse from the 1-D form to a 0-D form at DC. The theory of transmission lines has been presented by many authors. The nomenclature used here was drawn from [24].

3.1.1 Generation of Direct EM Coupling Models

Using the differential circuit representation in Figure 3-1, the equations of transmission-line theory can be developed [24].

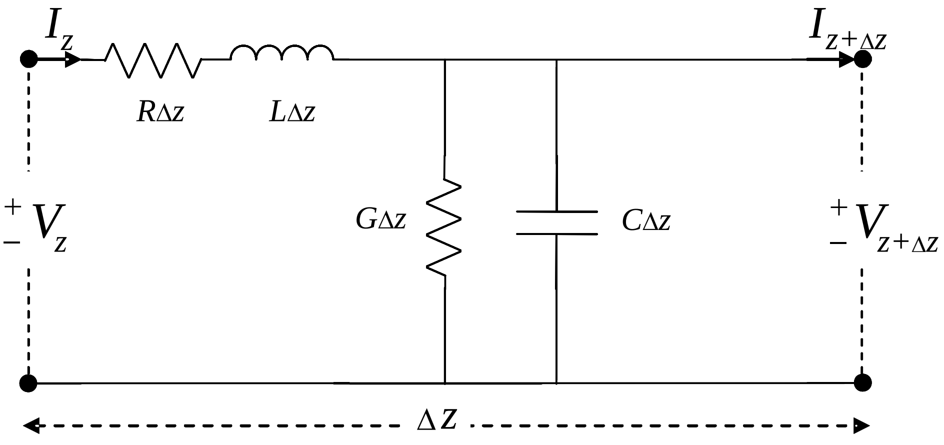

Figure 3-1 Equivalent circuit of a section of transmission line.

The transmission-line equations are given by

$$\left.\frac{d^2V}{dz^2}\right|_z = YZV$$

$$\left.\frac{d^2I}{dz^2}\right|_z = YZI$$

$$Y = G + i\omega C$$

$$Z = R + i\omega L$$

The complex propagation constant is given by

$$\Gamma^2 = YZ = \left(G + i\omega C\right)\left(R + i\omega L\right)$$

3.1.1.1 Parallel Wires

Two of the metallic penetrations into the mine are made up of parallel lines: the rails and the conveyor structure. It then follows that parallel lines seen as a transmission line should be considered. The formulation of the per unit length circuit parameters are given by [25]:

$$L = \frac{\mu}{2\pi} \ln \frac{\rho_0}{a_1 a_2}$$

$$C = \frac{2\pi\varepsilon'}{\ln\left(\rho_0 / a_1 a_2\right)}$$

$$R = \frac{1}{\pi a_1^2 \sigma_1} + \frac{1}{\pi a_2^2 \sigma_2}$$

$$G = \frac{2\pi\omega\varepsilon''}{\ln\left(\rho_0 / a_1 a_2\right)}$$

where ρ_0 is the distance between wires of radius a_1 and a_2 with conductivities σ_1 and σ_2.

3.1.1.2 Coaxial Cable

The most efficient transmission line in the mine is an isolated wire that operates as a trolley communication line. If this is considered as a center conductor and the walls of the mine tunnel as a return, then there is a semblance to a coaxial structure, shown in Figure 3-2.

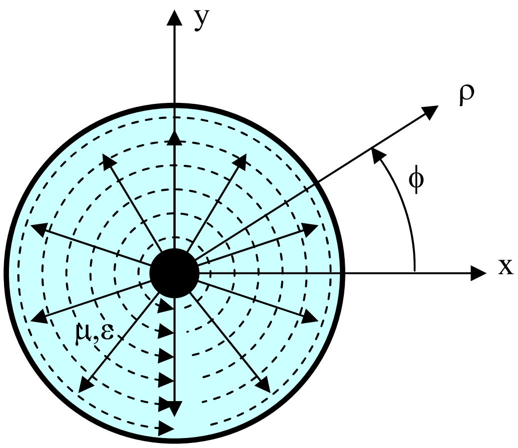

Figure 3-2 Coaxial cable geometry.

For a coaxial cable, we know that the TEM fields contained within are:

$$\overline{E} = \frac{V_0 \hat{\rho}}{\rho \ln\left(b/a\right)} e^{-\gamma z}$$

$$\overline{H} = \frac{I_0 \hat{\phi}}{2\pi\rho} e^{-\gamma z}$$

The transmission line parameters can be found using a field analysis, as follows.

$$L = \frac{\mu}{\left|I_0\right|^2} \int_S \overline{H} \cdot \overline{H}^* ds = \frac{\mu}{(2\pi)^2} \int_{\phi=\phi}^{2\pi} \int_{\rho=a}^{b} \frac{1}{\rho^2} \rho \, d\rho \, d\phi = \frac{\mu}{2\pi} \ln \frac{b}{a}$$

$$C = \frac{\varepsilon}{\left|V_0\right|^2} \int_S \overline{E} \cdot \overline{E}^* ds = \frac{\varepsilon'}{(\ln \quad b/a)^2} \int_{\phi=\phi}^{2\pi} \int_{\rho=a}^{b} \frac{1}{\rho^2} \rho \, d\rho \, d\phi = \frac{2\pi\varepsilon'}{\ln b/a}$$

$$R = \frac{R_S}{\left|I_0\right|^2}\int_{C_1+C_2} \bar{H}\cdot\bar{H}^* d\ell = \frac{R_S}{(2\pi)^2}\left(\int_{\phi=\phi}^{2\pi}\frac{1}{a^2}a \quad d\phi + \int_{\phi=\phi}^{2\pi}\frac{1}{b^2}b \quad d\phi\right) = \frac{R_S}{2\pi}\left(\frac{1}{a}+\frac{1}{b}\right)$$

$$G = \frac{\omega\varepsilon''}{\left|V_0\right|^2}\int_S \bar{E}\cdot\bar{E}^* ds = \frac{\omega\varepsilon''}{(\ln \quad b/a)^2}\int_{\phi=\phi}^{2\pi}\int_{\rho=a}^{b}\frac{1}{\rho^2}\rho \, d\rho \, d\phi = \frac{2\pi\omega\varepsilon''}{\ln b/a}$$

where $R_S = \sqrt{\dfrac{\pi f \mu_c}{\sigma_c}}$, b is the radius of the outer conductor, and a is the radius of the inner conductor.

3.1.1.3 Eccentric Coaxial Cable

Then, if the center conductor is moved from a concentric orientation to an offset position, as seen in Figure 3-3, the cable begins to become closer to reality.

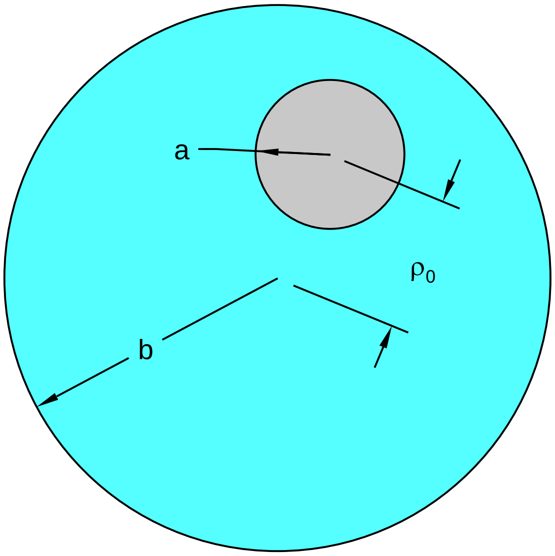

Figure 3-3 Eccentric coaxial cable geometry.

From the capacitance calculations in Smythe [26] between two cylinders, we have:

$$C = 2\pi\varepsilon\left[\cosh^{-1}\left(-\frac{\rho_0^2 - b^2 - a^2}{2ba}\right)\right]^{-1}$$

Utilizing Tesche's formulation of L in terms of C [25],

$L = \frac{\mu\varepsilon}{C}$, we can obtain the inductance per unit length for the eccentric coaxial cable.

$$L = \frac{\mu}{2\pi}\cosh^{-1}\left(-\frac{\rho_0^2 - b^2 - a^2}{2ba}\right)$$

Then, using the similarity relation,

$G = 2\pi\varepsilon''\left[\cosh^{-1}\left(-\frac{\rho_0^2 - b^2 - a^2}{2ba}\right)\right]^{-1}$, where $\varepsilon'' = j\omega\sigma$, and R is the same as in the centered coaxial case above.

3.1.1.4 Tunnel Coaxial Cable

Others have looked at using transmission line theory in the analysis of wires in tunnels [27,28]. Most of these have looked at the transmission of waves at frequencies of 1 MHz and above. Wait also investigated the quasi-static limit [29], which shall be discussed here.

With the same geometry as seen in Figure 3-3, the equations have been developed for Z and Y as:

$$Z = \frac{i\omega\mu_0}{2\pi}\left(\Lambda + \Omega\right) + Z_s$$

where $Z_s = \frac{\eta_w}{2\pi a}\frac{I_0(\gamma_w a)}{I_1(\gamma_w a)}$, $\gamma_w = \sqrt{i\omega\mu_w\sigma_w}$, and $\eta_w = \frac{i\omega\mu_w}{\gamma_w}$.

$$Y = \frac{i\omega 2\pi\varepsilon_0}{\Lambda}$$

$$\Lambda \cong \ln\frac{b}{a} - \ln\frac{b^2}{b^2-\rho_0^2}$$

$$\Omega = \frac{1}{\gamma_e b}\left\{\frac{K_0(\gamma_e b)}{K_1(\gamma_e b)} + 2\sum_{m=1}^{\infty}\left[\frac{K_m(\gamma_e b)}{K_{m+1}(\gamma_e b)} - \frac{\gamma_e b}{2m}\right]\left(\frac{\rho_0}{b}\right)^{2m}\right\} + \ln\frac{b^2}{b^2-\rho_0^2}$$

$$\gamma_e = \sqrt{i\omega\mu_e\left(\sigma_e + i\omega\varepsilon_e\right)}$$

3.1.2 Comparison of Direct EM Coupling Models to Measured Results

The complex propagation constant, Γ, was calculated from the measured current at location 1 and 7. It should be noted that the response of the current probe and the fiber optic unit have been removed. The current at location 1 (z_1) and location 7 (z_7) can be written in terms of Γ and a constant current I_0.

$I(z = z_1) = I_0 e^{-\Gamma z_1}$ and $I(z = z_7) = I_0 e^{-\Gamma z_7}$

Rearranging $I(z = z_1)$ and inserting it into $I(z = z_7)$ we have

$$I(z = z_7) = I(z = z_1)e^{-\Gamma(z_7 - z_1)} \Rightarrow e^{-\Gamma(z_7 - z_1)} = \frac{I(z = z_7)}{I(z = z_1)} = H$$

Then solving for Γ

$$\Gamma = -\frac{\ln H}{z_7 - z_1}$$

3.1.2.1 Trolley Communication Cable

The tunnel going into the Sago coal mine was approximately circular with a diameter of ~2 m. The trolley communication cable was a 10 gauge wire (with insulation jacket) strung along the roof of the tunnel going into the mine. The cable was held up by roof hangers (~2 inches long) periodically such that the average distance from the roof was ~6 inches. At the entrance to the mine the trolley communication cable was grounded to one rail of the tracks entering the tunnel, which was also the drive point for the measurements performed.

The real part of Γ calculated from the location 1 and 7 data is plotted in Figure 3-4. Clutter from the 60 Hz power present in the mine contaminated the data below 100 Hz and is not shown in this plot. The Trolley communication cable structure was modeled using the tunnel coaxial formulation with a ground resistivity of 0.1 and 100 Ω-m, both of which are plotted with the measured data. Also, if the rail is considered a parallel conductor, which is reasonable, then the structure can be modeled with the parallel wire transmission line formulation. However, the wires are grounded at the entrance of the mine. We can simulate this with an effective conductance, G_{eff}. If we replace the normal conductance, G, which would be zero due to the surrounding material being free space, with a $G_{eff} \sim$ 2e-7, then it is like a resistance between rail and trolley communication cable of ~1.4 kΩ. This is a reasonable value given the length of wire and the single point ground at the entrance. The parallel wire model is also overlaid in Figure 3-4.

The two tunnel coaxial models bound the measured data for a good part of the frequency band. The parallel wire transmission line model with a constant effective conductance does a good job of following an average value of the measured data.

The differences between the current at location 1 and 7 were quite small despite a distance of almost 3.5 km. Due to this small attenuation the measurements are more susceptible to noise and setup variations. The uncertainties due to setup variation, although small, are close to the order of the differences between the two measurements. These issues make the trolley communication line not the ideal penetration for modeling.

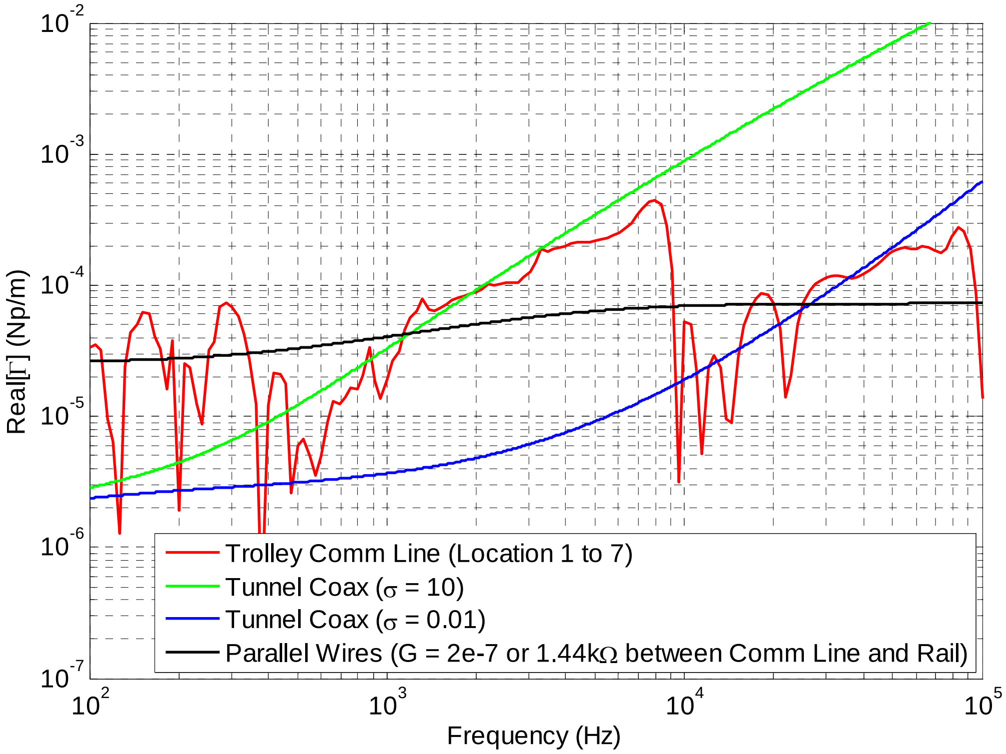

Figure 3-4 Real part of propagation factor for the Trolley Communication Line compared with various transmission line models.

3.1.2.2 Power Shield

The next conductive penetration considered is the shield of the power cable entering the mine. The power shield surrounds the power cable with an approximate radius of 3 inches. The power cable mostly runs along the side wall of the mine, closely secured to the wall. At each power center the power shield was unintentionally grounded by the ~2 m square power converter sitting on the ground. If we treat the power converter as a 1 m radius plate on a 10 Ω-m ground, then from the resistance calculation $R = \rho/4a$ [30] we have ~2.5 Ω to ground. Location 1 was located next to Power Center 1, location 2 next to Power Center 2, and location 3 next to Power Center 3. Therefore the resistance to ground could be between 0.83 and 2.5 Ω, if each power center ground was considered in a parallel configuration. However, while the power converter at Power Center 1 was sitting directly on the ground, the power converter at Power Center 3 was sitting partially on wooden blocks. Over the distance of 429 m from location 1 to 2, if we distribute the ground resistance between the power shield and the wall of the tunnel we have an effective conductance, G_{eff}, present in the transmission line formulations.

The real part of Γ from the measured data collected on the power shield, from location 1 to 2 and from location 1 to 3, is plotted in Figure 3-5. Looking at the power shield inside the tunnel as an eccentric coaxial cable, an effective conductance of 6.5e-3 S is needed for good correlation between measured data between 500 Hz and 30 kHz. However, if we look at the power shield as one wire and the rail as the other, then we can analyze it as a system of parallel wires approximately 0.5 m apart. Using an effective conductance of 1e-3 S or a resistance of 2.3 Ω at a single point between the power shield and the rail, then the agreement with measured data is quite good between 20 Hz and 30 kHz. For completeness, analyzing the power shield using the tunnel coaxial formulation with an added constant effective conductance of 1e-3 S yields fairly good results between 40 Hz and 30 kHz. It should be noted that for the power shield measurements the 60 Hz power to the mine was completely shut off. It is apparent from the data that the measured responses are useable from 20 Hz and above in frequency.

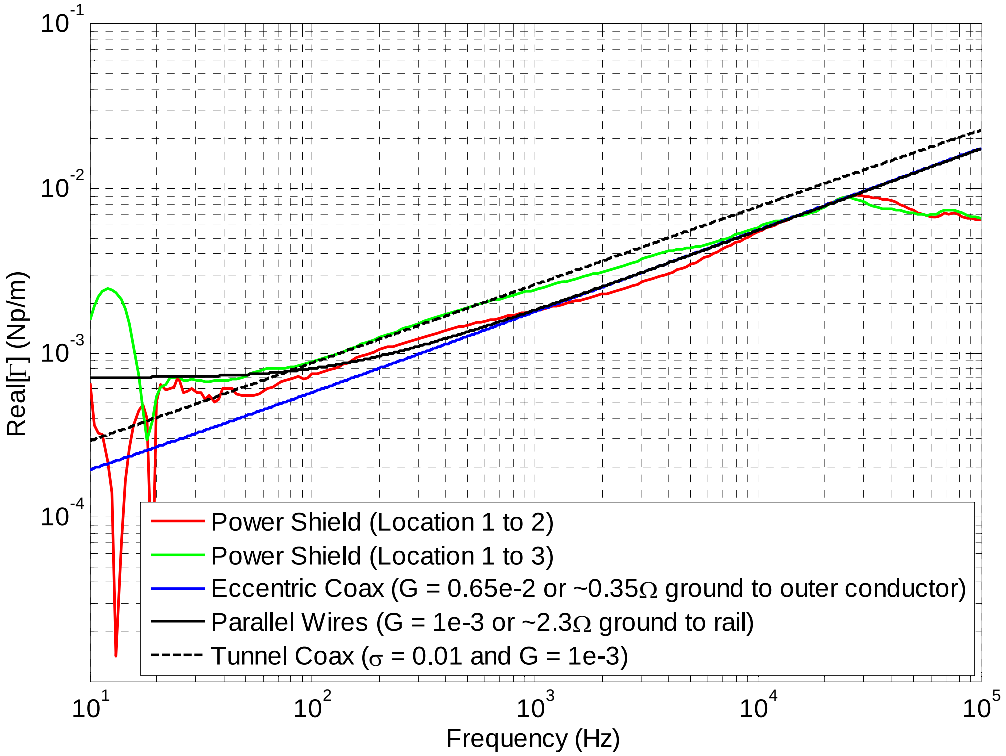

Figure 3-5 Real part of propagation factor for the Power Shield compared with various transmission line models.

3.1.2.3 Rail of Tracks for Man-Trip

The next conductive penetration considered is the left rail of the tracks entering the mine for the personnel transportation vehicles (or Man-Trips). The rail is of the usual rail road track cross-section and will be modeled as a cylinder with an approximate radius of 1 inch. The rails run along the floor of the tunnel with a separation of ~1 m between them. The rails are lying directly on the floor and have bolts securing them to the floor periodically.

The real part of Γ from the measured data collected on the rail, from location 1 to 2 and from location 1 to 3, is plotted in Figure 3-6. Looking at the rail inside the tunnel as a tunnel coaxial cable, if an effective conductance of 2e-2 S is used (indicating a resistance from rail to tunnel wall of 50 Ω every meter) there is good correlation between the model and measured data between 10 Hz and 300 Hz. However, if we look at the left rail as one wire and the right rail as the other return wire, then we can analyze it as a system of parallel wires approximately 0.5 m apart. Using an effective conductance of 2e-2 S or a resistivity of 50 Ω-m between the two rails (which given a 100 Ω-m rock/ground resistivity and a separation of 0.5 m is reasonable), the agreement with measured data is quite good between 10 Hz and 1.4 kHz.

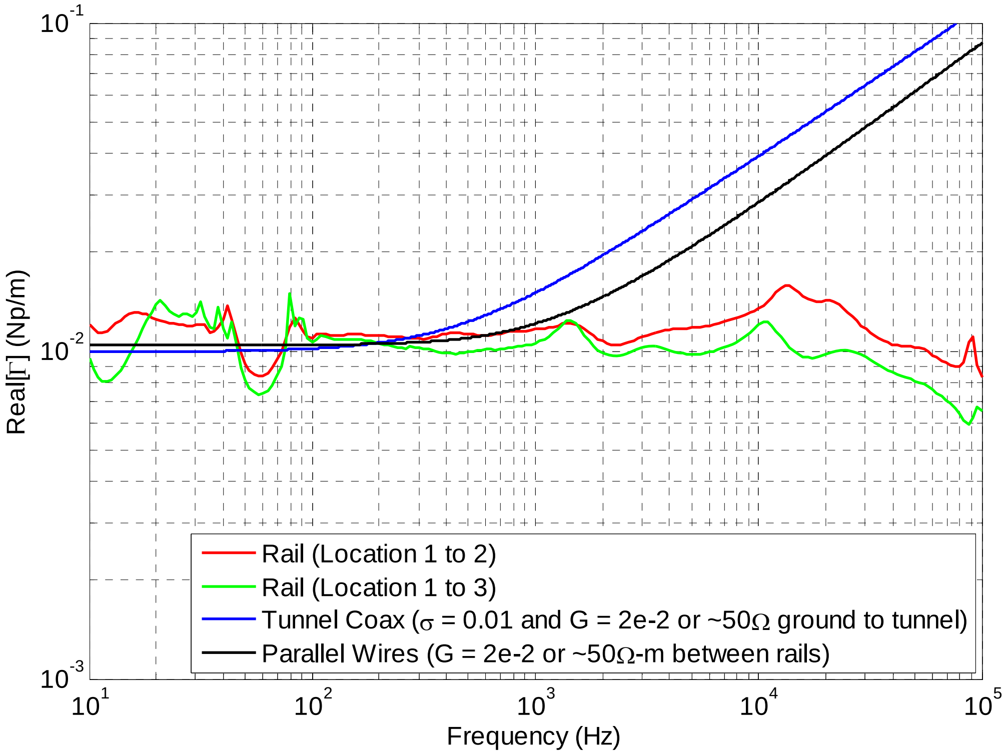

Figure 3-6 Real part of propagation factor for the Rail compared with various transmission line models.

3.1.2.4 Conveyor Belt Structure

The final conductive penetration considered is the conveyor belt structure used to transport coal out of the mine. The conveyor belt structure is a complex metal frame work suspended from the ceiling of a tunnel into the mine. The conveyor belts were suspended from the mine roof by metal chains attached to brackets bolted to the roof every ~3 to 5 m. The metal guarding and the metal supports for the guarding were anchored firmly against the mine roof and in contact with the wire mesh installed on the roof. The conveyor utilizes a separate tunnel into the mine than the trolley communication line, power cable, and rails. The conveyor structure will be modeled as two parallel cylinders with an approximate radius of 3 inches.

The real part of Γ from the measured data collected on the conveyor, from location 1 to 2 and from location 1 to 3, is plotted in Figure 3-7. Looking at the conveyor inside the tunnel as an eccentric coaxial cable, an effective conductance of 2e-2 S is needed for good correlation between measured data between 700 Hz and 5 kHz. However, if we look at the one side of the conveyor structure as one wire and the other side of the conveyor structure as a return, then we can analyze it as a system of parallel wires approximately 0.5 m apart. Using an effective conductance of 1e-2 S (or a resistivity of 100 Ω-m between the sides of the conveyor structure), then the agreement with measured data from location 1 to 2 is quite good between 10 Hz and 5 kHz. Analyzing the conveyor structure using the tunnel coaxial formulation with an added constant effective conductance of 5e-3 S (or a resistivity of 200 Ω-m between the structure and tunnel wall) yields fairly good results between 10 Hz and 3 kHz for the measured data from location 1 to 3. It should be noted that for the conveyor measurements the 60 Hz power to the mine was on, the conveyor was running, and coal was being transported on the conveyor out of the mine.

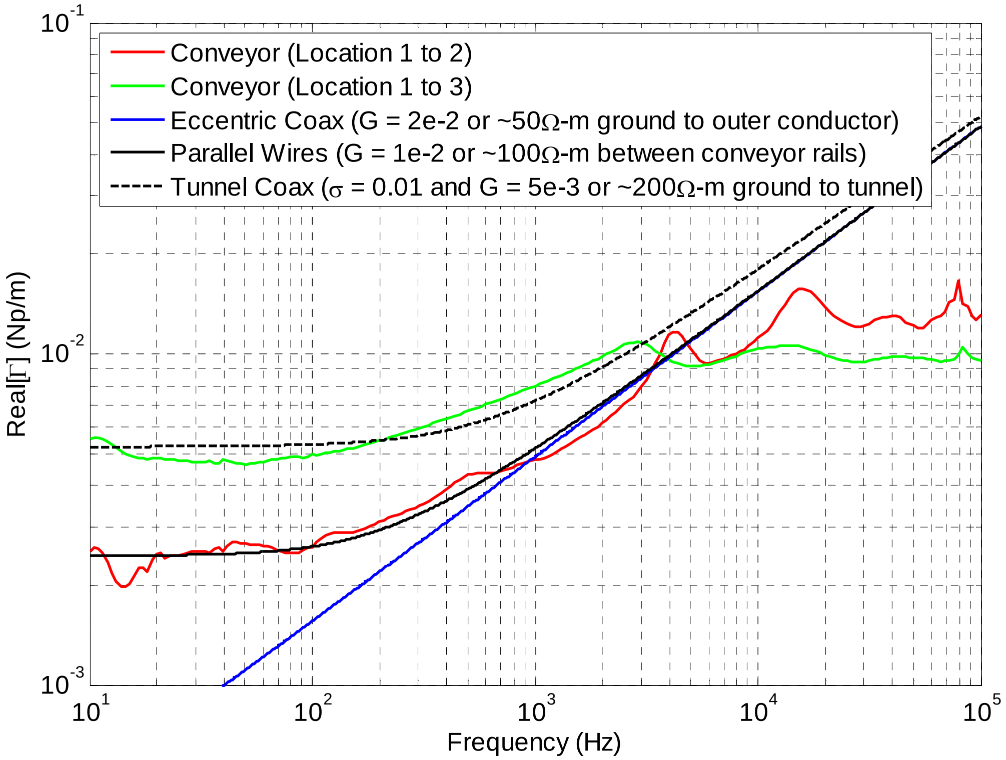

Figure 3-7 Real part of propagation factor for the Conveyor Structure compared with various transmission line models.

3.1.2.5 Summary of Direct EM Coupling Model Comparison

The four conductive penetrations going into the Sago coal mine were modeled as various canonical transmission lines and compared with measured current transfer function data. Modeling conductors as a transmission line using parallel wire geometry with a constant conductance between wires led to the best results. The trolley communication line had very little loss between the first and last measurement points, which made the complex propagation constant very susceptible to clutter, measurement setup variations, and resonance shifts in the data. These issues led to the fact that the trolley line was not ideal for modeling. The power shield had very good correlation between the parallel wire transmission line model and the measured data from 10 Hz to 30 kHz. The power shield data showed a stable complex propagation constant, making the comparison between measured data and models more productive. The complex propagation constant calculated from measured data of the rail was fairly constant over the entire frequency range. The model of the parallel wires (which seems to fit the geometry well), only compares well with measured data from 10 Hz to 1 kHz. A model with very little capacitance and inductance may be needed to decrease the frequency dependence of the propagation constant. Finally, the conveyor belt structure showed a good correlation between measured data and the parallel wire model from 10 Hz to 5 kHz. Again, the modeled results and measured results diverge at the high end of the frequency spectrum. However, the conveyor belt structure was a very complex geometry and the complex propagation constant from the measured data was somewhat inconsistent from location to location. Overall, the analytic canonical modeling produced very good results for the majority of the frequency band measured.

3.2 Indirect Electromagnetic Coupling via Soil and Rock

Calculating the electric fields below the surface of the earth due to a lightning flash can be a difficult task. To simplify matters, modeling will start with finding the fields in the earth due to a linear current source. This section starts with the simplest case of a DC current source injected into a homogeneous half-space. Then the next subsection introduces a time-varying, infinite length current source above the surface of the earth. This case will also be very useful in simulating the electric fields underground due to a horizontal arc of lightning or cloud-to-cloud lightning. The development continues as the current source is brought to the surface of the earth. Analytic models are shown for both an infinite and finite length current sources in Section 3.2.3. Computational models using Eiger are shown for the finite wire case with various current distributions. The complexity increases as the conductive half-space is stratified into layers of differing conductivities. Analytic infinite line and computational finite line current sources are modeled and the results are shown for the stratified media cases in Section 3.2.4. Finally, the various models developed throughout this section are compared with the measured electric field data from the indirect drive coupling experiments performed at the Sago coal mine.

3.2.1 Static Coupling Model for Current Injected into Homogeneous Half-Space

The geometry for the simplest model for DC current coupling is shown in Figure 3-8 and is analyzed in [26].

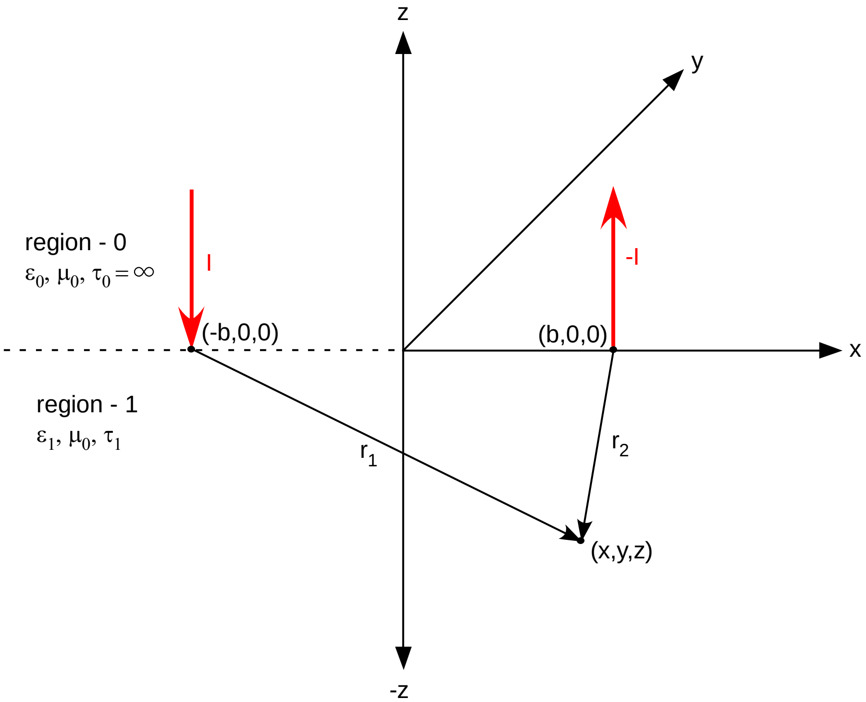

Figure 3-8 DC current drive with homogeneous conducting half-space.

Current *I* is driven into the conductive half-space at (-b,0,0) and the current is extracted at (b,0,0). The upper half-space, region-0, has infinite resistivity and the lower half-space, region-1 has resistivity, τ_1. From simple considerations, V(x,y,z), the potential at Cartesian coordinate (x,y,z) with respect to infinity is given by

$$V(x,y,z) = \frac{\tau_1 I}{2\pi}\left(\frac{1}{\sqrt{(x+b)^2 + y^2 + z^2}} - \frac{1}{\sqrt{(x-b)^2 + y^2 + z^2}}\right)$$

The electric field at point (x,y,z) is easily calculated from

$$\bar{E}(x,y,z) = -\nabla V(x,y,z)$$

And calculating the x-component of interest

$$E_x(x,y,x) = -\frac{\partial}{\partial x}V(x,y,z)$$
$$= \frac{\tau_1 I}{2\pi}\left(\frac{(x+b)}{\left[(x+b)^2+y^2+z^2\right]^{\frac{3}{2}}} - \frac{(x-b)}{\left[(x-b)^2+y^2+z^2\right]^{\frac{3}{2}}}\right)$$

The next coupling models to be considered are generalizations where the current is time varying ($e^{i\omega t}$) and the displacement currents are neglected because region-1 is assumed to be a good conductor. Also the current is confined to a line source of infinite length (to begin with) and horizontal to the half-space interface for the following models. This may not be a good representation for the path that currents from lightning would travel in the earth; however it is a good representation of the experimental setup and any conductors that may have lightning currents directly injected onto them.

3.2.2 Infinite Line Source above Homogeneous Half-Space

This model will be used to simulate the coupling of the horizontal portion of a cloud-to-ground flash or horizontal cloud-to-cloud lightning to underground as in Section 4.4. The current drive geometry of an infinitely long, horizontal wire placed a distance, h, above a conductive half-space is shown in Figure 3-9. Similar configurations are analyzed in [31-35].

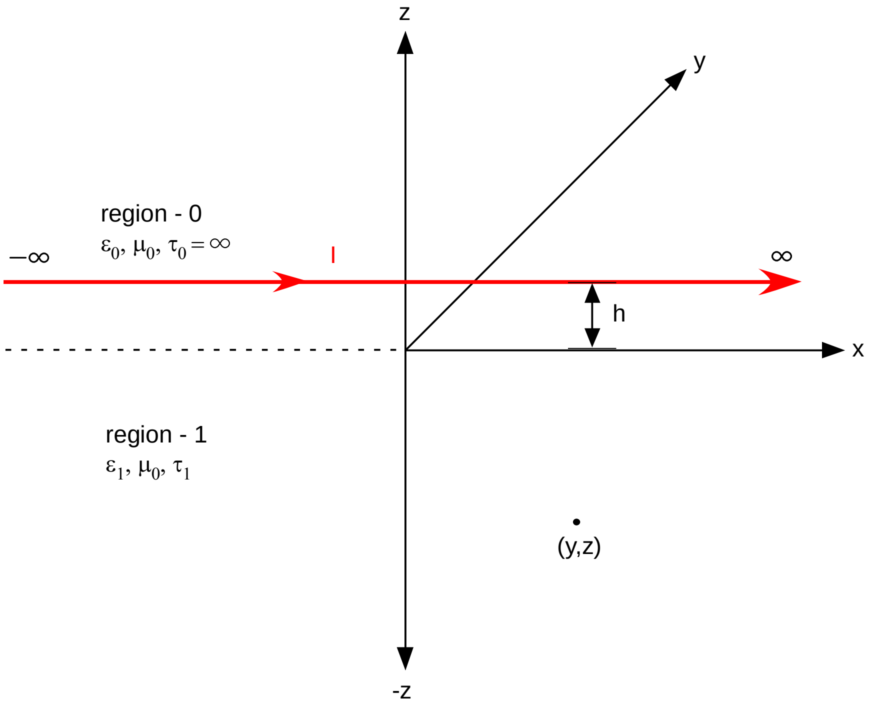

Figure 3-9 Infinite length, harmonically time varying horizontal current drive over a conductive half-space.

The current drive is harmonically time-varying and is directed along the positive x-axis at height, h, above it. Since the current is infinite in extent and constant in amplitude, there is no dependence on *x*. The upper half-space has infinite resistivity and the lower half-space has resistivity, τ_1. If one neglects displacement current and relates current density, $i_x(y,z)$ and electric field, $E_x(y,z)$, in region-1 through $E_x(y,z)=\tau_1 i_x(y,z)$ then the current density in the lower half-space, region-1, can be determined by

$$E_x\left(y,z\right)=\frac{ik\varsigma_0}{\pi}\int_0^\infty \frac{e^{qz}e^{-uh}}{u+q}\cos uy\,du$$

where

$$k = \omega\sqrt{\mu_0 \varepsilon_0}$$

$$q = \sqrt{u^2 + ip^2}$$

$$p^2 = \frac{\omega\mu_0}{\tau_1} = \frac{2}{\delta_1^2}$$

$$\delta_1 = \sqrt{\frac{2\tau_1}{\omega\mu_0}}$$

Numerical calculations of this integral result in Figure 3-10.

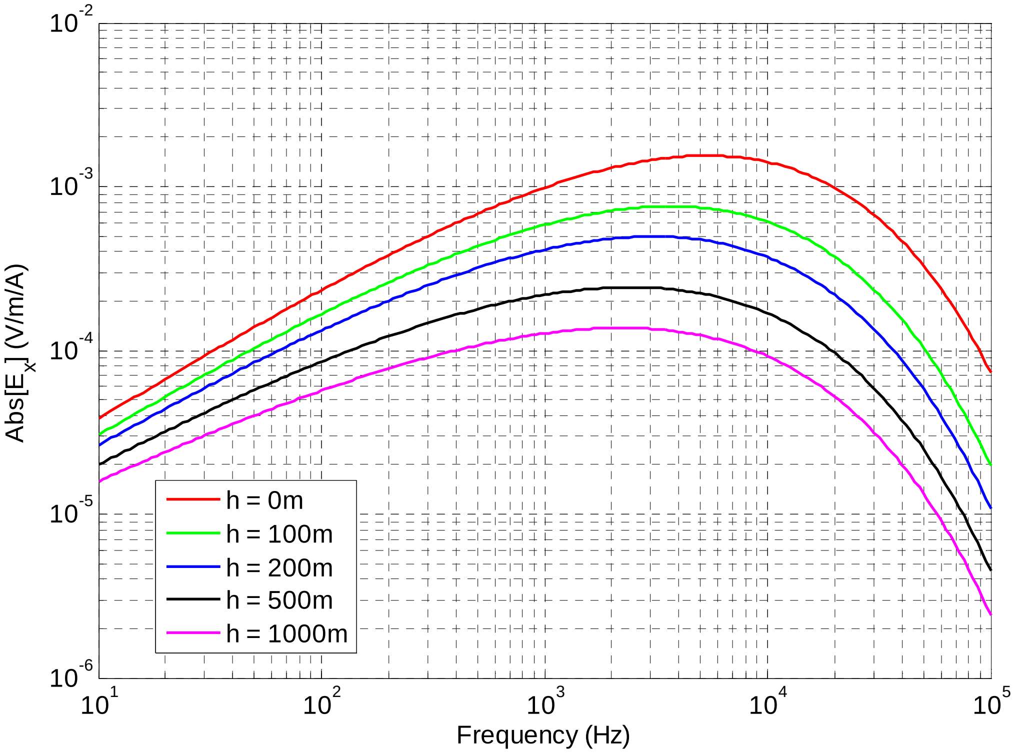

Figure 3-10 Electric field magnitude from an infinite line current source at various heights when measured at z = -100 m, y = 0 m, and τ_1 = 80 Ω-m.

Note that the skin depth, δ, plays an important role as a parameter in all diffusion coupling calculations. For convenience it is plotted for resistivities of 10, 100, and 1000 Ω-m in Figure 3-11. At a given frequency, the lower the resistivity the smaller the skin depth, meaning a majority of the current is contained closer to the surface. Hence, there will be better coupling deeper underground for ground with resistivity of 100 Ω-m than for ground with resistivity of 10 Ω-m.

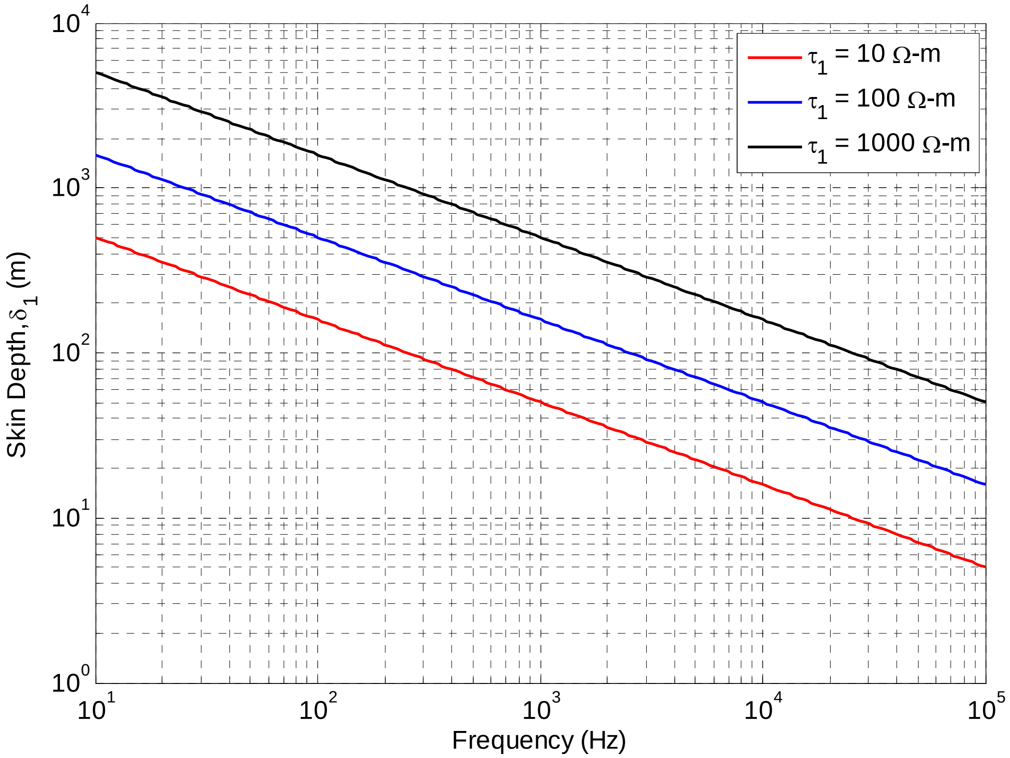

Figure 3-11 Skin depth, δ_1, as a function of frequency for resistivities of 10, 100, and 1000 Ω-m.

3.2.3 Line Source at Surface of Homogeneous Half-Space

For this section the line source is brought to the interface between the half-spaces. Three models are compared for a line source at the surface of a homogeneous half-space. First looking at an infinite line source, and then moving to a finite line source using analytic solutions. Finally, computational results are shown for the finite line source.

3.2.3.1 Infinite Line Source

If the line current source is brought to the surface of the conducting homogeneous half-space, where h=0, integrating E_x from Section 3.2.2 for y=0 to get the horizontal electric field immediately below the current source yields [36]

$$E_x(y=0,z)=\frac{\tau_1 I}{\pi}\frac{1}{\delta_1^2}\left\{\left[(1+i)\frac{1}{\left(\frac{z}{\delta_1}\right)}+\frac{1}{\left(\frac{z}{\delta_1}\right)^2}\right]e^{-(1+i)\frac{z}{\delta_1}}-i2K_0\left[(1+i)\frac{z}{\delta_1}\right]-(1+i)\frac{1}{\left(\frac{z}{\delta_1}\right)}K_1\left[(1+i)\frac{z}{\delta_1}\right]\right\}$$

where K_0 and K_1 are modified Bessel functions. Note that we are now using positive z in the downward direction in the formula. A plot of the electric field at z = 100 m depth for resistivities of 10, 100, and 1000 Ω-m are shown in Figure 3-12 and Figure 3-13.

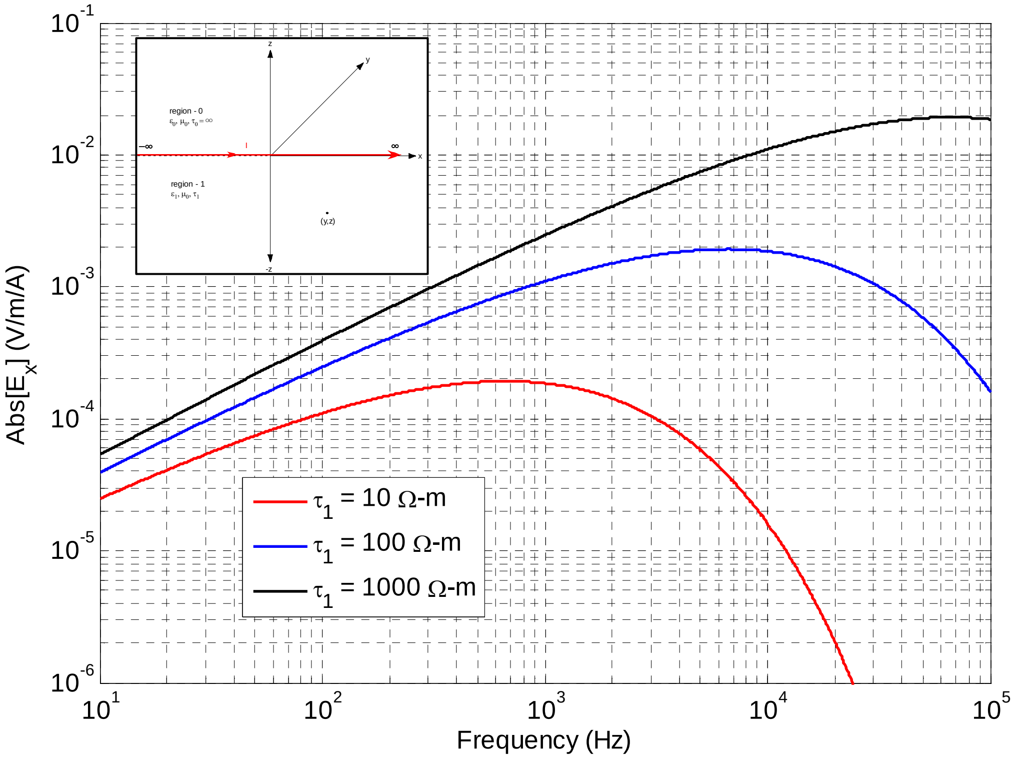

Figure 3-12 Amplitude of electric field as a function of frequency at depth of 100m with resistivities of 10, 100, and 1000 Ω-m.

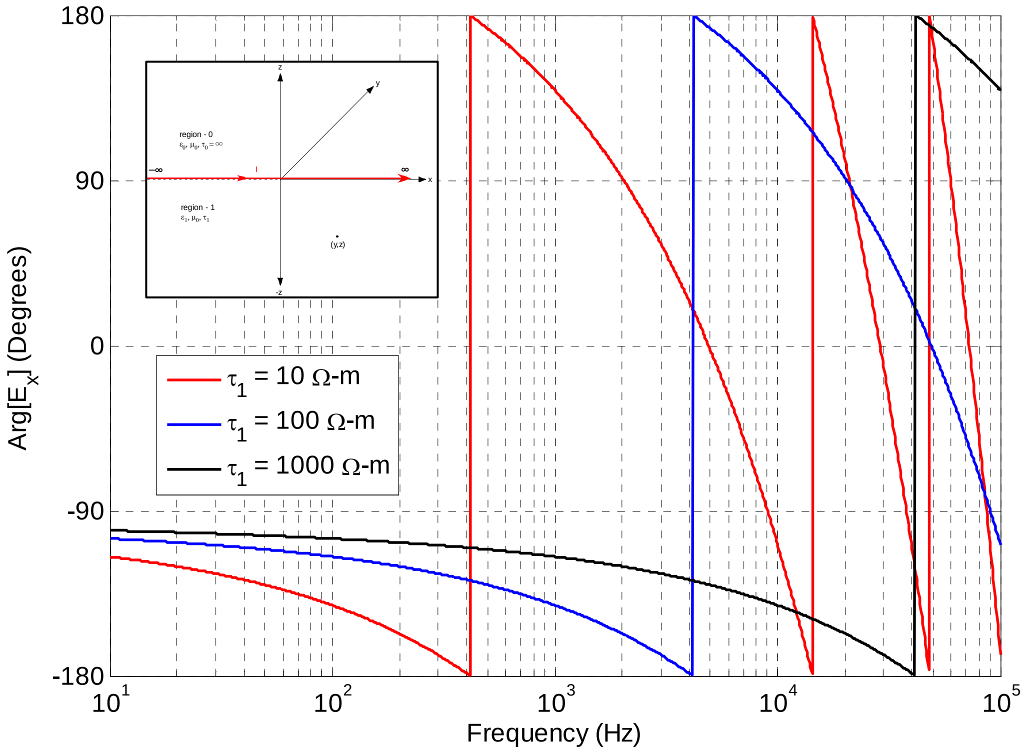

Figure 3-13 Phase of electric field as a function of frequency at depth of 100m with resistivities of 10, 100, and 1000 Ω-m.

3.2.3.2 Finite Line Source

The time-harmonic fields underground due to a finite line current have been studied by Hill and Wait [37].

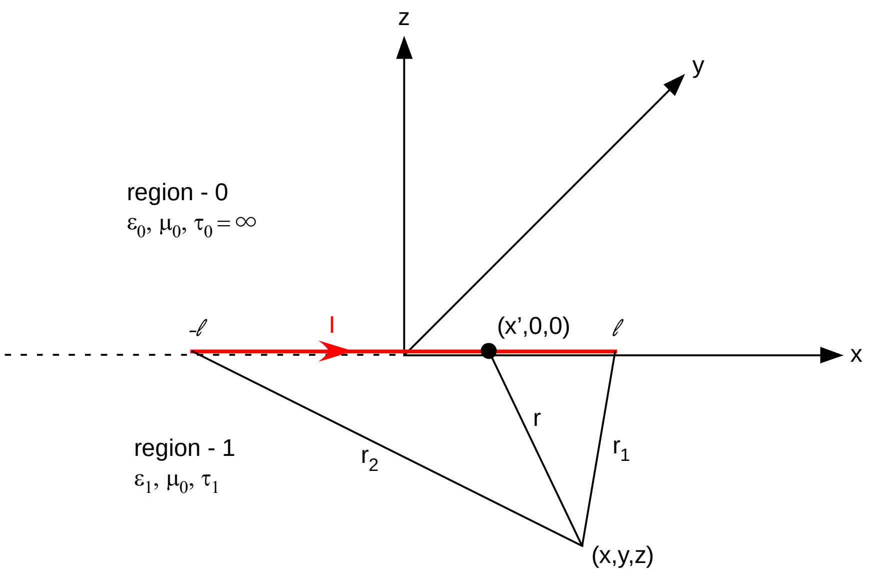

Figure 3-14 Finite length, harmonically time varying horizontal current drive at interface of a conductive half-space.

Again, displacement currents are neglected due to the low frequency of interest. The field components calculated are as follows:

$$E_x\left(x,y,z\right)=\frac{-I}{2\pi\sigma}\int_{-l}^{l}\left(A+B\right)dx',$$

$$A=\frac{\exp(-\gamma r)}{r^3}\left[\left(\frac{3z^2}{r^2}-1\right)+\gamma r\left(\frac{3z^2}{r^2}-1\right)+\gamma^2 z^2\right]$$

$$B=\frac{\gamma}{2}\left[\begin{array}{l}\frac{\gamma z}{r^2}\left(1-\frac{3y^2}{r^2}\right)I_0K_0+\frac{\gamma z}{r^2}\left(-1+\frac{3y^2}{r^2}+\frac{2y^2}{r^2-z^2}\right)I_1K_1\\+\frac{1}{r^2}\left(-1+\frac{3y^2}{r^2}+\frac{z\left(1-\gamma^2y^2\right)}{r}-\frac{3zy^2}{r^3}\right)I_0K_1+\frac{1}{r^2}\left(-1+\frac{3y^2}{r^2}-\frac{z\left(1-\gamma^2y^2\right)}{r}+\frac{3zy^2}{r^3}\right)I_1K_0\end{array}\right]$$

The argument of I_0 and I_1 is $\frac{\gamma\left(r+z\right)}{2}$ and the argument of K_0 and K_1 is $\frac{\gamma\left(r-z\right)}{2}$.

Numerically integrating E_x for a depth of 100 m and a conductor length of 500 m (the same depth and length as the measurement setup) results in Figure 3-15 and Figure 3-16. The inclusion of the finite length of the conductor is clearly seen with the asymptotic behavior to a DC constant value, instead of the decreasing value with decreasing frequency seen with the infinite wire model.

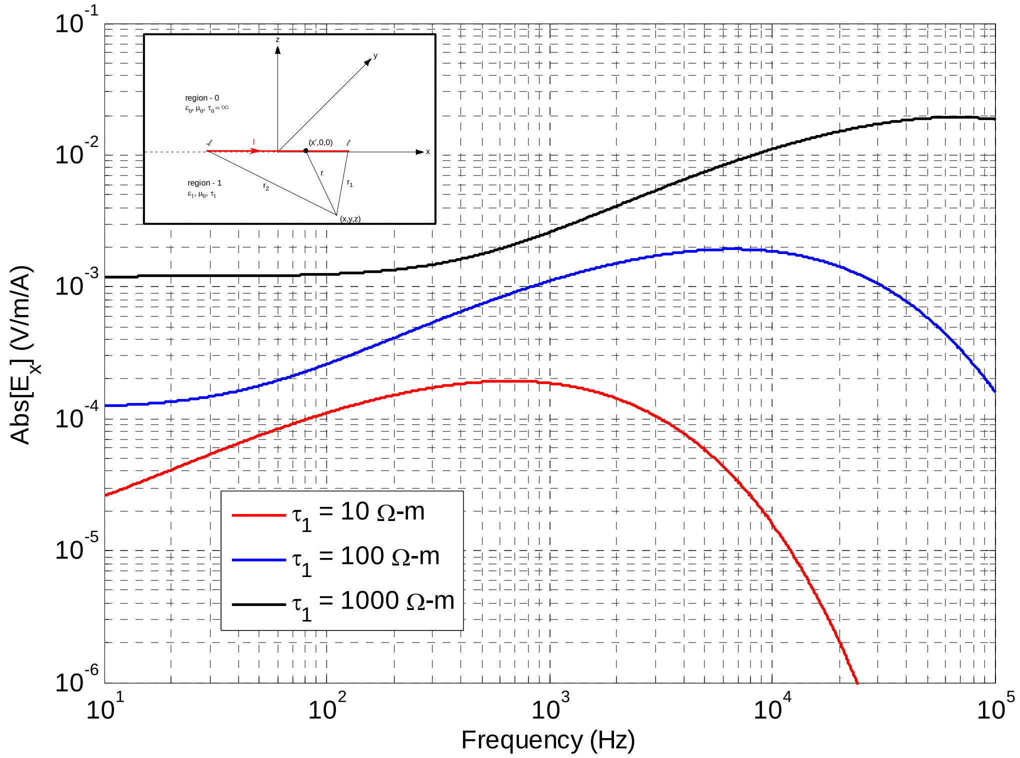

Figure 3-15 Amplitude of electric field as a function of frequency at depth of 100 m with resistivities of 10, 100, and 1000 Ω-m.

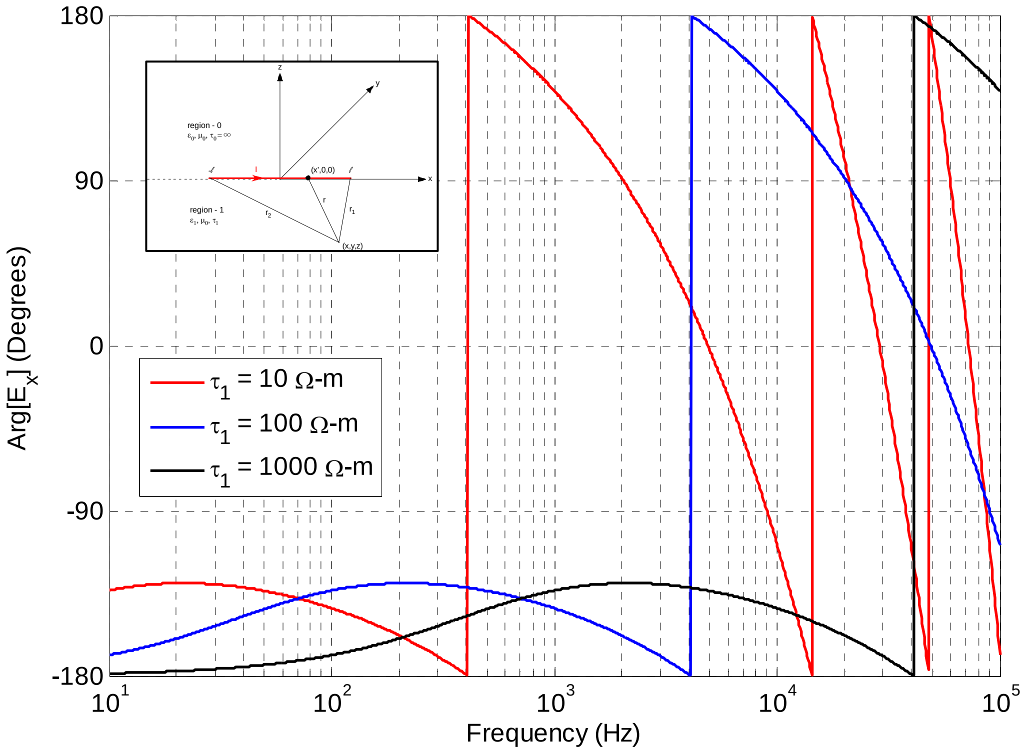

Figure 3-16 Phase of electric field as a function of frequency at depth of 100 m with resistivities of 10, 100, and 1000 Ω-m.

3.2.3.3 Numerical Modeling in EIGER

The geometry of Figure 3-14 was modeled numerically and run on the open source EIGER (Electromagnetic Interactions GenERalized) code suite. The Eiger code suite consists of four types of codes: a geometry translator (I2j); a pre-processor (Jungfrau); a physics code (Eiger); and a post-processor (Moench). The geometry translator takes a universal mesh file created from a commercial software package and converts it to a standard ascii input file (*.jfg) that is used in the pre-processor. Jungfrau is used to input all the relevant physical parameters and constraints of the problem into a form that can be read by Eiger. The some of the physical parameters include the mesh file, frequency(ies) to be solved, definition of layered media (position, size, complex permittivity, and complex permeability), and definition of excitations. Eiger, the physics code, is used to solve for the electric and magnetic currents on boundary elements when the excitations are time-harmonic. Eiger solves for the currents using the method of moments (MOM). The method of moments is a procedure for solving a linear operator equation ($L(f) = g$) by transforming it into a system of simultaneous linear equations (or a matrix equation). The description of the method of moments was originally presented by Harrington [38,39].

The basic method of moments procedure is:

1. Get the integral equation
   a. Use equivalence theorems to replace all matter by free space and equivalent currents.
   b. Integral equation is an expression of boundary conditions or equivalence theorems.
2. Solve the integral equations by MOM
   a. Expand equivalent current ($\mathbf{J} = \sum_{n=1}^{N} I_n \mathbf{J}_n$) to create matrix equation
   b. Enforce N weighted averages of integral equations ($[L]A = G$)
   c. Solve the matrix equation so that $A = [L]^{-1} G$ (usually solved by a LU decomposition)

Once Eiger solves for the principal unknowns, Moench calculates the secondary quantities. Examples of secondary quantities are the electric and magnetic fields (both near and far fields) in the regions surrounding the surfaces of the problem. The reason that secondary quantities are important is that the principal unknowns are difficult to measure, so experiments usually measure the secondary quantities. Moench reuses much of the software from Eiger. The near fields are calculated using a pseudo-MOM where the fields are calculated at a point (fictious element) from the potentials on the wire.

For the simulations presented in this dissertation, the physics code (Eiger) was not actually used. The currents on the wire were specified, so there were no unknown currents to be solved for. The output file from Eiger (a *.mnh file) was created manually for each geometry and case studied. The needed files were then input into Moench for the near field calculation from the wire drive. Example input and output files are contained in Appendix C.

The three models (analytic infinite wire, analytic 500m wire, and numerical 500m wire) are compared in Figure 3-17. All three curves are the x-component of the electric field directly below the center of the drive wire, at position (0, 0, -100). A ground resistivity of 80 Ω-m was chosen as representative of the measurement site.

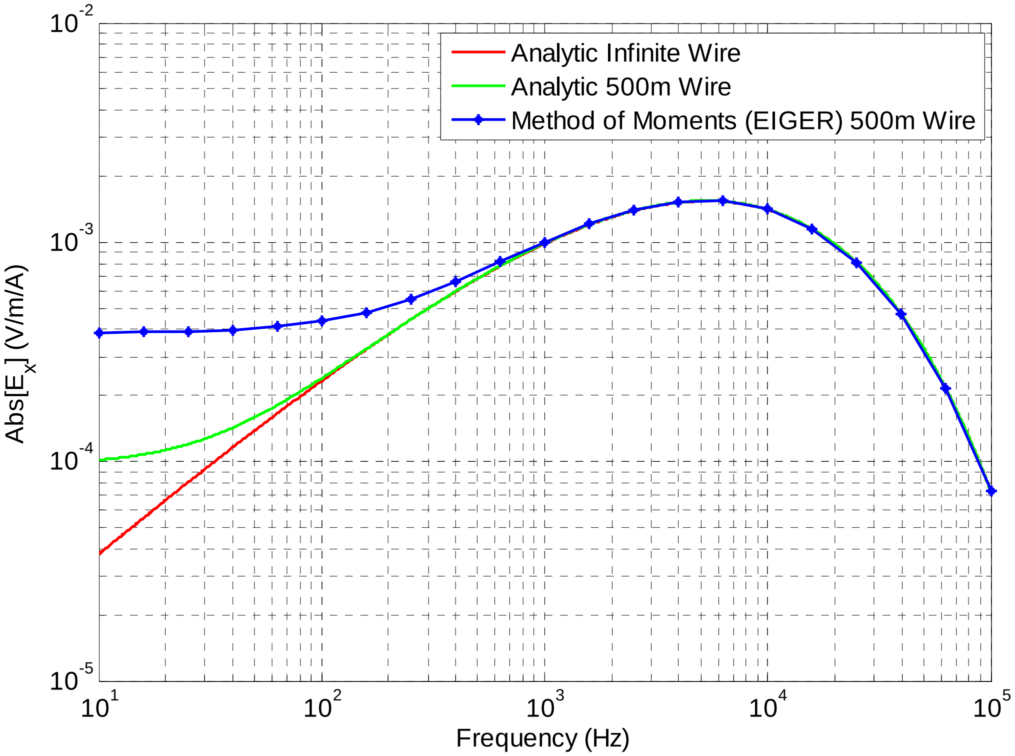

Figure 3-17 Comparison of the amplitude of E_x from a computational finite wire model with analytic finite and infinite wire models, using τ_1 = 80 Ω-m and z = -100 m.

It is unrealistic to think that there would be a constant current along the entire length of the 500m long wire. The resulting amplitude of the x component of the electric field from a finite length wire with a triangular and a sinusoidal current distribution are plotted in Figure 3-18 with the constant current drive. Note that the amplitude at the low end of the frequency spectrum is enhanced with the non-constant current distribution; these values approach the measured fields more closely than the constant drive.

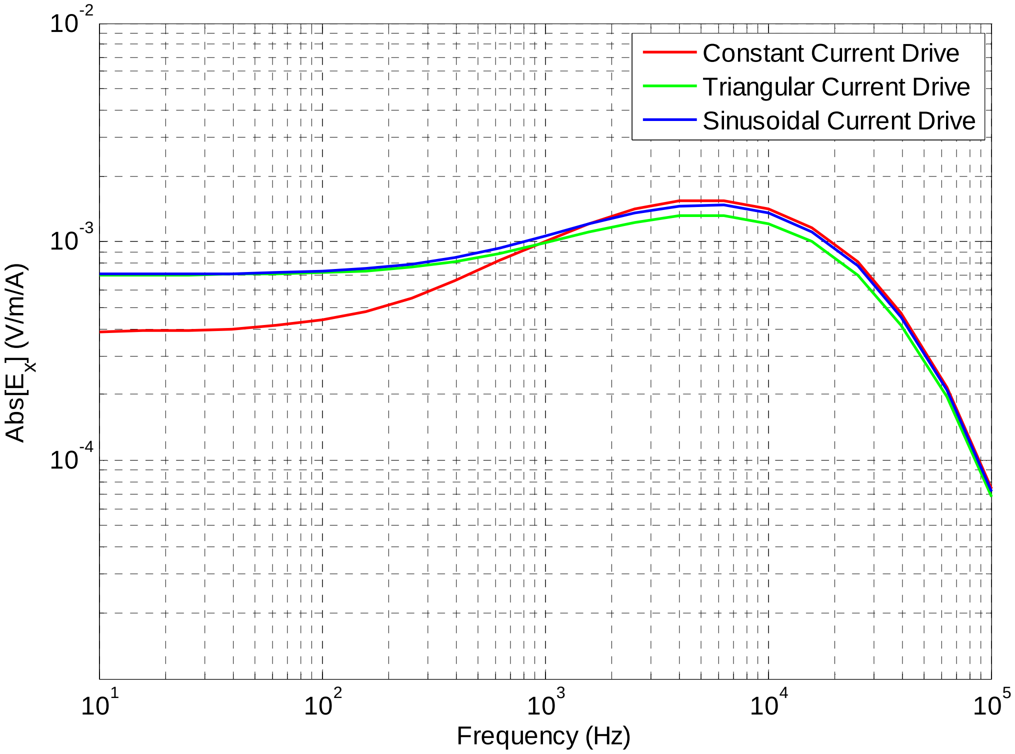

Figure 3-18 Comparison of the amplitude of E_x from a constant, triangular, and sinusoidal current distribution in a computational finite wire model, using τ_1 = 80 Ω-m and z = -100m.

3.2.4 Line Source at Surface of Stratified Half-Space

Two models are compared for a line source at the surface of a stratified (or layered) half-space.

3.2.4.1 Infinite Line Source

The geometry for the infinite current source at the surface of a stratified conductive half-space is shown in Figure 3-19. The situation is the same as in Section 3.2.3.1, except the half-space has a finite layer of conductive media with $\tau_1 \neq \tau_2$.

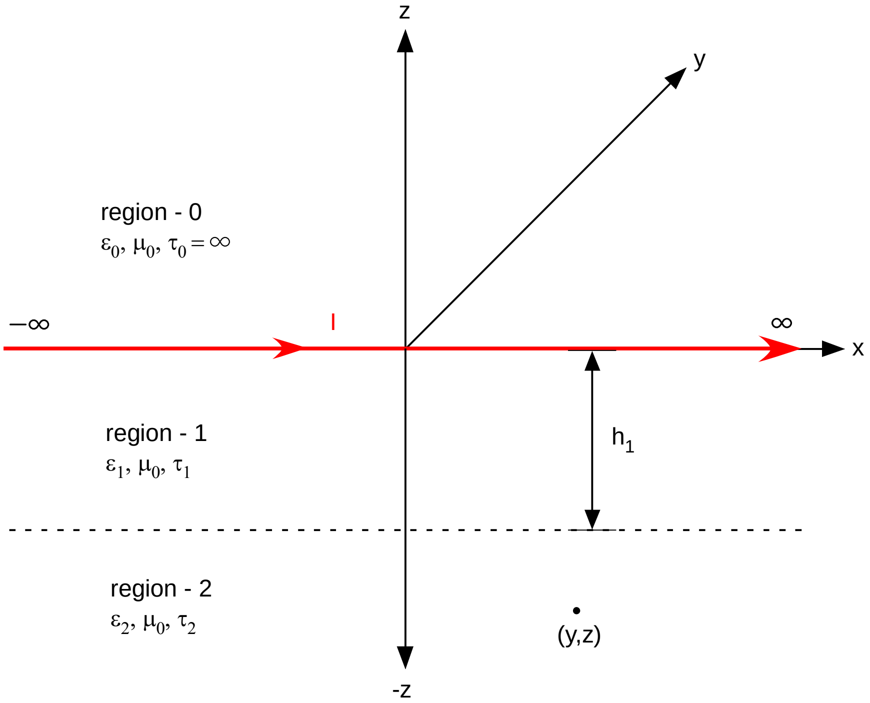

Figure 3-19 Infinite length, harmonically time varying horizontal current drive at surface of a stratified conductive half-space.

Again we neglect displacement currents and relate the electric field to the current in the infinite wire, $E_x(y,z) = \tau_2 i_x(y,z)$. If we let $y = 0$, then the electric field results in [36]:

$$E_x\left(y=0,z\right) = -\frac{i4\tau_2 I}{\pi}\frac{1}{\delta_2^2}\int_0^\infty \frac{u_1 e^{u_2 h_1}}{\left(u+u_1\right)\left(u_1+u_2\right)e^{u_1 h_1}+\left(u-u_1\right)\left(u_1-u_2\right)e^{-u_1 h_1}} e^{-u_2 z}\,du$$

$$u_1 = \sqrt{u^2 + ip_1^2}$$

$$p_1^2 = \frac{\omega\mu_0}{\tau_1} = \frac{2}{\delta_1^2}$$

$$\delta_1 = \sqrt{\frac{2\tau_1}{\omega\mu_0}}$$

$$u_2 = \sqrt{u^2 + ip_2^2}$$

$$p_2^2 = \frac{\omega\mu_0}{\tau_2} = \frac{2}{\delta_2^2}$$

$$\delta_2 = \sqrt{\frac{2\tau_2}{\omega\mu_0}}$$

Equations similar to the above have been published in [31,32,35], however there are no closed form solutions to the integral equation. Carrying out the integration numerically allows us to obtain the curves for the electric field for three different cases, shown in Figure 3-20.

The first case represents a somewhat thin layer of higher conductive media over a lower conductive rock bed. This is a common type of situation for the earth in many parts of the country. The second case has a large lower conductivity layer over a higher conductive half-space. Both of these cases have a geometrical average conductivity at a depth of 100 m of ~ 80 Ω-m. The third case shows that if a layer of 80 Ω-m media is on top of an 80 Ω-m half-space, the results are identical to that of the 80 Ω-m half-space alone. The resulting electric field curves for case 1 and 2 are very similar to the 80 Ω-m half-space results. In fact at the low end of the frequency spectrum case 1 overlays case 3. There is at most a factor of 4 difference in amplitude between the cases.

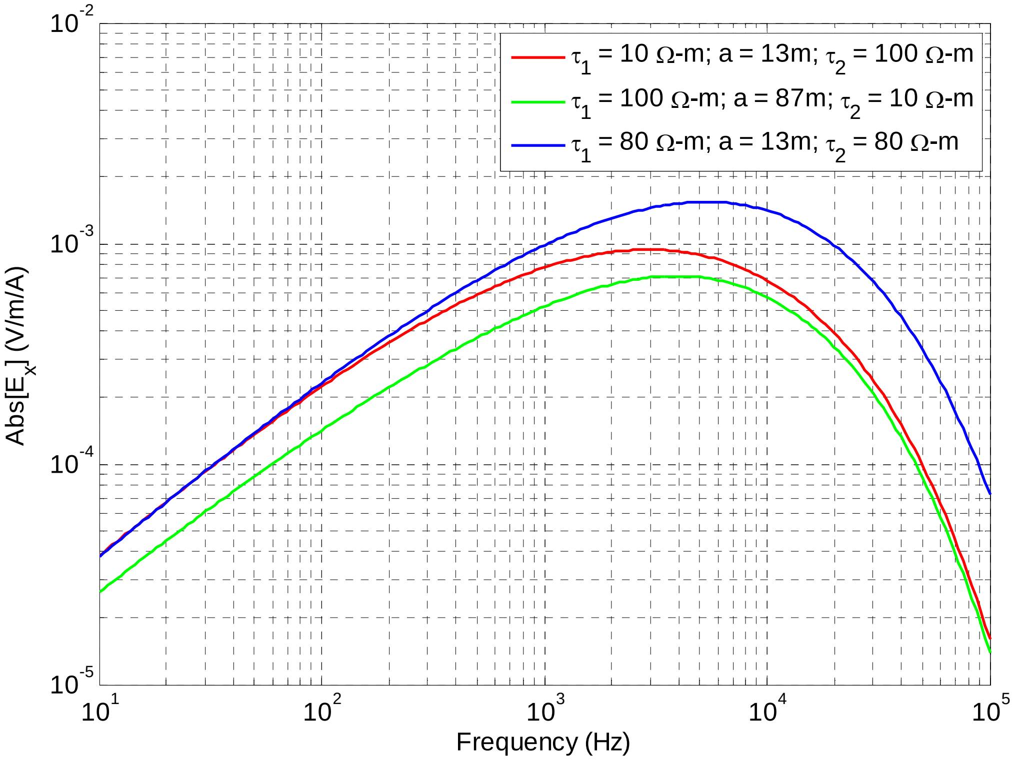

Figure 3-20 Amplitude of E_x at depth of 100 m for three configurations of two layered ground.

3.2.4.2 Numerical Models

The geometry of Figure 3-19, except a finite length wire replaced the infinite current drive, was modeled with Eiger and is compared in Figure 3-21. The numerical results are consistant with the analytical results from Figure 3-20.

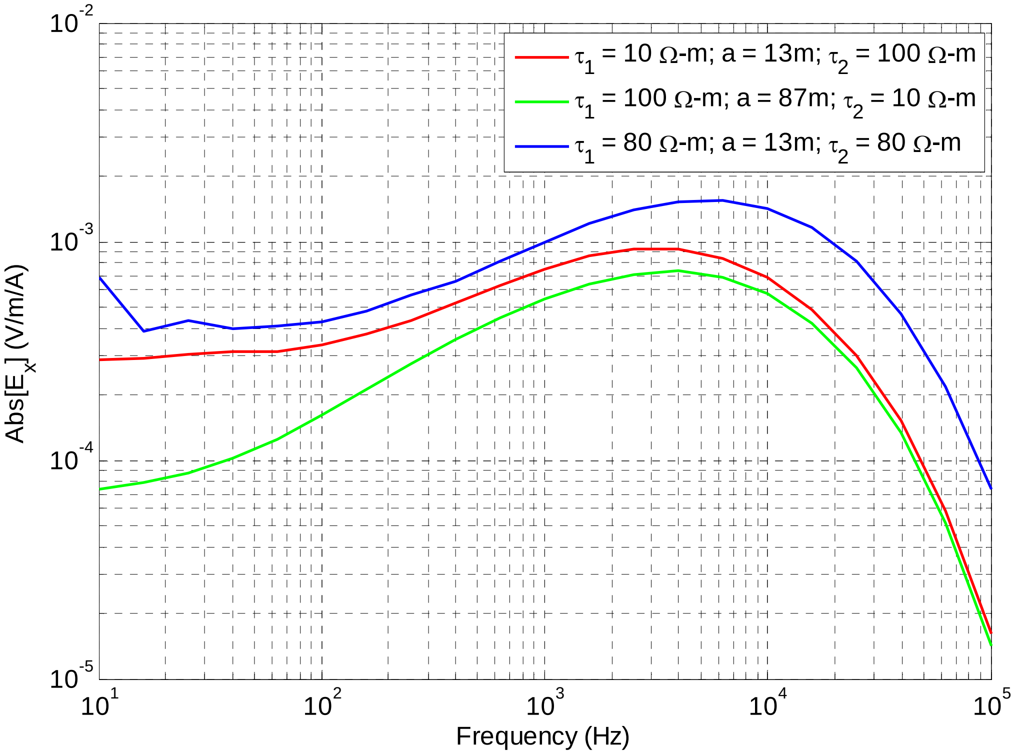

Figure 3-21 Amplitude of E_x at depth of 100 m for three configurations of two layered ground from computational model.

Several case studies were performed to analyze the necessity of using a layered earth representation. The thickness and resistivity of the layers were extracted from [11] which shows the multiple layered geometry in Figure 3-22 fits their sounding data the best. Figure 3-23 shows the resulting x-directed electric field for the multi-layered geometry and is overlaid with the two layered half-space results. A comparison with the measured data is discussed in the next section.

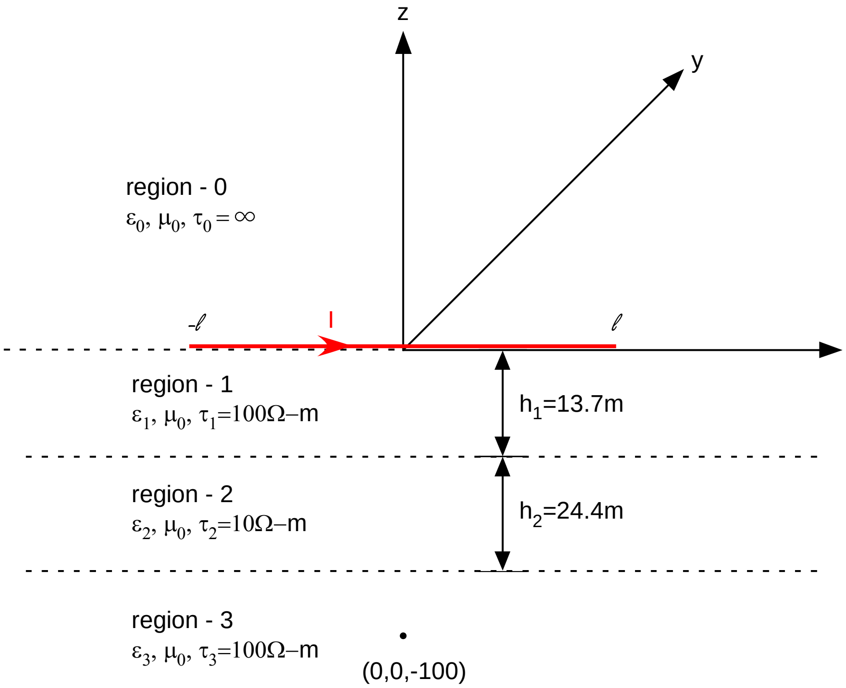

Figure 3-22 Geometry of three layered stratified media extracted from [11].

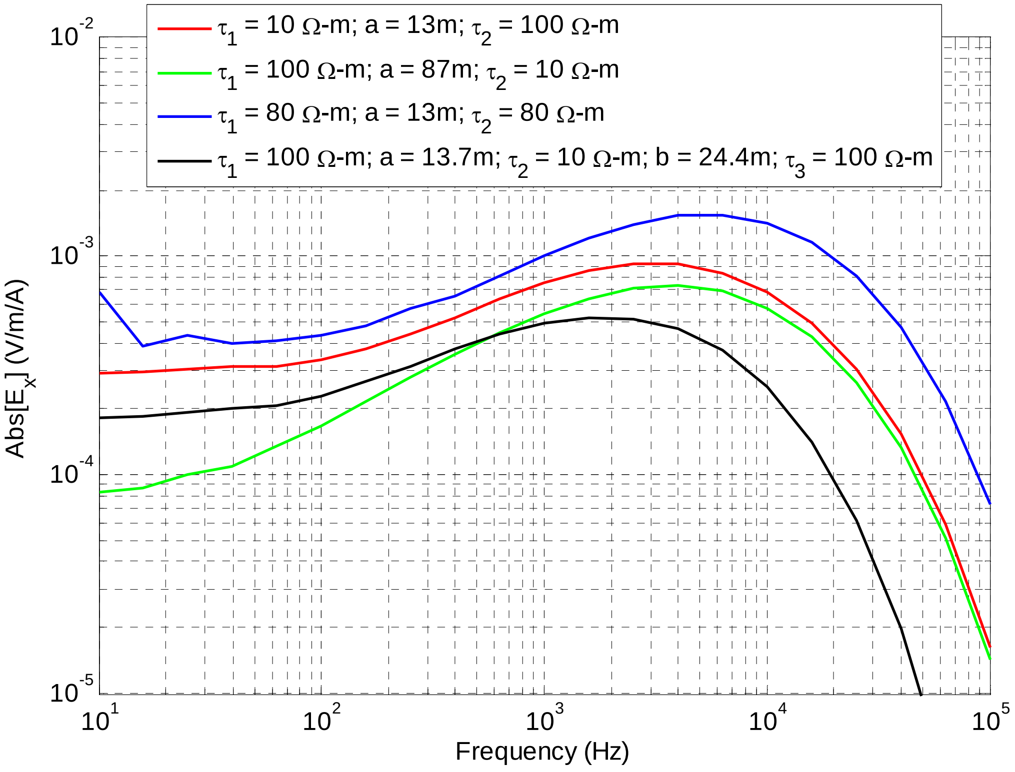

Figure 3-23 Amplitude of E_x at depth of 100 m for three configurations of two layered ground from computational model with three layered configuration from [11].

3.2.5 Models Compared with Measured Results

Models for diffusion coupling from an infinite and finite current source above a homogeneous half-space were presented in Section 3.2.3. These models are compared with the measured electric field inside the sealed area of the mine. Using an effective soil resistivity of 80 Ω-m, the analytic models plotted in Figure 3-24 match very closely the horizontal (P-directed) electric field measured with a parallel current drive. The correlation between model and measured data is extremely good from 10 to 100 kHz. This confirms that the major coupling mechanism from the surface to the sealed area is field diffusion coupling. The measured data is contaminated by 60 Hz resonances and clutter below 1 kHz for this polarization. The data deviates from the model of coupling beneath an infinite and finite line at frequencies below 1 kHz. The measured data stays at a constant level of approximately 0.0006 V/m/A (this is estimated from the cable voltage measurements shown in Chapter 2), whereas the analytical models predict a downward slope. Much of this deviation can be attributed to the field caused by the DC component from the finite spacing of the ground rods. A comparison of the average of the P-directed electric field measurements from P2 to P8 with the analytic and computational models are shown in Figure 3-25. The average field is a more meaningful value to compare since it has local variations removed. The amplitude and shape show amazing correlation between the measured data and the single layered computational model (with sinusoidal current distribution). The three layered computational model with values extracted from [11] did not perform well. This shows that for the frequencies of interest it is better to take the geometric average of the stratified media (~80 Ω-m), than each layer individually.

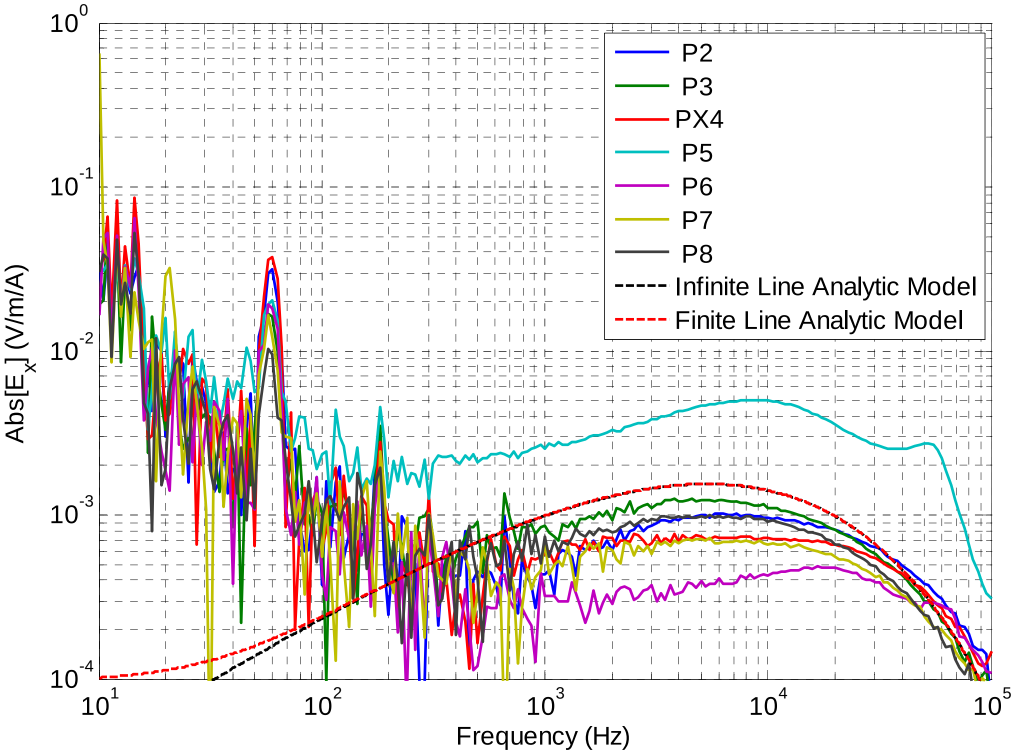

Figure 3-24 P-directed electric fields compared with the analytic models with an effective resistivity of 80 Ω-m.

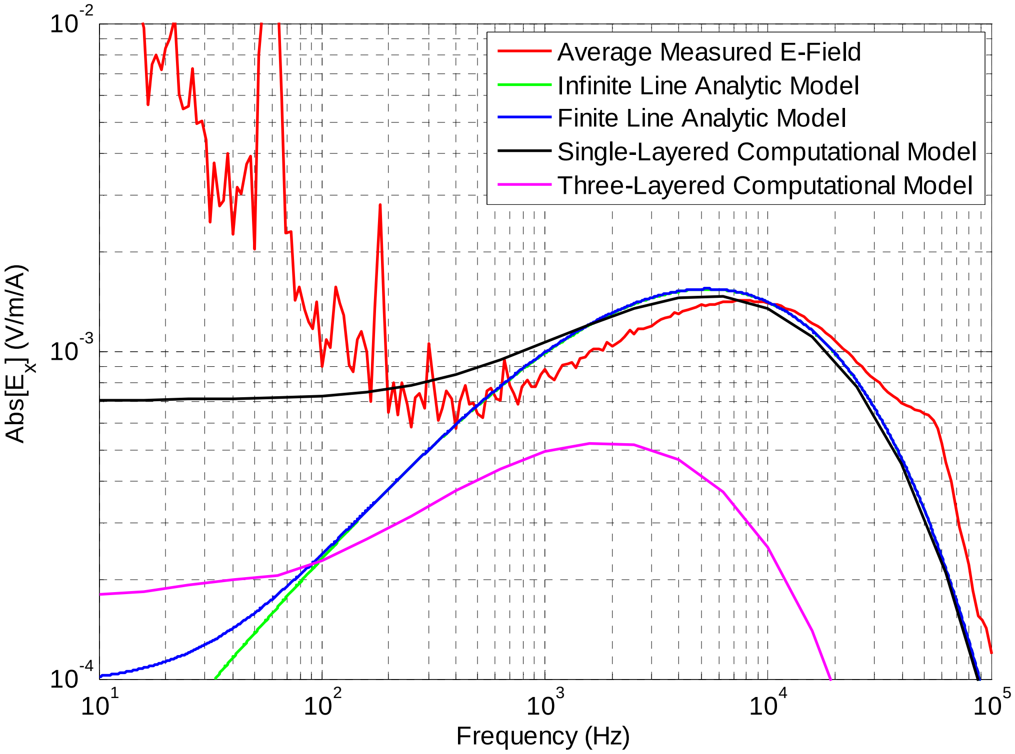

Figure 3-25 Average of P-directed fields from P2 to P8 compared with various models.

3.3 Fields coupling to multi-conductor cable model

A comparison of the induced voltage on the pump cable and coupling models are now presented. The extreme low frequency allows for simple coupling models to be sufficient. Three models will be presented: A simple model of multiplying the length of the cable by the x-directed electric field at the center of the driving antenna; A model of multiplying the average electric field over the length of the receiving antenna by the effective height for an antenna of a given length; and a model using transmission line theory to couple the spatially varying electric field to the wire.

3.3.1 Simple Model

The simplest model for electric fields coupling to wires is multiplying the length of the wire by the x-directed field at the center of the driving antenna. If we let the center of the driving antenna to be at the origin and the receiving antenna to be a distance z away, then $V(0,0,z) = LE_x(0,0,z)$, where L is the length of the receiving wire.

3.3.2 Effective Height Model

An improvement over the previous model is to treat the receiving wire as an antenna and calculate the effective height (or effective length), then multiply it by the average x-directed incident electric field over its length. The effective height is defined as

$$h_{eff} = \frac{V_{oc}}{E_{inc}}$$

Then the far-zone field E_a radiated by an antenna with current I_g in the terminals is [40]

$$E_a = -j\eta_0 \frac{k_0 I_g}{4\pi r} h_{eff} e^{-jk_0 r}$$

So by calculating the far-field of the receiving antenna from a test voltage, V_g, the effective height can be calculated. From Balanis [40]

$$I_g = \frac{V_g}{(R_r + R_L + R_g) + j(X_A + X_g)}$$

Assuming that the $Z_g = R_g + X_g = 50\Omega$, the antenna reactance X_A is negligible compared with the radiation resistance, R_r, and

$$R_L = \frac{1}{2}\frac{L}{2\pi b}\sqrt{\frac{\omega\mu_0}{2\sigma}}$$

For a long wire antenna [41]

$$R_r = 60\left(1.415 + \ln\left(\frac{kL}{\pi}\right) - C_i(2kL) + \frac{\sin(2kL)}{2kL}\right)$$

and

$$E_\theta = \frac{-j\eta_0 I_g \sin\theta \; e^{-jk_0 r} e^{-jk_0 (Lu/2)} \sin\left(\frac{kLu}{2}\right)}{2\pi r u}$$

where $u = 1 - \cos\theta$.

The open circuit voltage of the receiving antenna is then

$$V_{oc} = E_{inc} h_{eff} = E_{inc} \left. \frac{4\pi r E_\theta}{-j\eta_0 k_0 I_g e^{-jk_0 r}} \right|_{\theta=\pi/2}$$

3.3.3 Transmission Line Field Coupling Model

Using transmission line theory and treating the incident electric field as a distributed source has been used in previous areas by Vance and Warne and Chen [42,43]. Using a transmission line formulation for coupling at extremely low frequencies is acceptable due to the extreme thinness of the receiving antenna (pump cable). If we consider the receiving wire in the mine as a wire over a lossy earth ground, where the radius of the wire is *a* and the wire is a distance *d* above the ground. Then if we let

$$k = \sqrt{-ZY} \text{ and } Z_c = \sqrt{\frac{Z}{Y}}$$

For the admittance we use the usual formulation of a wire over a perfect ground for the capacitance, such that

$$Y = i\omega C = \frac{-i\omega 2\pi\varepsilon_0}{\operatorname{arccosh}\left(d/a\right)}$$

For the impedance the perturbation due to the non-perfect ground is included using Sunde's [30,44] formulation

$Z = Z_1 + Z_2$, where Z_1 is the formulation of a wire over a perfect ground and Z_2 is the correction term

$$Z_1 = \frac{-i\omega\mu_0 \operatorname{arccosh}\left(d/a\right)}{2\pi}$$

$$Z_2 = \frac{-i\omega\mu_0\Delta}{2\pi}$$

where $\Delta = \ln\left(\frac{1-idk_d}{-idk_d}\right)$ and $k_d = \sqrt{\omega\mu_0\left(i\sigma_d + \omega\varepsilon_d\right)}$.

Then, the transmission line equations start as

$$\frac{dV}{dx} = -ZI + E_x^{inc}$$

$$\frac{dI}{dx} = -YV$$

Combining the equations by differentiating (second equation), yields

$$\left(\frac{d^2}{dx^2} + k^2\right) I = -YE_x^{inc}$$

If we let E_x be a constant then solving the second order differential equation, yields

$$I(x) = \frac{-E_x^{inc}}{Z}\left(\tan(kL)\sin(kx) + \cos(kx) - 1\right)$$

And at x = 0 (where the measurements were made)

$$V(0) = \frac{kE_x^{inc}}{YZ}\tan(kL)$$

If E_x is allowed to be a function of x, then using the method of variation of parameters, we find

$$I(x) = \left(C_1 + P(x)\right)e^{-kx} + \left(C_2 + Q(x)\right)e^{kx}$$

where

$$P(x) = \frac{1}{2Z_c}\int_{x_1}^{x} e^{kv} E_x^{inc}(v)\,dv$$

$$Q(x) = \frac{1}{2Z_c}\int_{x}^{x_2} e^{-kv} E_x^{inc}(v)\,dv$$

$$C_1 = \rho_1 e^{kx_1}\,\frac{\rho_2 P(x_2)e^{-kx_2} - Q(x_1)e^{kx_2}}{e^{k(x_2-x_1)} - \rho_1\rho_2 e^{-k(x_2-x_1)}}$$

$$C_2 = \rho_2 e^{-kx_2}\,\frac{\rho_1 Q(x_1)e^{kx_1} - P(x_2)e^{-kx_1}}{e^{k(x_2-x_1)} - \rho_1\rho_2 e^{-k(x_2-x_1)}}$$

$$\rho_1 = \frac{Z(x_1) - Z_c}{Z(x_1) + Z_c} \text{ and } \rho_2 = \frac{Z(x_2) - Z_c}{Z(x_2) + Z_c}.$$

The impedance at x_1 (x = 0) is set to be 10 MΩ which is essentially an open circuit and the impedance at x_2 (x = 300m) is set to be 0, or a short circuit. These conditions lead to $P(x_1)$ and $Q(x_2)$ equal to zero, ρ_1 equal to 1 and ρ_2 equal to -1. The voltage at x_1 is

$$V(x_1) = Z_c \left(\frac{-Q(x_1)\sinh(kx_2) - P(x_2)e^{-kx_2}}{\cosh(kx_2)} - Q(x_1) \right).$$

At very low frequencies the transmission line coupling model becomes less reliable, because of the finite length of the receiver, the finite depth below ground, and the very large skin depth. The transition point between where it is more accurate to use antenna theory [45] and transmission line theory for a 300 m long wire is at ~500 Hz. The error introduced by using transmission line coupling at 10 Hz is only 10% and the error is less than 1% at 100 Hz. Therefore it was determined the error was small enough to use the transmission line coupling for the entire frequency regime, so that a single model would be utilized.

3.3.4 Measured Wire Voltage compared with models

The three models for electric field to cable voltage coupling are applied to the horizontal component of the electric field from the finite current source. The fields used are those from the computational simulations seen in Figure 3-18. Fore each current distribution, each cable coupling model is compared with the measured cable voltage from the sealed area in the Sago coal mine.

In Figure 3-26, the constant current drive electric field present at a depth of 100 m was applied to each cable coupling model. It is clear from the data that the current distribution on the wire is incorrect to be compared with the measured data. All of the modeled voltages are too high at the 6 kHz peak and over most of the frequency band. Also the shapes of the curves do not match.

In Figure 3-27, the triangular current drive electric field present at a depth of 100 m was applied to each cable coupling model. It can be seen that the most simple model does a nice job of obtaining the correct shape of the measured voltage curve, but has too high of amplitude by a factor of ~2. The effective height model and the transmission line model with constant field both track the measured voltage well from 2 kHz to 70 kHz (100 kHz for the effective height model). But the clear winner is the transmission line model that accounts for the spacially varying electric field. The shape of the curve is correct and the amplitude is just a bit low.

Finally, in Figure 3-28, the sinusoidal current drive electric field present at a depth of 100 m was applied to each cable coupling model. The same conclusion can be made as from the triangular distribution case, in terms of the models comparing with each other. Again, the transmission line model that accounts for the spacially varying electric field most closely matches the shape and amplitude of the measured cable voltage. The modeled curve overlays the measured data almost perfectly.

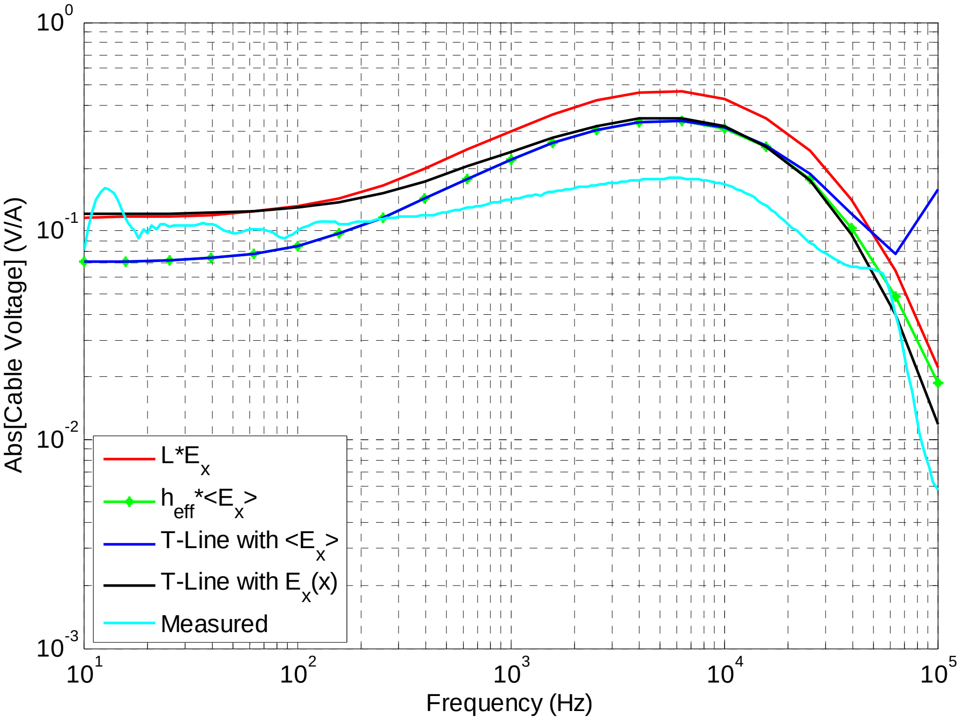

Figure 3-26 Constant current drive on wire at surface.

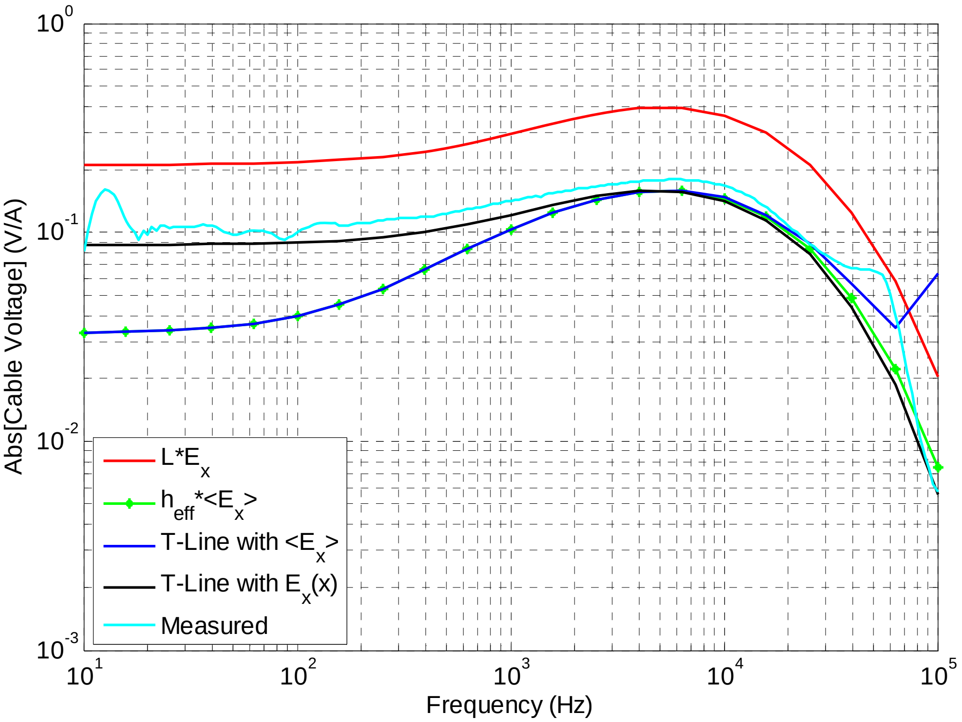

Figure 3-27 Triangular current drive on wire at surface.

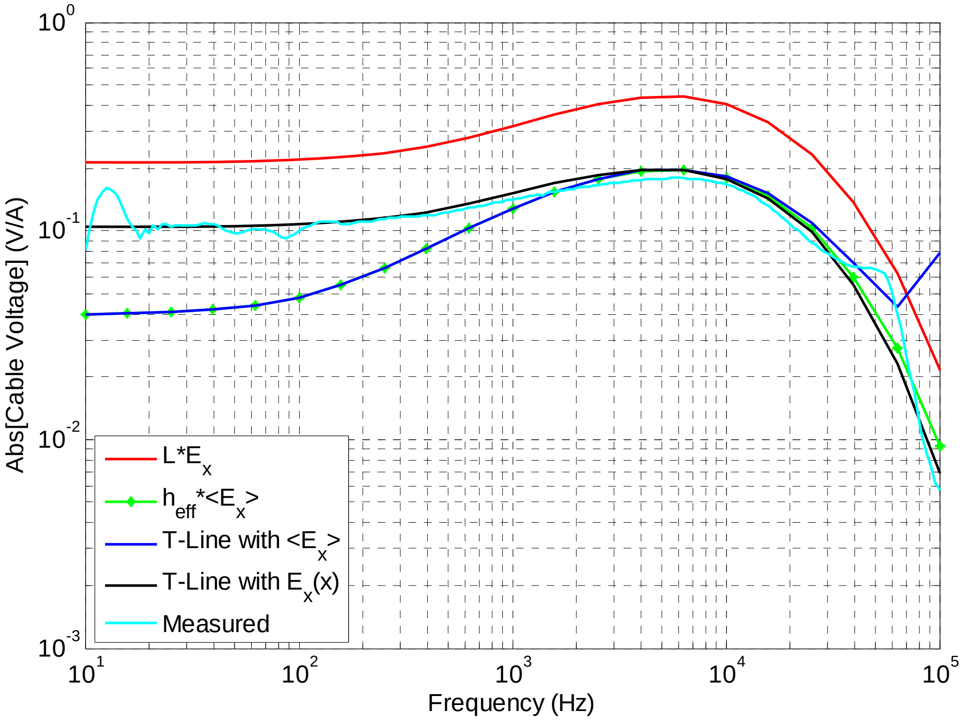

Figure 3-28 Sinusoidal current drive on wire at surface.

3.4 Vertical Buried Wire Drive

An interesting anomaly in the data was that the measured vertical electric field was the dominant component. A short computational study was made to determine the effects of current on a vertical gas well (~ 114.3 m or 375 ft away from the measurement locations in the sealed area) on the vertical electric field component. Figure 3-29 shows the x and z (vertical) components of the electric field due to a vertical current source 114.3 m away in a conductive half-space. The vertical component dominates and is on the same order of magnitude as the measured vertical electric field shown in Chapter 2. There are discrepancies between the measured waveform shape and the computational waveform. However, this was a plausibility study to help explain the presence of a large vertical electric field measured from a horizontal drive current. Actual measurements on the current induced on the gas pipes would be helpful in confirming this hypothesis.

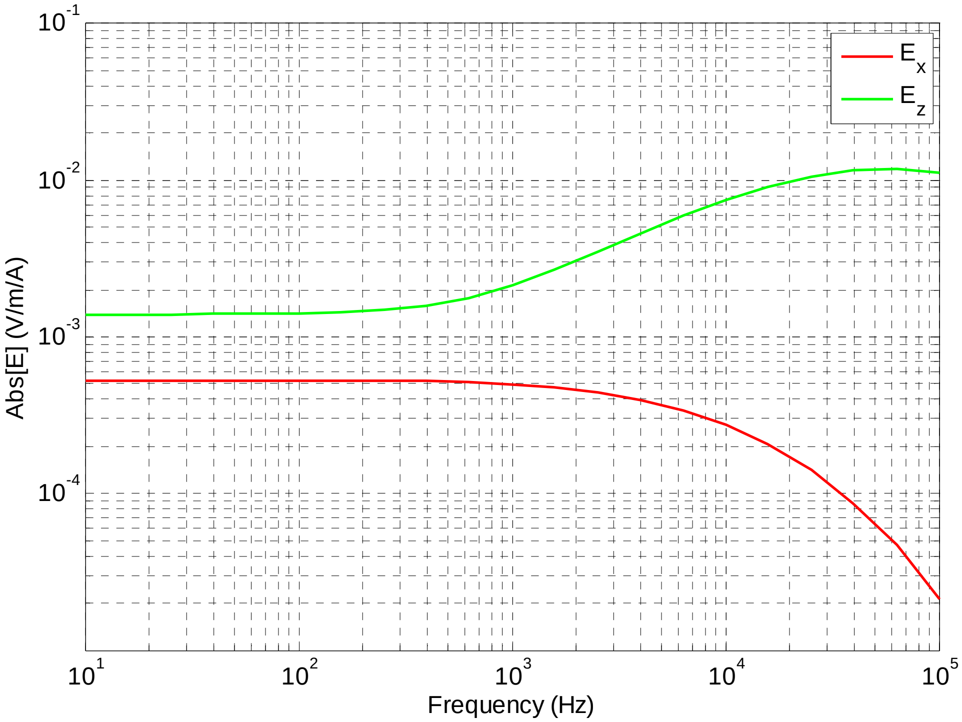

Figure 3-29 Abs of E_x and E_z due to a vertical current source 114m away in a conductive half-space.

3.5 Uniform Magnetic Field at Surface above Homogeneous Half-Space

The fields produced in the sealed area during the explosion were from natural lightning, not linear current sources, except for the case of a horizontal arc channel. In Section 1.3.2 the magnetic field from a fully developed vertical lightning stroke was shown. This magnetic field can be calculated at a distance on the surface from the stroke attachment point, but we still need to propagate the field to the sealed area below the surface. This section develops the equations that allow a uniform magnetic field to propagate into a conductive half-space and calculate the electric field in said half-space.

Assume that a uniform y-directed magnetic field of intensity, H_0, is instantaneously applied above a conducting half-space (region 1), as shown in Figure 3-30.

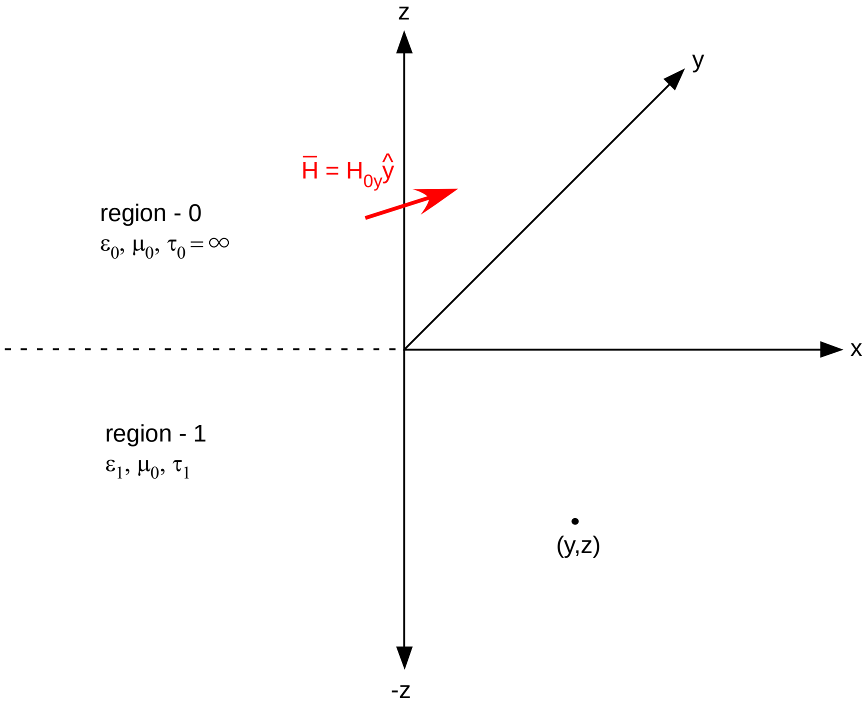

Figure 3-30 Harmonically time-varying magnetic field drive over conductive half-space.

For a good conductor [46],

$$\alpha \approx \sqrt{\frac{\omega\mu\sigma}{2}} = \frac{1}{\delta}$$

$$\beta \approx \sqrt{\frac{\omega\mu\sigma}{2}} = \frac{1}{\delta}$$

And the surface impedance is written as

$$Z_S = (1+j)\sqrt{\frac{\omega\mu_1}{2\sigma_1}}$$

Taking the normal unit vector to be in the z direction, or

$\hat{n} = \hat{z}$,

and applying the boundary condition of surface impedance, yields the tangential electric field as

$$\overline{E}_t = Z_S \overline{J}_S = Z_S(\hat{n} \times \overline{H}) = -\hat{x} Z_S H_{0y}.$$

Inserting the formula for the surface impedance and skin depth, and rearranging yields the electric field just below the surface of the interface,

$$E_{1x}(z=0^-) = -(1+j)\sqrt{\frac{\omega\mu_1}{2\sigma_1}} H_{0y} = -(1+j)\frac{1}{\sigma_1}\frac{1}{\delta_1} H_{0y} = -\tau_1 \frac{(1+j)}{\delta_1} H_{0y}.$$

However, it is more important to know the electric field below the surface at some depth, z = -d. So, for attenuation in the negative z direction

$$E_{x1}(z) = E(z=0^-)e^{(\alpha + j\beta)z}.$$

Combining the above equations yields the x component of the electric field due to a uniform magnetic field at the surface as

$$E_{x1}(z) = -\tau_1 \frac{(1+j)}{\delta_1} H_{0y} e^{(1+j)z/\delta_1}.$$

Alternatively, starting with Maxwell's equation and relating an x-directed electric field with a y-directed magnetic field, we find

$$\bar{H} = -\frac{1}{j\omega\mu}\nabla \times \bar{E} = -\hat{y}\frac{1}{j\omega\mu}\frac{\partial E_x}{\partial z}$$

Then, knowing the conduction current is related to electric field as

$$\bar{E} = \frac{1}{\sigma}\bar{J}\ .$$

Then we can rewrite the equation, relating surface current to magnetic field as

$$H_y = -\frac{1}{j\omega\mu\sigma}\frac{\partial J_x}{\partial z}\text{, or}$$

$$\frac{\partial J_x}{\partial z} = -j\omega\mu\sigma H_y\ .$$

From boundary conditions, we see that

$$\nabla \times \bar{H} = \bar{J}_i + \bar{J}_c + j\omega\bar{D}$$

If we let the impressed current (J_i) be set equal to zero and the displacement current ($j\omega D$) be neglected, then

$$\nabla \times \bar{H} = \bar{J}_c$$

Now letting H only have a y component

$$\nabla \times \bar{H} = \hat{x}\left(-\frac{\partial H_y}{\partial z}\right) + \hat{z}\left(\frac{\partial H_y}{\partial x}\right) = \bar{J}_c$$

Then putting the restriction on J_c to have only a x-directed component,

$$\frac{\partial H_y}{\partial z} = -J_{cx}$$

Differentiating the above equation and combining equations yields the second order differential equation

$$\frac{\partial^2 H_y}{\partial z^2} - k^2 H_y = 0$$

where $k = \sqrt{j\omega\mu\sigma} = (1+j)\sqrt{\frac{\omega\mu\sigma}{2}} = \frac{(1+j)}{\delta}$.

The general solution to the differential equation is

$$H_y(z) = Ae^{kz} + Be^{-kz}$$

If we want the magnetic field to decay to zero as *z* goes to negative infinity, then *B* must equal zero. Also at $z = 0$, the magnetic field is some constant value H_0.

$$H_y(z) = H_0 e^{kz}$$

Then since

$$E_x = \frac{1}{\sigma} J_{cx} = -\frac{1}{\sigma}\frac{\partial H_y}{\partial z}$$

The x component of the electric field due to the uniform magnetic field is

$$E_x(z) = -\frac{k}{\sigma} H_0 e^{kz} = -\tau \frac{(1+j)}{\delta} H_0 e^{(1+j)z/\delta},$$

the same as the previous derivation. Also note that this formulation describes the electric field due to the uniform surface current produced by a cloud-to-ground lightning stroke.

Chapter 4 Results Coupled with Lightning

The results from the direct drive measurements, and the indirect coupling measurements and analysis are coupled with recorded and hypothetical lightning strokes in this section. The analysis performed in this section uses the recorded amplitude, when appropriate; however, for all other cases, nominal amplitudes of 100 kA were used. The value of 100 kA was used for two reasons: first, there was a cloud-to-ground stroke recorded close in time and distance to the explosion area on the order of 100 kA; and second, the value of 100 kA is easy to scale. It should be noted that the voltages presented in Section 4.2 and 4.3 were calculated using the uniform magnetic field excitation formulation shown in Section 3.5. The voltages from a hypothetical long, low altitude horizontal current channel from a cloud-to-ground stroke of Section 4.4 were calculated using infinite line current source above a half-space shown in Section 3.2.2. The basic lightning waveforms used in this section as inputs into the transfer functions are shown in Figure 4-1. The negative lightning waveform was created using a double exponential formula found in [47]. There is no analytic or mathematical model for a positive lightning waveform found in published literature. Hence, a positive lightning waveform was created using a 15th order polynomial of the author's design and appending a 100 ms tail on the backend. The positive lightning waveform characteristics were tailored from values found in [48,12]. Some pertinent waveform characteristics of the modeled lightning waveforms are shown in Table 4-1.

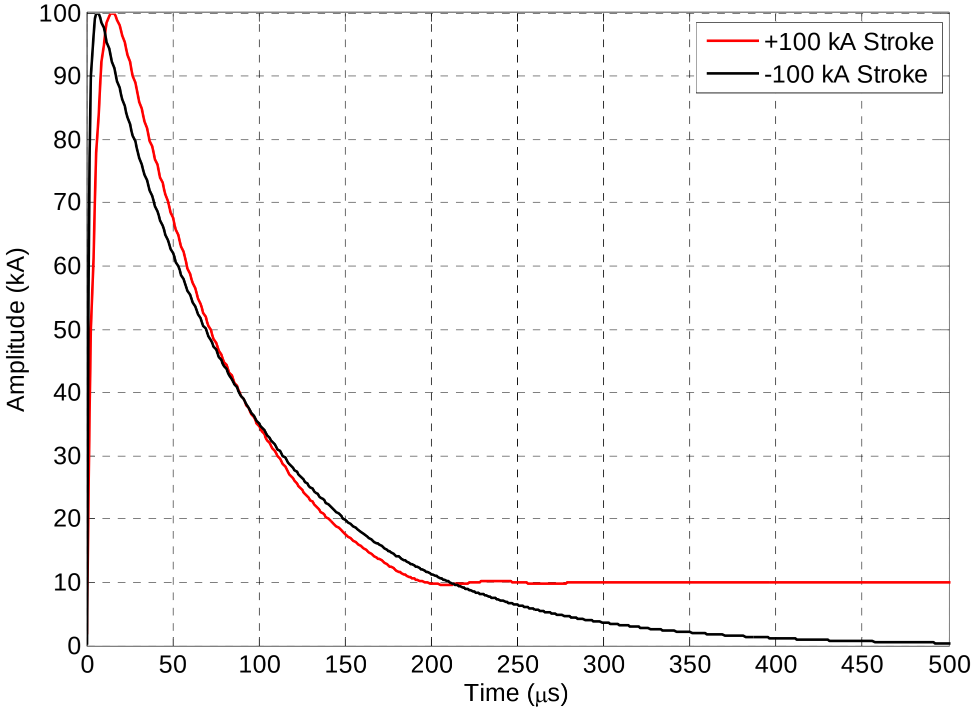

Figure 4-1 Basic positive and negative lightning waveforms used as inputs for analysis.

Table 4-1 Characteristics of positive and negative lightning waveforms used in analysis

Amplitude (kA)	Full Width at Half Maximum, FWHM (μs)	dI/dt (kA/μs)
-100	68	16.7
+100	69	6.5
+30	69	2.0

4.1 Direct Drive Transfer Functions Coupled with Lightning Strokes

If we assume that lightning directly coupled onto the conductive penetrations into the entrance of the Sago mine with either a positive or negative 100 kA stroke, then peak voltages and currents can be calculated. Only the direct drive transfer functions measured with the fence ground are used in this analysis because the fence ground is more representative of a current distribution due to a real lightning stroke.

The peak currents and voltages on the trolley communication line, conveyor, rail, and power cable shield were calculated using the following procedure. First, the lightning waveforms shown in Figure 4-1 were transformed into the frequency domain with a fast Fourier transform (FFT). Then the lightning data was multiplied by the complex transfer function of a given conductor at a given location. The resulting frequency waveform was then transformed back into the time domain with an inverse fast Fourier transform (IFFT). The peak voltage or current was recorded for each waveform. This was then repeated for each conductor at each location measured. Voltage was not measured on the trolley communication line because it was an insulated cable. The measurement locations cross-referenced to break number and approximate distance from the entrance are summarized in Table 4-2 for convenience.

Since the transfer function of the shield of the power cable was only measured out to the #3 power center, an extrapolation was performed to estimate the voltage and current at location 7 (at the 2nd Left Switch). The extrapolated values of voltage and current on the shield of the power cable are shown in the green highlighted cells of the “Power Cable Shield” columns of Table 4-3 and Table 4-5. The voltage was extrapolated using an exponential curve fit, while the current was extrapolated using a simple logarithmic curve fit. These extrapolations were matched with the trend of the first three points, and are a best-guess speculation. The peak currents and voltages from a positive 100 kA lightning stroke attached directly to the entrance of the mine for each conductor at each location are shown in Table 4-3 and Table 4-4. The peak currents and voltages due to a negative 100 kA stroke are shown in Table 4-5 and Table 4-6.

Table 4-2 Direct drive measurement locations

Location	Mine Feature	Break Number	Approximate Distance from Entrance
1	#1 Power Center	Belt 1, Break 1	30 m (98 ft.)
2	#2 Power Center	Belt 2, Break 1	459 m (1506 ft.)
3	#3 Power Center	Belt 3, Break 1	669 m (2195 ft.)
4	1st Right Spur	Belt 3, Break 16	1076 m (3530 ft.)
5	2nd Right Spur	Belt 4, Break 11	2178 m (1.35 miles)
6	1st Left Switch	Belt 4, Break 50	3255 m (2.02 miles)
7	2nd Left Switch	Belt 4, Break 59	3491 m (2.17 miles)

Table 4-3 Peak currents and voltages from a positive 100 kA lightning stroke, for conductive penetrations with old mine grounding

	Trolley Comm Line	Conveyor	Conveyor	Rail	Rail	Power Cable Shield	Power Cable Shield
Location	I_{max} (A)	I_{max} (A)	V_{max} (V)	I_{max} (A)	V_{max} (V)	I_{max} (A)	V_{max} (V)
1						6213	8369
2	162			37	643	2841	3229
3	154			17	233	2547	1582
4							
5							
6							
7						480*	1*

* Extrapolated values.

Table 4-4 Peak currents and voltages from a positive 100 kA lightning stroke, for conductive penetrations with current mine grounding

	Trolley Comm Line	Conveyor	Conveyor	Rail	Rail	Power Cable Shield	Power Cable Shield
Location	I_{max} (A)	I_{max} (A)	V_{max} (V)	I_{max} (A)	V_{max} (V)	I_{max} (A)	V_{max} (V)
1	293	2884	10931	14087	136693		
2							
3	279	495	881	9	996		
4	279	11	62	9	436		
5	220	27	11	30	1079		
6	190	11	2	42	321		
7	198	9	1	35	106		

Table 4-5 Peak currents and voltages from a negative 100 kA lightning stroke, for conductive penetrations with old mine grounding

	Trolley Comm Line	Conveyor	Conveyor	Rail	Rail	Power Cable Shield	Power Cable Shield
Location	I_{max} (A)	I_{max} (A)	V_{max} (V)	I_{max} (A)	V_{max} (V)	I_{max} (A)	V_{max} (V)
1						6193	7989
2	295			60	668	2711	3078
3	279			22	218	2417	1438
4							
5							
6							
7						280*	1*

* Extrapolated values.

Table 4-6 Peak currents and voltages from a negative 100 kA lightning stroke, for conductive penetrations with current mine grounding

	Trolley Comm Line	Conveyor	Conveyor	Rail	Rail	Power Cable Shield	Power Cable Shield
Location	I_{max} (A)	I_{max} (A)	V_{max} (V)	I_{max} (A)	V_{max} (V)	I_{max} (A)	V_{max} (V)
1	434	2926	11279	13606	143340		
2							
3	467	515	1052	13	1615		
4	417	14	77	17	934		
5	343	31	13	34	1367		
6	320	29	3	54	650		
7	301	9	1	19	62		

An item of interest is the relatively high current on the shield of the power cable (480 A) at the 2nd left switch (location 7) in Table 4-3. The power cable does not stop at the 2nd left switch, but turns approximately 90 degrees to the left and travels down the 2nd Left Main and onto the 2 Left Power Center. This presents a similar coupling mechanism as the indirect case where a long line current drive on the surface produces electromagnetic fields that propagate through earth. Only in this case, instead of the lightning currents on the surface being the drive, the induced current on the shield of the power cable inside the mine provides the drive mechanism for coupling onto the pump cable. Assuming a direct

100 kA positive stroke onto the shield of the power cable at the entrance to the mine, an analysis of this scenario results in <50 V peak induced on the pump cable, too low to be of concern.

4.2 Indirect Drive from NLDN and USPLN Positive Stroke 1-3

The locations of the three recorded lightning strokes, on the NLDN and USPLN, are shown in Figure 4-2 with the calculated distances and angles. Note that it is highly probable that the 38.8 kA and 35 kA strokes represent a single stroke with a location discrepancy, as discussed in Section 1.5. The angles shown are the angles between the line made up from the lightning stroke to the center of the pump cable, and the line formed by the direction where the pump cable lay. The first stroke analyzed is the 38.8 kA positive lightning stroke, 5.44 km (3.4 miles) away from the sealed area and an angle of 52.8 degrees. The second stroke has an amplitude of 35 kA at a distance of 4.02 km (2.5 miles) away from the sealed area and an angle of 49.3 degrees. The last stroke has an amplitude of 101 kA, a distance of 2.91 km (1.8 miles), and an angle of 85.5 degrees. The resulting induced voltage pulses on the pump cable (at the end of the cable nearest the explosion area) are shown in Figure 4-3, with peak amplitudes of 66.1 V, 87.9 V, and 42.8 V for the three strokes, respectively. The transmission line coupling models developed in Section 3.3.3 were used for coupling the electric field to voltage on the pump cable in Figure 4-3 with a cable length of 300 m (984 ft.). Since there is concern about the actual length of intact pump cable present at the time of the explosion, analysis was performed on a pump cable with a length of 61 m (200 ft.) to account for the length of the cable piece found closest to the explosion area. The resulting induced voltage pulses on the 61 m (200 ft.) length of pump cable are shown in Figure 4-4. None of the induced voltages from these recorded strokes have the necessary amplitude to cause an arc inside the sealed area. It should be noted that taking the indirect coupling model approximation out to 3 km and beyond represents an upper bound on the coupling.

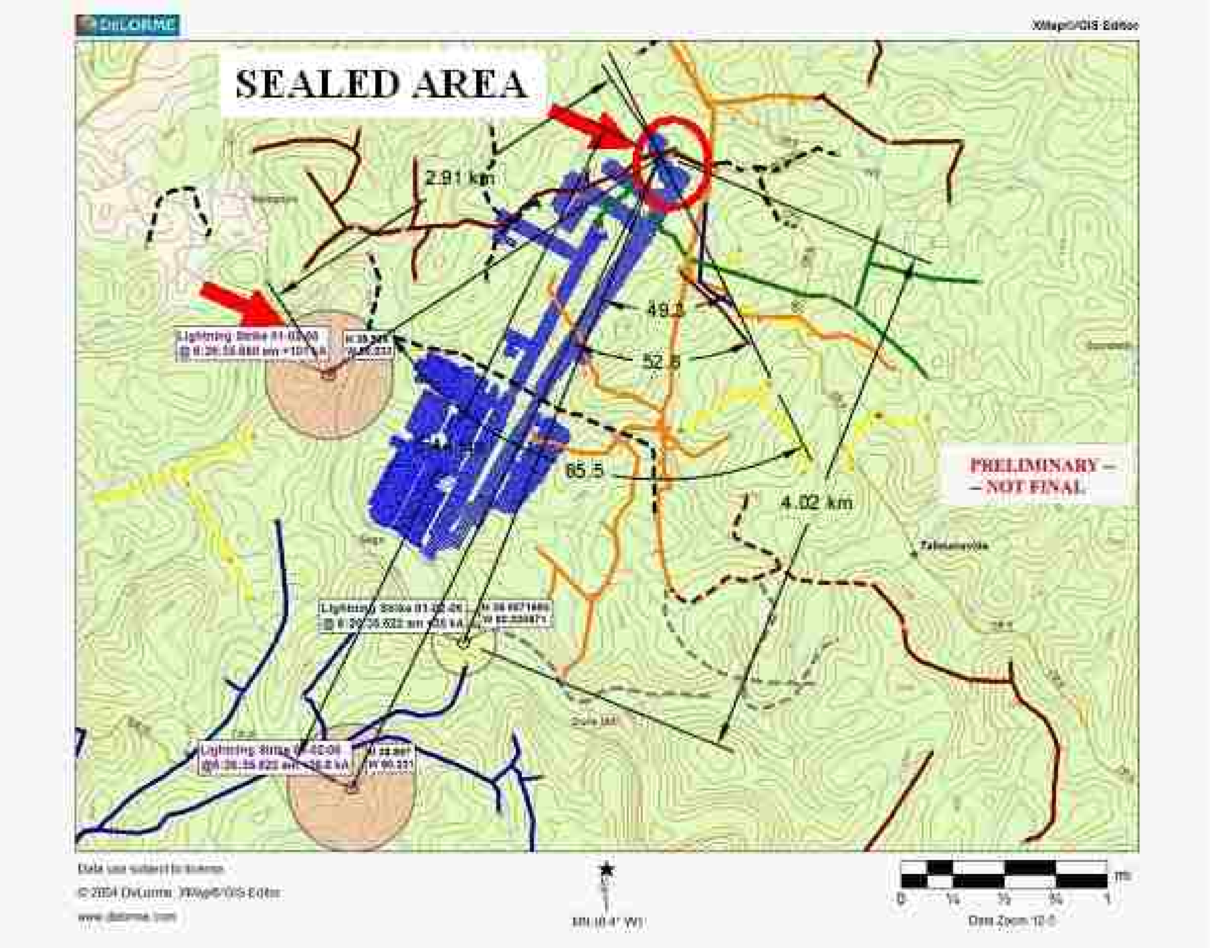

Figure 4-2 Locations of recorded lightning strokes with respect to the sealed area, with distances and angles.

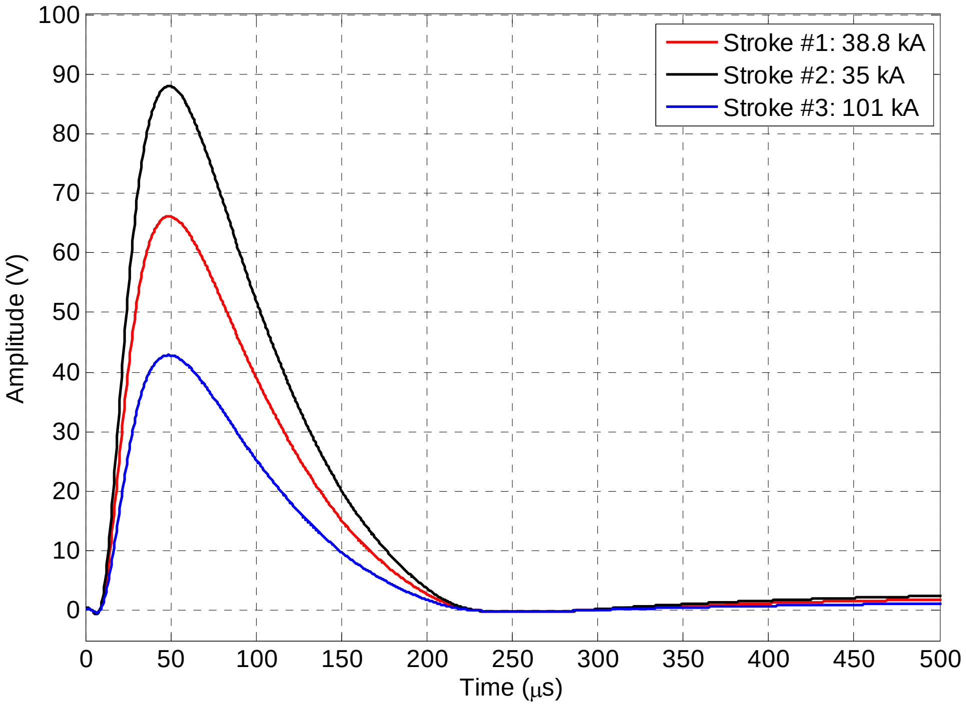

Figure 4-3 Voltage induced on pump cable (length of 300 m or 984 ft.) due to the three positive lightning strokes recorded on the NLDN and USPLN.

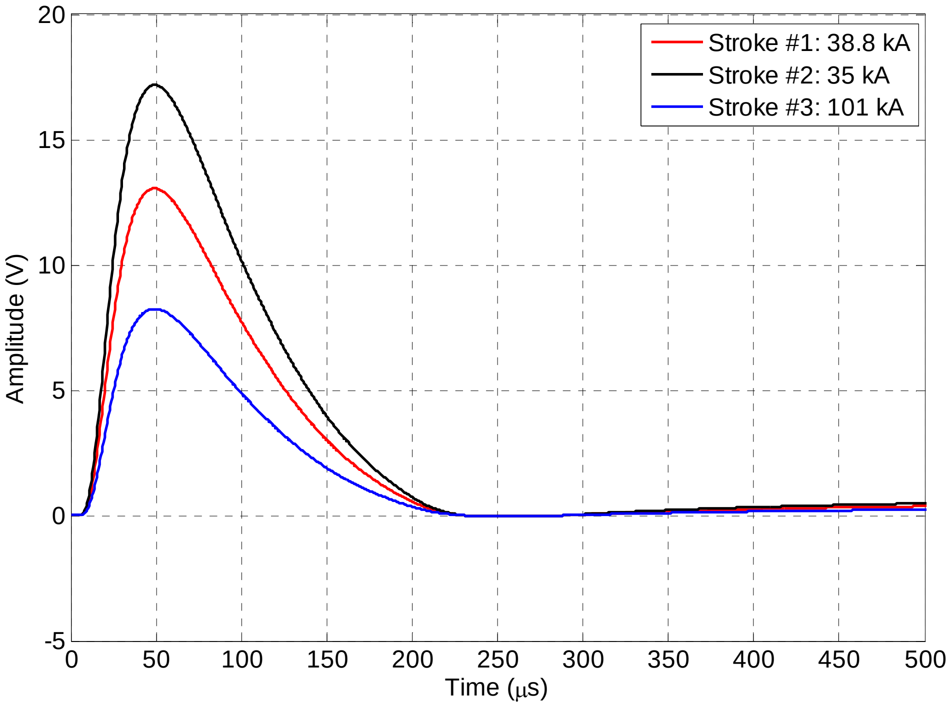

Figure 4-4 Voltage induced on pump cable (length of 61 m or 200 ft.) due to the three positive lightning strokes recorded on the NLDN and USPLN.

4.3 Indirect Drive from Hypothetical Stroke Directly over Sealed Area

If we assume a 100 kA negative or positive lightning stroke attached within 160 m (525 ft.) from directly over the center of the pump cable in the sealed area on the surface, it could induce a sufficiently high voltage in conductors in the sealed area to cause an electrical arc. This effect would be maximized if the stroke were directly inline with the pump cable direction at an angle of zero degrees. The induced voltage on the pump cable (with a length of 300 m or 984 ft.) from a 100 kA positive and negative cloud-to-ground stroke is shown in Figure 4-5. The maximum voltages are 24.9 kV from the positive pulse and 23.3 kV from the negative lightning pulse. Again, since there is concern about the actual length of intact pump cable present at the time of the explosion, analysis was performed on a pump cable with a length of 61 m (200 ft.) to account for the cable piece found closest to the explosion area. The resulting induced voltage pulses on the 61 m (200 ft.) length of pump cable are shown in Figure 4-6. The maximum voltages expected on the shorter cable length are 10.5 kV from the positive pulse and 9.8 kV from the negative lightning pulse.

Lightning currents as low as 20 kA (either positive or negative), which is closer to the statistical average peak current of cloud-to-ground lightning strokes, can produce thousands of Volts on the pump cable. This level of voltage is more than capable of initiating an electrical arc under the right conditions. The peak voltage amplitude expected on the pump cable scales linearly with the peak current amplitude of the driving lightning stroke. The results from the 100 kA case shown in Figure 4-5 can be scaled to the 20 kA case by dividing the peak amplitude of the voltage on the cable by a factor of five.

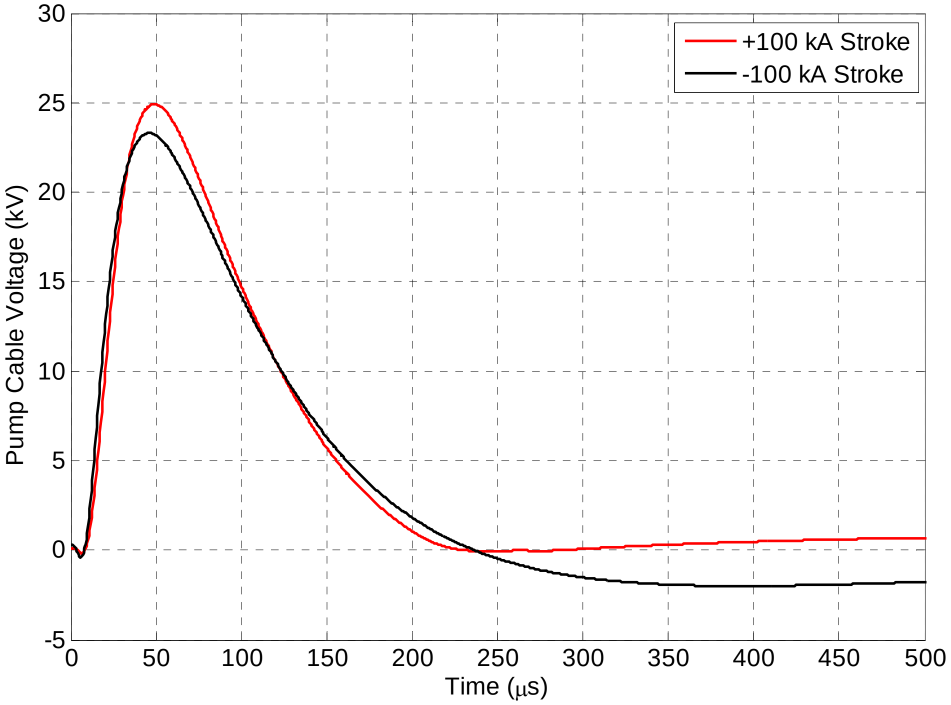

Figure 4-5 Induced voltage pulse on pump cable (length of 300 m or 984 ft.) due to a hypothetical positive and negative 100 kA cloud-to-ground lightning stroke 160 m from directly above sealed area.

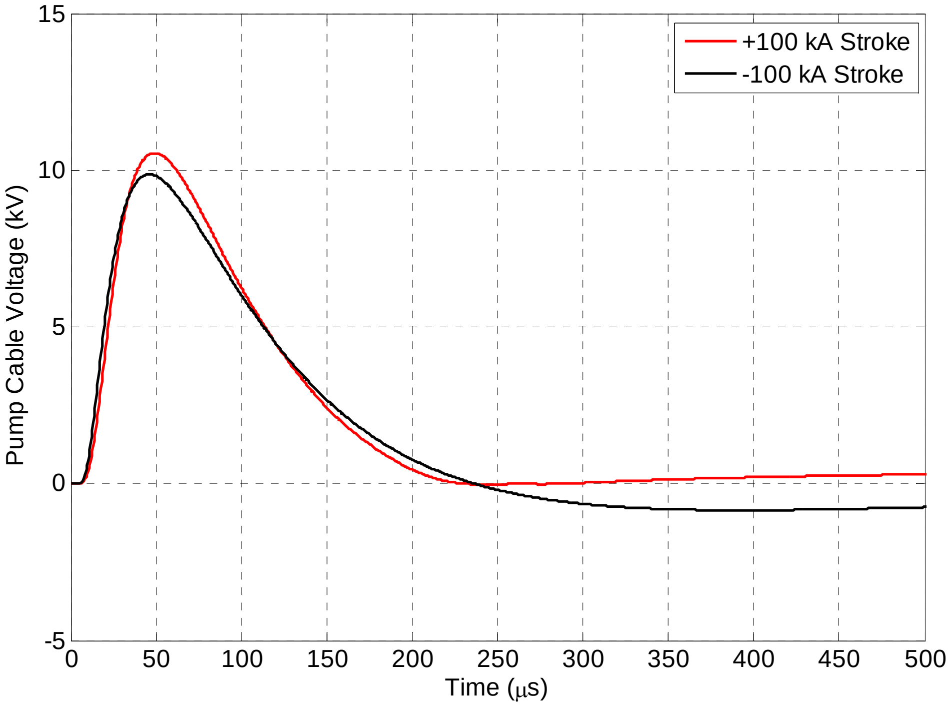

Figure 4-6 Induced voltage pulse on pump cable (length of 61 m or 200 ft.) due to a hypothetical positive and negative 100 kA cloud-to-ground lightning stroke 100 m from directly above sealed area.

4.4 Indirect Drive from a Hypothetical Cloud-to-Ground Stroke with a Current Channel over Sealed Area

If we assume a 100 kA positive cloud-to-ground stroke with a long, low altitude horizontal current channel directly over the sealed area and inline with the pump cable direction at an angle of zero degrees, it could be capable of inducing voltages on the pump cable sufficient to produce electrical arcing. Pump cable (with a length of 300 m or 984 ft.) voltages are shown for a positive cloud-to-ground stroke with horizontal current channel at heights (H) of 0 m (0 ft.), 100 m (328 ft.), 200 m (656 ft.), 500 m (1640 ft.), and 1000 m (3281 ft.) above the surface in Figure 4-7. The maximum voltages from the positive current channel at the heights given are 38.5 kV, 18.0 kV, 11.5 kV, 5.4 kV, and 2.8 kV, respectively. Induced voltages for a negative cloud-to-ground stroke with a current channel directly over the sealed area are shown in Figure 4-9. The maximum voltages from the negative current channel at the heights given are 36.3 kV, 16.9 kV, 10.8 kV, 5.1 kV, and 2.7 kV, respectively.

Again, since there is concern about the actual length of intact pump cable present at the time of the explosion, analysis was performed on a pump cable with a length of 61 m (200 ft.) to account for the cable piece found closest to the explosion area. The resulting induced voltage pulses on the 61 m (200 ft.) length of pump cable are shown for a positive cloud-to-ground stroke with horizontal current channel at heights (H) of 0 m (0 ft.), 100 m (328 ft.), 200 m (656 ft.), 500 m (1640 ft.), and 1000 m (3281 ft.) above the surface in Figure 4-8. The maximum voltages from the positive current channel at the heights given are 7.8 kV, 3.7 kV, 2.3 kV, 1.1 kV, and 0.6 kV, respectively. Induced voltages for a negative cloud-to-ground stroke with a current channel directly over the sealed area are shown in Figure 4-10. The maximum voltages from the negative current channel at the heights given are 7.3 kV, 3.4 kV, 2.2 kV, 1 kV, and 0.5 kV, respectively.

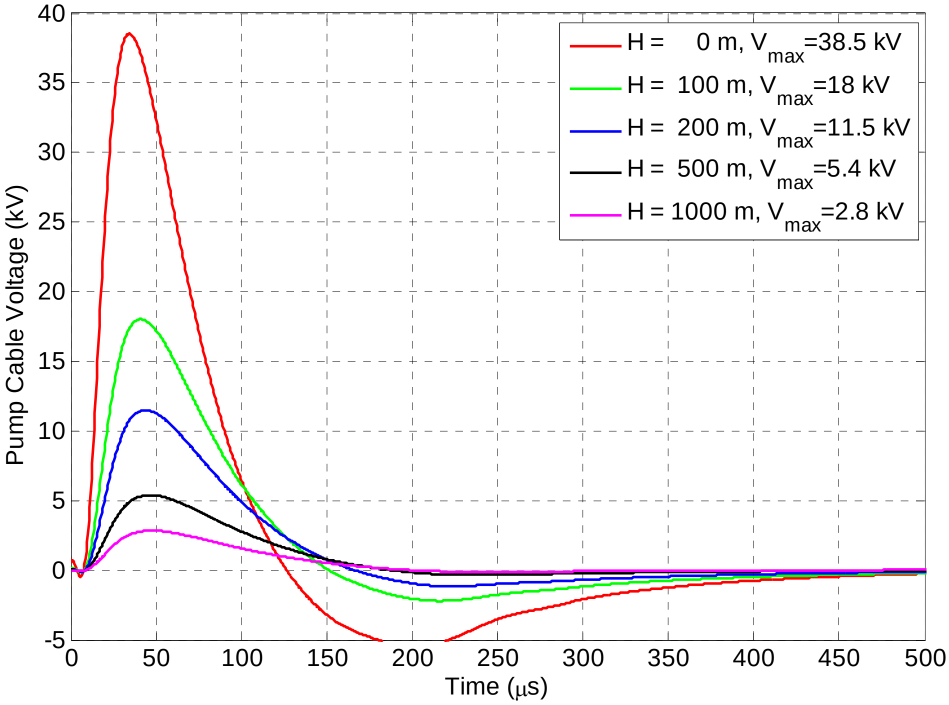

Figure 4-7 Induced voltage pulse on pump cable (with length of 300 m or 984 ft.) from hypothetical horizontal current channel from a cloud-to-ground +100 kA stroke, H is distance of the current channel above the ground.

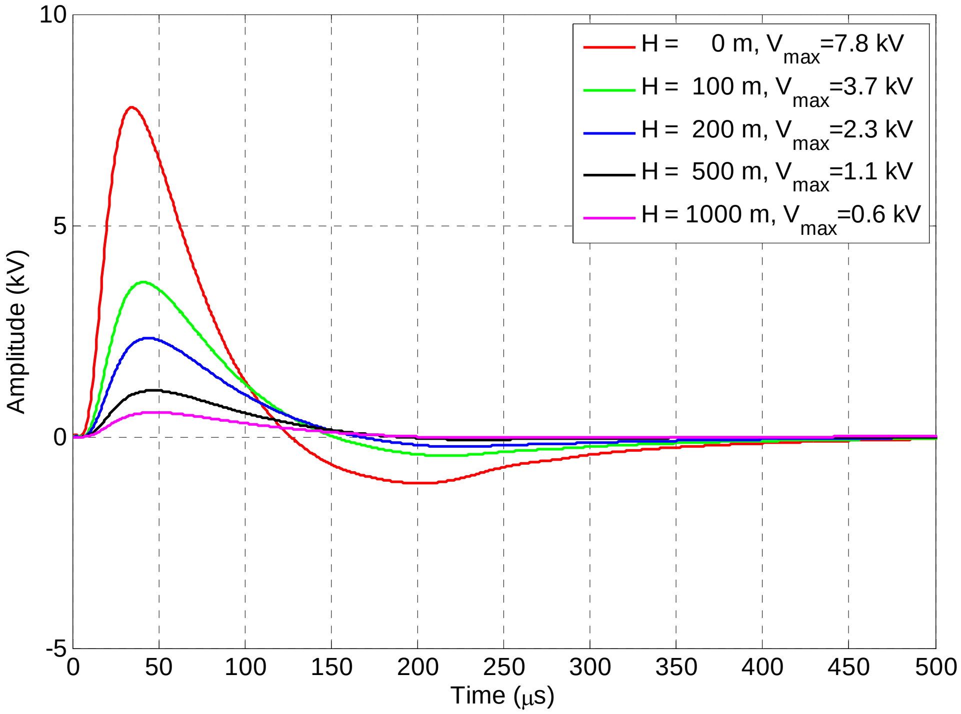

Figure 4-8 Induced voltage pulse on pump cable (length of 61 m or 200 ft.) from hypothetical horizontal current channel from a cloud-to-ground +100 kA stroke, H is distance of the current channel above the ground.

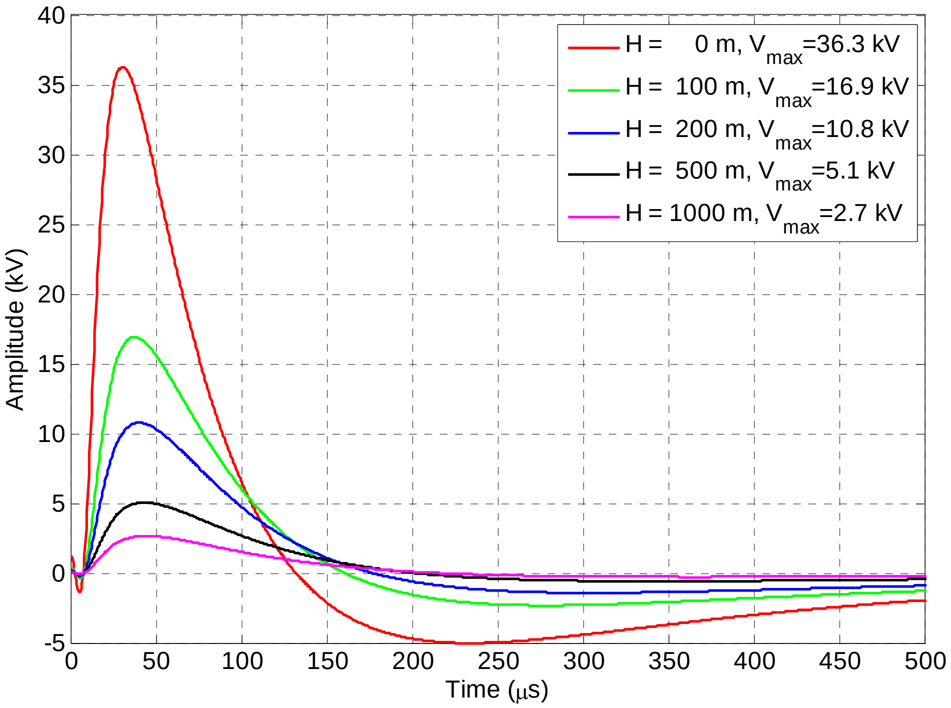

Figure 4-9 Induced voltage pulse on pump cable (length of 300 m or 984 ft.) from hypothetical horizontal current channel from a cloud-to-ground -100 kA stroke, H is distance of the current channel above the ground.

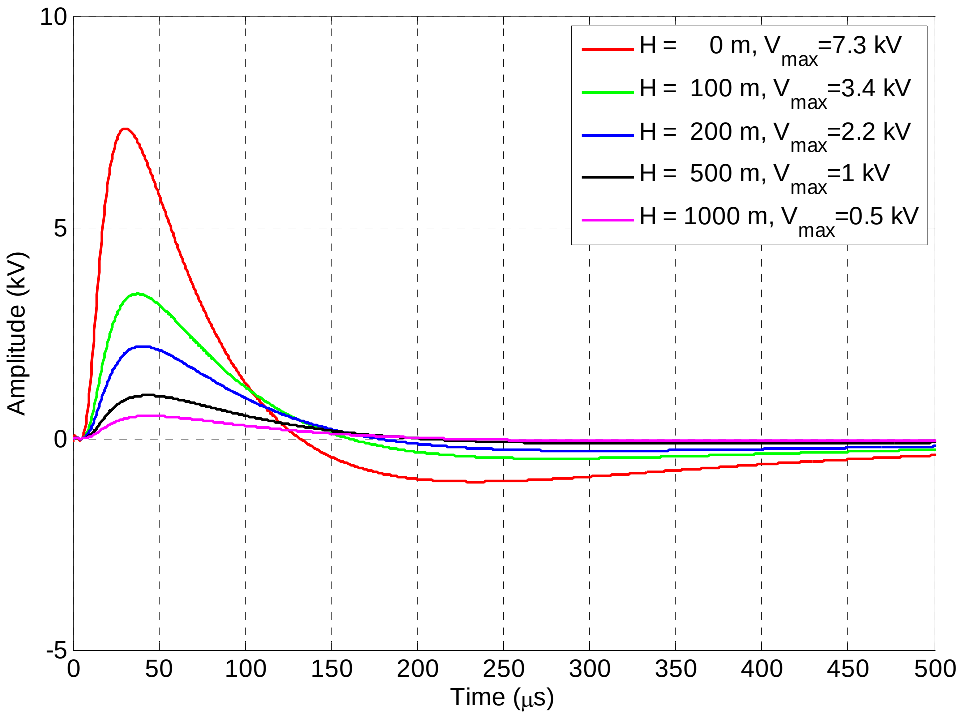

Figure 4-10 Induced voltage pulse on pump cable (length of 61 m or 200 ft.) from hypothetical horizontal current channel from a cloud-to-ground -100 kA stroke, H is distance of the current channel above the ground.

Chapter 5 Conclusions, Recommendations, and Future Work

The conclusions made in this dissertation are specific to the geometry of the Sago mine site where measurements were taken. The results cannot and should not be generalized to any other mining systems.

5.1 Direct Coupling Conclusions

The current and voltage on metallic penetrations into the mine were calculated given the direct drive transfer functions and a mathematical representation of a positive-polarity, 100 kA peak cloud-to-ground lightning stroke. This calculation assumes that the lightning stroke attaches directly onto the metallic penetration at the entrance to the mine. While there is no evidence that lightning struck the entrance of the mine, this assumption represents the worst-case placement of an attachment for this analysis.

The farthest point into the mine that the direct drive measurements were made was at the entrance to the 2nd Left Parallel, 3,491 m (or 2.17 miles) into the mine, as close to the seal that was breached by the explosion as possible. At this location, the peak currents and voltages calculated at this location given the input of a positive 100 kA peak lightning stroke attaching at the mine entrance are shown in Table 5-1. The voltage was not measured for the trolley communication line because it was insulated and not an exposed conductor.

Table 5-1 Current and voltage at the 2nd Left Switch due to a 100 kA peak, positive cloud-to-ground lightning stroke at the entrance of the mine

Metallic penetration	Current	Voltage
Trolley Communication line	198 A	Not measured
Conveyor Structure	9 A	1 V
Rail	35 A	106 V
Shield of Power Cable[5]	480 A	1 V

The voltages and currents on the conveyor, rail, and shield of the power cable outside the sealed area are incapable of coupling sufficient energy into the sealed area. The voltage on the trolley communication line is not anticipated to be significantly larger than those of the conveyor, rail, and power cable shield.

- *It is highly unlikely that direct drive coupling, even under a worst-case scenario, could have produced significant voltage on the cable in the sealed area.*

Because of the substantial initial grounding of metallic penetrations that enter the mine, and because of the multiplicity of grounding points of these systems as they penetrate into the mine, the lightning current would be divided sufficiently so that only a relatively small amount of current would be injected into the mine near the sealed area. All metallic penetrations were intentionally terminated outside the sealed area. Consequently, the amplitude of current flowing on conductors outside the sealed area is insufficient to generate adequate voltage on the cable inside the sealed area to cause a significant buildup of voltage. At low frequencies, the parallel nature of the multiplicity

---

[5] The current and voltage for the shield of the power cable were extrapolated from measurements made at the Power Centers 1, 2, and 3.

of grounding points is sufficient to divide the lightning current. At higher frequencies, the metallic penetrations can be treated as non-ideal (lossy) transmission lines with periodic grounding that attenuates the high-frequency components of the current even more than lower frequencies. ***Although this coupling mechanism is likely insufficient to cause arcing, the voltage and current is sufficient to cause electrical shocks to personnel contacting these metallic penetrations, even miles back into the mine.***

5.2 Indirect Coupling Conclusions

Three things are needed to conclude that indirect coupling of lightning energy into the sealed area produced high voltage in the sealed area of the Sago mine on the morning of January 2, 2006. They are:

- lightning energy propagating from the surface through the overburden into the sealed area;
- an antenna, or receiver (such as a cable), of this energy present in the sealed area; and
- lightning of sufficient magnitude and proximity to the sealed area at the time of the explosion.

The indirect measurements coupled with analytical models discussed in this dissertation confirm that electromagnetic energy with the frequency content of lightning driven on the surface penetrates the ground into the sealed area. Measurements and analyses also confirm that the pump cable acts as a receiver of this energy and is the most likely coupling agent in the sealed area.

Two cloud-to-ground lightning strokes were recorded in the vicinity of the Sago mine within one second of the explosion in the sealed area. Based on the results in this dissertation, these lightning strokes were too far away to have generated a significant voltage on the pump cable in the sealed area. A thorough, expert analysis of the raw data provided by several lightning detection databases did not uncover evidence to support the detection of another cloud-to-ground stroke in the correct timeframe.

- *It is unlikely that indirect drive from the* ***vertical components*** *of the* ***recorded lightning strokes*** *(recorded amplitude and location) around the Sago mine could have produced significant voltage on the cable present in the sealed area.*

The simultaneous events of recorded lightning strokes and the explosion in the sealed area of the mine; the multiple personal accounts above the sealed area describing simultaneous flash and thunder [1] (indicating extremely close lightning); the lack of data from the lightning detection networks from upward positive lightning initiated from tall structures [12,13]; the inability of the lightning detection networks to resolve the presence of horizontal lightning arc channels [12,13]; and the unlikely, but possible, scenario of an undetected cloud-to-ground lightning flash [14] of sufficient magnitude and proximity to the sealed area at the time of the explosion led to the investigation of various hypothetical lightning stroke events. The expected voltage on the abandoned cable was calculated for each scenario using the indirect coupling models developed in this dissertation.

The first hypothetical case explores the possibility of the presence of a horizontal lightning arc channel acting as a source of energy. For this scenario, a 100 kA-peak horizontal arc channel is assumed to be parallel to the pump cable in the sealed area at distances of 100 m (328 ft), 200 m (656 ft), 500 m (1,640 ft), and 1000 m (3,281 ft) above the ground above the sealed area. For a positive-polarity flash, the resultant voltages on the pump cable were 18.0 kV, 11.5 kV, 5.4 kV, and 2.8 kV, respectively. For a negative-polarity flash, the resultant voltages on the pump cable were 16.9 kV, 10.8 kV, 5.1 kV, and 2.7 kV, respectively. While these calculations use favorable coupling circumstances (high peak arc-channel current and parallel orientation of the arc channel to the pump cable and cable length of 300m), this hypothetical scenario presents a reasonable case where significant voltages build up on the pump cable.

- *It is reasonable to assume that **if** a horizontal, low-altitude arc channel occurred from one of the lightning strokes recorded by the NLDN (or USPLN) or from an unrecorded lightning stroke, it could have produced significant voltage on the cable in the sealed area.*

The second hypothetical case explores the possibility of an undetected cloud-to-ground stroke of sufficient magnitude and proximity to the sealed area. Applying a 100 kA-peak, cloud-to-ground stroke of optimum orientation to the pump cable (300 m length) within

160 m (525 ft) of the sealed area, the results are peak voltages on the pump cable of 24.9 kV for a negative-polarity flash, and 23.3 kV for a positive-polarity flash. For the same conditions, the induced voltage decreases as distance of a lightning stroke from the sealed area increases.

- *It is reasonable to assume that* ***if*** *an average or above average cloud-to-ground lightning stroke occurred above the sealed area at Sago, that it could produce significant voltage on the cable in the sealed area.*

The conclusions of this dissertation are that lightning of sufficient magnitude and proximity to the sealed area would create high voltage on the pump cable. The simultaneity in time of recorded lightning strokes and the explosion occurring is very strong evidence of cause and effect. Furthermore, eyewitness accounts of simultaneous lightning and thunder at the time of the explosion, plus the analysis of credible hypothetical scenarios which cannot be confirmed by lightning detection networks, lend credibility to the idea that lightning-induced electrical arcing.

5.3 Recommendations

The results of this work demonstrate the usefulness of transfer function measurement techniques and analytical modeling to evaluate lightning effects in mining environments. The effects described in this dissertation are significant. A more comprehensive research and development program should be conducted to expand on this work to extend this research for use in other underground coal mining operations. The research program would be conducted using similar transfer function measurement techniques, experiments at other sites with rocket-triggered and natural lightning, and analytical and computational modeling using validated state-of-the-art codes adapted for this application. Once completed, it is reasonable to expect that mitigation techniques and safety standards could be developed to secure coal mining systems from future lightning threats.

Much of the modeling of the transmission line coupling from lightning can be applied directly to buried telephone lines and power lines. Both of which are affected during electrical storms and are susceptible to outages due to direct attachment and horizontal cloud-to-cloud lightning. The models also could be extended in the frequency response to include electric fields coupling onto improvised explosive devices (IEDs) or detonator wires going to explosives.

5.4 Potential Further Areas of Study

The following items are potential areas for further study. Their effects on the coupling mechanisms characterized in this dissertation are unknown, but believed to be of minimal effect.

Future work includes further development of transmission line models for coupling voltages and currents directly into the mine via unintentional transmission lines.

5.4.1 Nonlinearities

Surface arcing and arcing through soil and rock are well-known phenomena that can propagate lightning energy over a distance of a hundred feet or less. Because these phenomena occur only at the full amplitudes of natural or triggered lightning strokes, their behavior and effect on coupling could not be studied using the low-amplitude transfer function measurement techniques of this study. There is no evidence an arc can travel a distance of 300 feet through soil and rock, therefore, it is unlikely this would have any effect on this analysis.

5.4.2 Coupling from Vertical Pipes near Sealed Areas

The effect on the coupled electromagnetic field caused by direct drive of the vertical gas well that passed near the sealed area was not measured in this study. Because we could not guarantee that damage to cathodic protection systems or other instrumentation would not be caused by our drive system, the owners of the system would not allow attachment to the pipe without indemnification. Direct drive of the vertical pipe could have caused some enhancement of the coupled electric fields in the sealed area, but would not change the conclusions. The modeled results of the fields induced by current on the closest vertical gas well were shown in Section 3.4, but measured data would be helpful.

5.4.3 Distributed Drives for Metallic Penetrations

Although the localized drive at the entrance to the mine of all metallic penetrations to the mine was studied, the propagation of voltages and currents on these penetrations can be enhanced by current flow on the surface of the earth above the penetrations. Simple considerations indicate that the voltage and current amplitudes are not enhanced significantly. The measurement that could have elucidated this phenomenon was cancelled because of the physical and political impracticality of stringing a wire from the entrance of the mine through dense forests and livestock-occupied pastureland to a location above the sealed area.

5.4.4 Effect of Grounded Roof Meshes

Voltages induced between sections of roof meshes in the sealed area were not measured because the substantial grounding of these meshes via rods driven every three feet or so to provide roof support was thought to prevent buildup of voltages. We found at the site that the use of nonconductive epoxies may prevent good contact between the epoxy bolts and the rock. The voltage buildup between sections of roof mesh and the effect of the roof mesh on electric fields and voltages within the sealed area was not studied in this work. Resistance between roof bolts ranged from 2 mΩ to 150 Ω for bolt spacing up to 15 m (~50 feet) [49]. The majority of the samples showed resistances closer to the 2 mΩ value. The maximum resistance found would yield soil resistivity on the order of 10 Ω-m, which would still be considered a fairly good conductor.

5.4.5 Coupling Paths Not Present in Sago Mine

Lightning coupling paths into sealed areas that are common in other underground coal mines but are absent from the Sago mine, such as coupling along metal-cased boreholes that extend from the surface into the sealed area and coupling through other metallic penetrations used for monitoring or other instrumentation were not studied in this dissertation.

5.4.6 Geologic Irregularities Affecting Coupling

The extent to which geologic irregularities such as faults and mineral deposits that affect the coupling of lightning energy into underground coals was not quantified in this study. However, studies conducted by hydroGEOPHYSICS indicate that there were no significant irregularities in the vicinity of the area where the explosion occurred. [11]

5.4.7 Lightning Current Return Path Assumptions

The analysis used in this dissertation assumes that lightning current is uniform in the radial direction. The extent to which large-scale inhomogenieties affect the current paths, and the extent to which the variation with depth affects the coupling, were not quantified in this study.

References

1. West Virginia Office of Miners' Health, Safety, and Training, *Report of Investigation into the Sago Mine Explosion which occurred January 2, 2006*, Upshur Co. West Virginia, December 11, 2006.

2. Checca, Elio and D. R. Zuchelli, *Lightning Strikes and Mine Explosions*, Proceedings of 7th US Mine Ventilation Symposium, June 5-7, 1995, pp 245-250.

3. Checca, Elio L., *Investigative Report No. C-042094–Oak Grove Mine Methane Gas Ignition*, U. S. Department of Labor, Mine Safety and Health Administration, Pittsburg Safety and Health Technology Center, Pittsburg, PA, April 6-12, 1994.

4. Scott, Doniece S., E. Larry Checca, Clete R. Stephan, and Mark J. Schultz, *Accident Investigation Report (Underground Coal Mine) Non-Injury Methane Explosion, Oak Grove Mine (I.D. No. 01-00851)*, U. S. Department of Labor, Mine Safety and Health Administration, District 11, January 29, 1996.

5. Scott, Doniece S., and Clete R. Stephan, *Accident Investigation Report (Underground Coal Mine) Non-Injury Methane Explosion, Oak Grove Mine (I.D. No. 01-00851)*, U. S. Department of Labor, Mine Safety and Health Administration, District 11, July 11, 1997.

6. Morris, Marvin E., Richard J. Fisher, George H. Schnetzer, Kimball O. Merewether, and Roy E. Jorgenson, *Rocket-Triggered Lightning Studies for the Protection of Critical Assets,* M. E. Morris *et al.*, IEEE Transactions on Industry Applications, Vol. 30, No. 3, pp 791-804, May/June 1994 (1994 Prize Paper Award from IEEE Power Systems Society).

7. Chen, Kenneth C., Kimball O. Merewether, Tom Y. T. Lin, and Parris Holmes, Jr., *Final Report: U12g Tunnel Lightning Evaluation*, Sandia National Laboratories Report, SAND2004-1619, Sandia National Laboratories, Albuquerque, NM, April 2004.

8. Dinallo, Michael A., and Roy E. Jorgenson, *Recommended Lightning Protection Practices for Operations Being Conducted in G-Tunnel at the Nevada Test Site*, Sandia National Laboratories Report SAND2006-1049P, Sandia National Laboratories, Albuquerque, NM, February 2006.

9. Staff-Mining Research, *Methane Control in Eastern U. S. Coal Mines*, Proceedings of the Symposium of the Bureau of Mines/Industry Technology Transfer Seminar, Morgantown, WV, May 30-31, 1973.

10. Insulating materials for design and engineering practice, John Wiley and Sons, 1962, Library of Congress Catalog Card Number 62-17460.

11. Rucker, Dale, Marc Levitt, Shawn Calendine, John Fleming, and Robert McGill, *Geophysical Survey for the Old 2 Left Section of the Sago Mine, Buckhannon, WV,* hydroGEOPHYSICS, Inc., Tucson, AZ, August 18, 2006.

12. Martin A. Uman, University of Florida (private communication).

13. E. Philip Krider, University of Arizona (private communication and memorandum, see Appendix E).

14. Cummins, Kenneth L., et. al., *The U.S. National Lightning Detection Network: Post-Upgrade Status*, Proceedings of the Second Conference of Meteorological Applications of Lightning Data, 86th AMS Annual Meeting, Atlanta, GA, 29 January - 2 February 2006. American Meteorological Society.

15. Novak, Thomas, and Thomas J. Fisher, *Lightning Propagation Through the Earth and Its Potential for Methane Ignitions in Abandoned Areas of Underground Coal Mines*, IEEE Transactions on Industrial Applications, Vol. 37, No. 6, Nov/Dec 2001, pp1555-1562.

16. Sacks, H. K., and Thomas Novak, *Corona Discharge Initiated Mine Explosion*, IEEE Transactions on Industrial Applications, Vol. 41, Sept/Oct 2005.

17. Liu, Jian-Bang, Paul D. Ronney, and Martin A. Gundersen, *Premixed Flame Ignition by Transient Plasma Discharges*,

18. Ronney, Paul D., *Technical Progress Report on Corona Discharge Initiation*, University of Southern Californa, Dept. of Aerospace and Mechanical Engineering, Los Angeles, CA, Sept 12, 2003.

19. Berger, K., *Protection of Underground Blasting* Operations, edited by R. H. Golde, in. *Lightning – Vol 2, Lightning Protection*, Academic Press, New York, NY, 1977, pp633-658.

20. Geldenhuys, H. J., A. J. Eriksson, W. B. Jackson, and J. B. Raath, *Research into Lightning-Related Incidents in Shallow South African Coal Mines*, Proceedings of the 21st Internal Conference on Safety in Mines Research, 1985, pp775-782.

21. Golledge, P., *Sources and Facility of Ignition in Coal Mines*, *in Ignitions, Explosions, and Fires*, 1981, pp2-1–2-12.

22. Geldenhuys, H. J., *The Measurement of Underground Lightning-Induced Surges in a Colliery*, Symposium on Safety in Coal Mining, South Africa National Electrical Engineering Research, Pretoria, South Africa, October 5-8, 1987.

23. Zeh, K. A., *Lightning and Safety in Shallow Coal Mines*, 23rd International Conference of Safety in Mines, 1989, pp691-700.

24. Pozar, David M., *Microwave Engineering, Third Edition*, John Wiley & Sons, New York, NY, 2005.

25. Tesche, Frederick M., Michel V. Ianoz, and Torbjorn Karlsson, *EMC Analysis Methods and Computational Models*, John Wiley & Sons, New York, NY, 1997.

26. Smythe, William R., *Static and Dynamic Electricity*, A Summa Book, Albuquerque, NM, 1989.

27. Wait, J.; and Hill, D., *Guided electromagnetic waves along an axial conductor in a circular tunnel*, IEEE Transactions on Antennas and Propagation, Volume 22, Issue 4, July 1974, pp. 627 - 630.

28. Mahmoud, S., *Characteristics of Electromagnetic Guided Waves for Communication in Coal Mine Tunnels*, IEEE Transactions on Communications, Volume 22, Issue 10, October 1974, pp. 1547 - 1554.

29. Wait, James R., *Quasi-static limit for the propagating mode along a thin wire in a circular tunnel*, IEEE Transactions on Antennas and Propagation, Volume 25, Issue 3, May 1977, pp. 441 - 443.

30. Sunde, Erling D., *Earth Conduction Effects in Transmission Systems*, pp. 112 & 272, D. Van Nostrand Company, Inc., New York, NY, 1949.

31. Wait, James R., *Electromagnetic Waves in Stratified Media*, The Macmillan Company, New York, NY, 1962

32. Tegopoulis, J. A., and E. E. Kriezis, *Eddy Currents in Linear Conducting Media*, Elsevier, New York, NY, 1985.

33. Stoll, Richard L., *The Analysis of Eddy Currents*, Clarendon Press, Oxford, UK, 1974.

34. Krawczyk, A., and J. A. Tegopoulis, *Numerical Modeling of Eddy Currents*, Clarendon Press, Oxford, UK, 1993.

35. Kaufman, A. A., and P. Hoekstra, *Electromagnetic Soundings*, Elsevier, New York, NY, 2001.

36. Higgins, Matthew B., and Marvin E. Morris, *Measurement and Modeling of Transfer Functions for Lightning Coupling into the Sago Mine*, SAND2006-

7976, Sandia National Laboratories Report, Sandia National Laboratories, Albuquerque, NM, April 2007.

37. Hill, David A., and James R. Wait, *Subsurface Electric Fields of a Grounded Cable of Finite Length for both Frequency and Time Domain*, Pure and Applied Geophysics, Vol. 111, No. 1, pp. 2324 – 2332, December 1973.

38. Harrington, R. F., *Field Computations by Moment Methods*, Macmillan, New York, 1968.

39. Harrington, R. F., *Matrix Methods for Field Problems*, Proc. IEEE, 55:136-149, February 1967.

40. Balanis, C.A., *Antenna Theory: Analysis and Design (Second Edition)*, Wiley, New York, 1997.

41. Wolff, E. A., *Antenna Analysis*, Wiley, New York, 1966.

42. Vance, E., *Coupling to Shielded Cables*, Wiley, New York, 1978.

43. Warne, Larry K., and Kenneth C. Chen, *Long Line Coupling Models*, SAND2004-0872, Sandia National Laboratories Report, Sandia National Laboratories, Albuquerque, NM, March 2004.

44. Chen, K.C., and Damrau, K.M., *Accuracy of approximate transmission line formulas for overhead wires*, IEEE Transactions on Electromagnetic Compatibility, Volume 31, Issue 4, November 1989, pp. 396 - 397.

45. Schelkunoff, S.A., and H. T. Friis, *Antennas Theory and Practice*, Wiley, New York, 1952.

46. Balanis, C.A., *Advanced Engineering Electromagnetics*, Wiley, New York, 1989.

47. Cianos, N., and Pierce, E. T., *A Ground-Lightning Environment for Engineering Usage*, Technical Report 1, SRI Project 1834, August 1972.

48. Rakov, Vladimir A., and Martin A. Uman, *Lightning*, Lightning Physics and Effects, Cambridge University Press, New York, NY, 2003.

49. Phillips, Robert, *Resistivity Measurements*, personal communications from Robert Phillips

Appendix A Calibration Documentation of Measurement Equipment

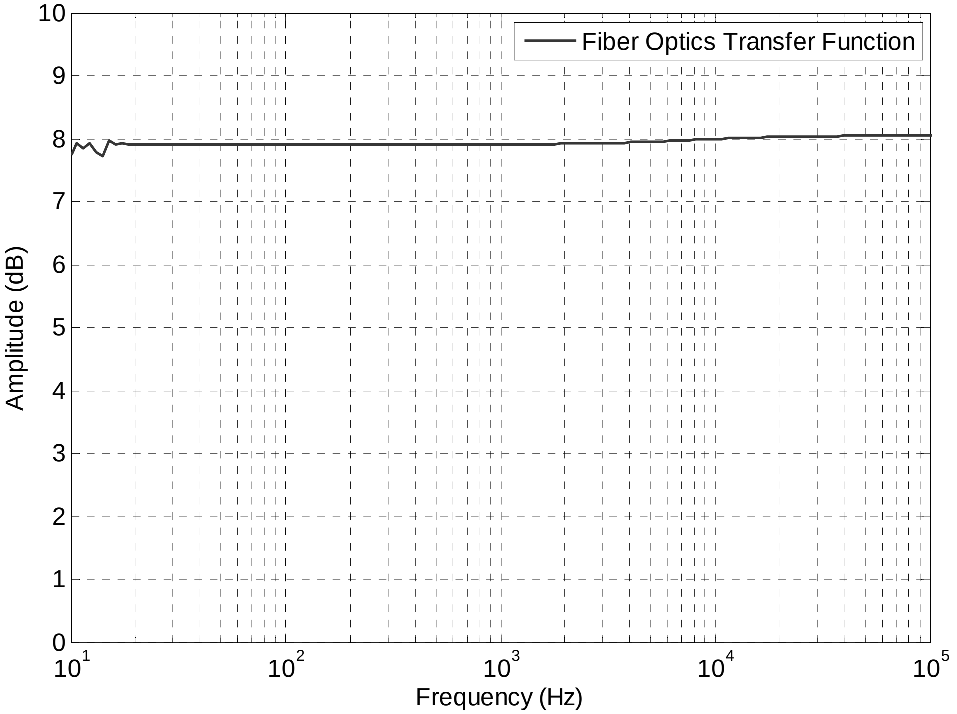

Figure A-1 Calibration frequency response of fiber-optic transmitter/receiver pair.

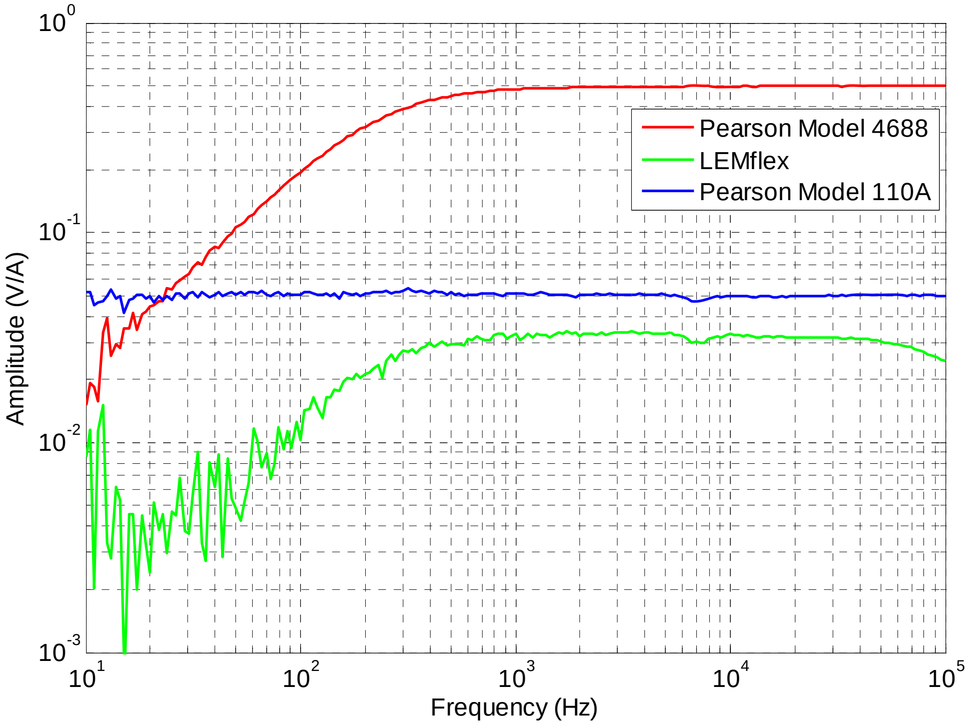

Figure A-2 Calibration frequency response of current probes used.

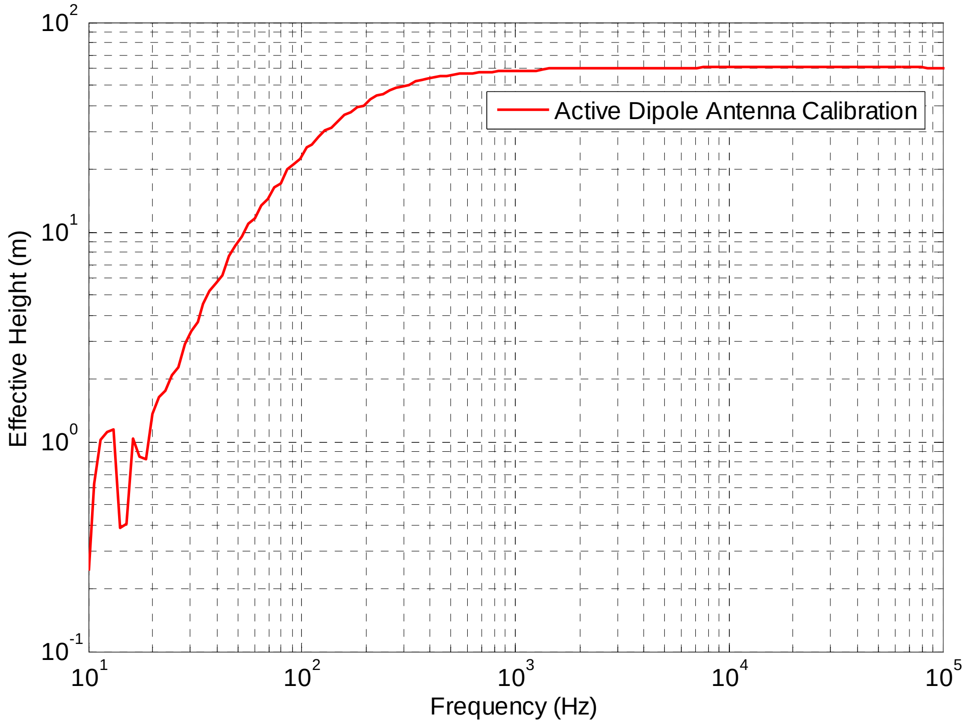

Figure A-3 Calibration frequency response of active dipole antenna.

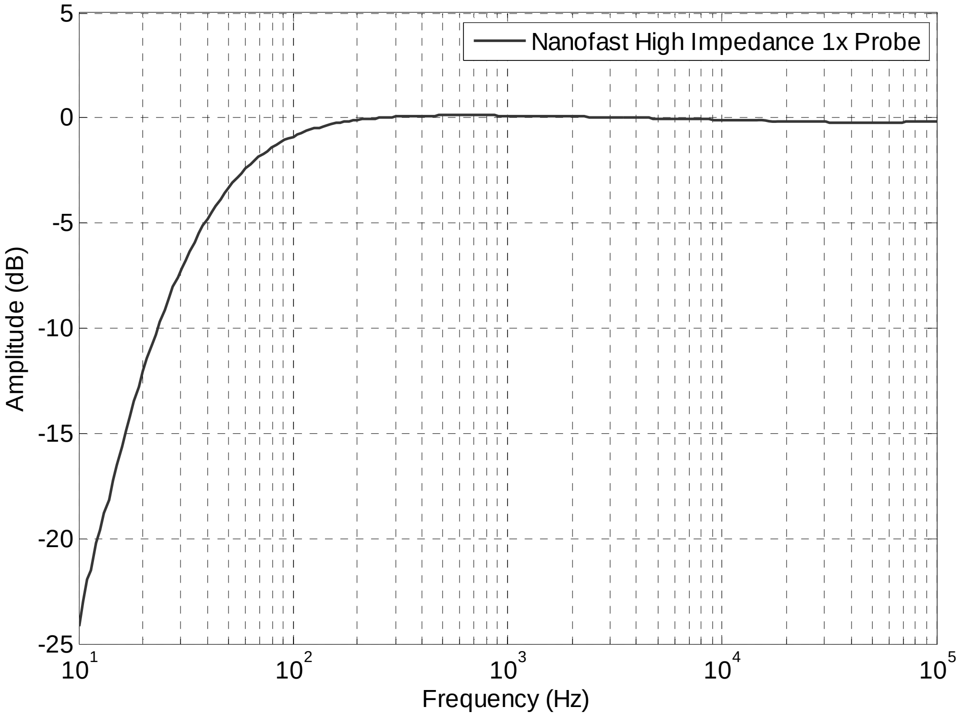

Figure A-4 Calibration frequency response of Nanofast high-impedance probe.

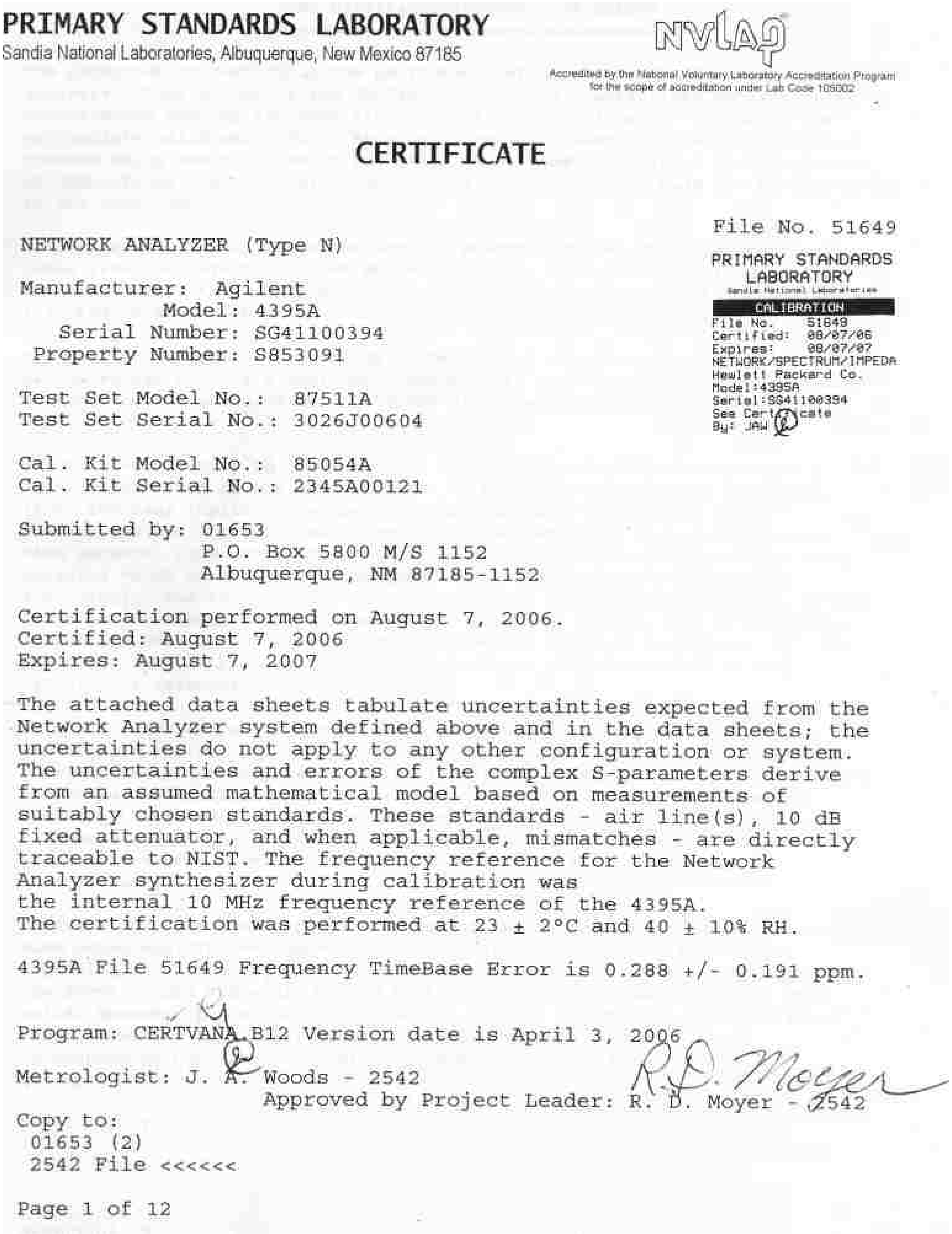

PRIMARY STANDARDS LABORATORY
Sandia National Laboratories, Albuquerque, New Mexico 87185

NVLAP
Accredited by the National Voluntary Laboratory Accreditation Program
for the scope of accreditation under Lab Code 105002

CERTIFICATE

File No. 51649

PRIMARY STANDARDS
LABORATORY
Sandia National Laboratories
CALIBRATION
File No. 51649
Certified: 08/07/06
Expires: 08/07/07
NETWORK/SPECTRUM/IMPEDA
Hewlett Packard Co.
Model:4395A
Serial:SG41100394
See Certificate
By: JAW

NETWORK ANALYZER (Type N)

Manufacturer: Agilent
Model: 4395A
Serial Number: SG41100394
Property Number: S853091

Test Set Model No.: 87511A
Test Set Serial No.: 3026J00604

Cal. Kit Model No.: 85054A
Cal. Kit Serial No.: 2345A00121

Submitted by: 01653
P.O. Box 5800 M/S 1152
Albuquerque, NM 87185-1152

Certification performed on August 7, 2006.
Certified: August 7, 2006
Expires: August 7, 2007

The attached data sheets tabulate uncertainties expected from the Network Analyzer system defined above and in the data sheets; the uncertainties do not apply to any other configuration or system. The uncertainties and errors of the complex S-parameters derive from an assumed mathematical model based on measurements of suitably chosen standards. These standards - air line(s), 10 dB fixed attenuator, and when applicable, mismatches - are directly traceable to NIST. The frequency reference for the Network Analyzer synthesizer during calibration was the internal 10 MHz frequency reference of the 4395A. The certification was performed at 23 ± 2°C and 40 ± 10% RH.

4395A File 51649 Frequency TimeBase Error is 0.288 +/- 0.191 ppm.

Program: CERTVANA.B12 Version date is April 3, 2006

Metrologist: J. A. Woods - 2542
Approved by Project Leader: R. D. Moyer - 2542

R. D. Moyer

Copy to:
01653 (2)
2542 File <<<<<<

Page 1 of 12

Figure A-5 Certificate of calibration for 4395A network analyzer.

Appendix B Compilation of Measured Data

Direct Drive Transfer Function Data:

The following transfer functions were measured with the mine grounding system in current state.

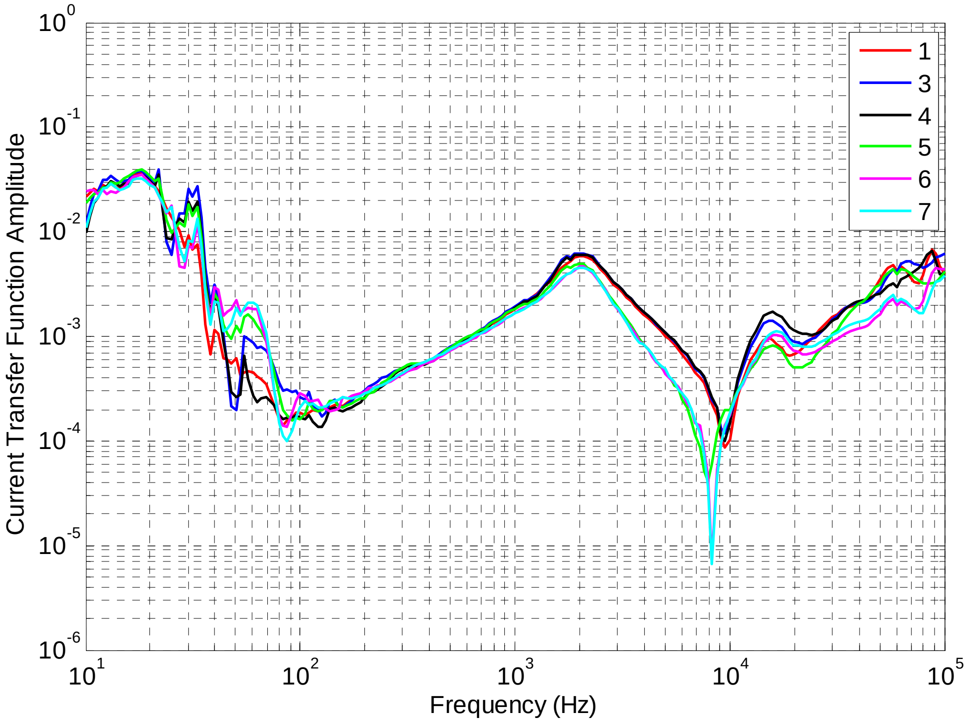

Figure B-1 Direct drive current transfer function of trolley communication line with a local ground.

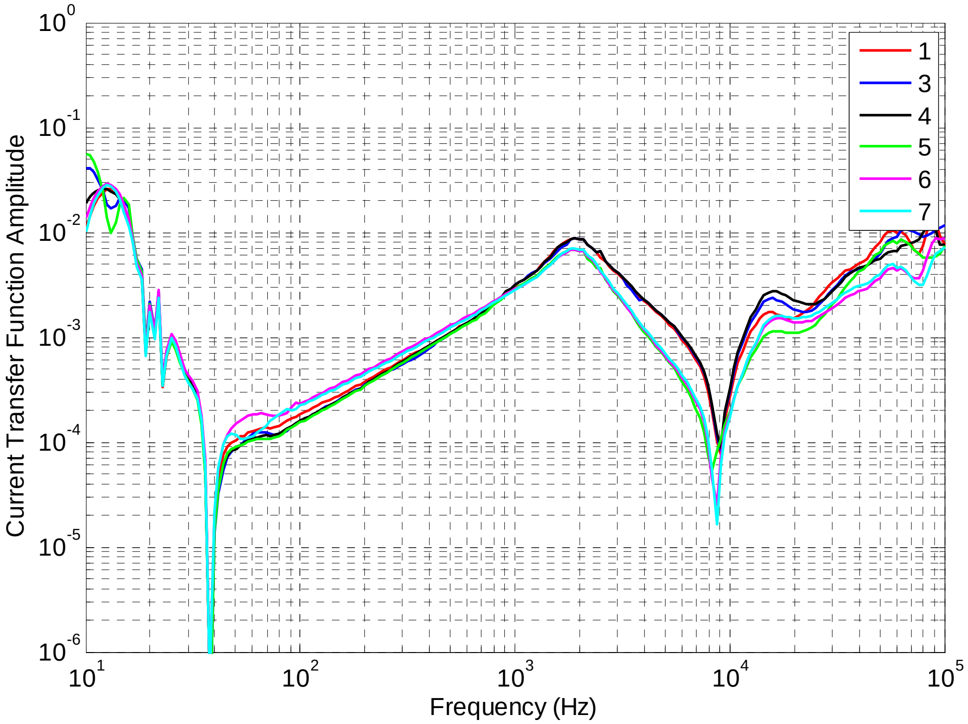

Figure B-2 Direct drive current transfer function of trolley communication line with a fence ground.

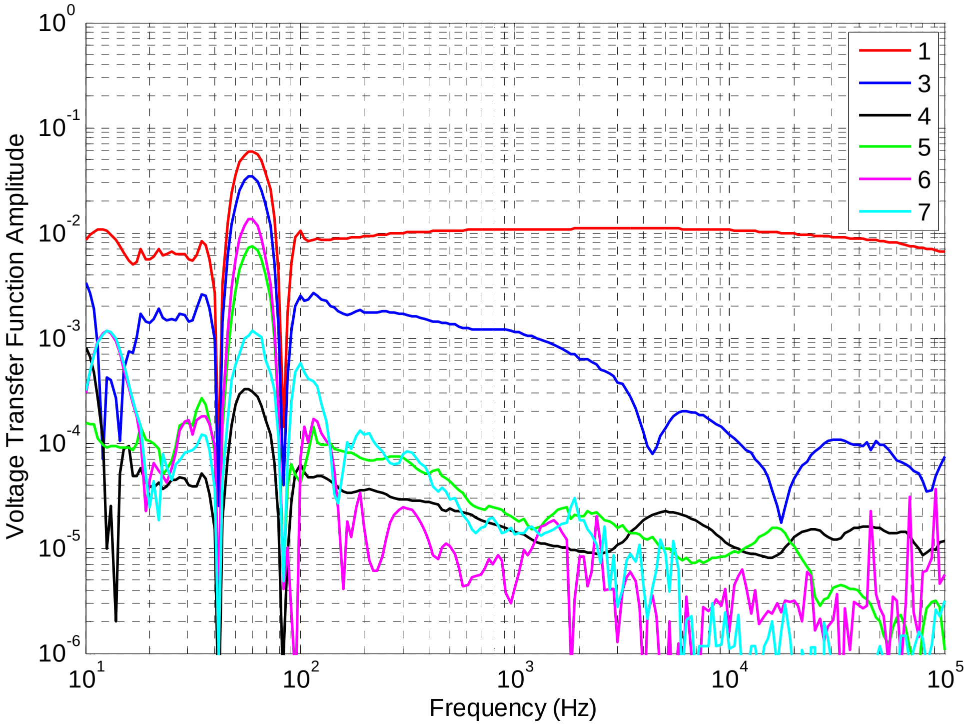

Figure B-3 Direct drive voltage transfer function of conveyor structure with a local ground.

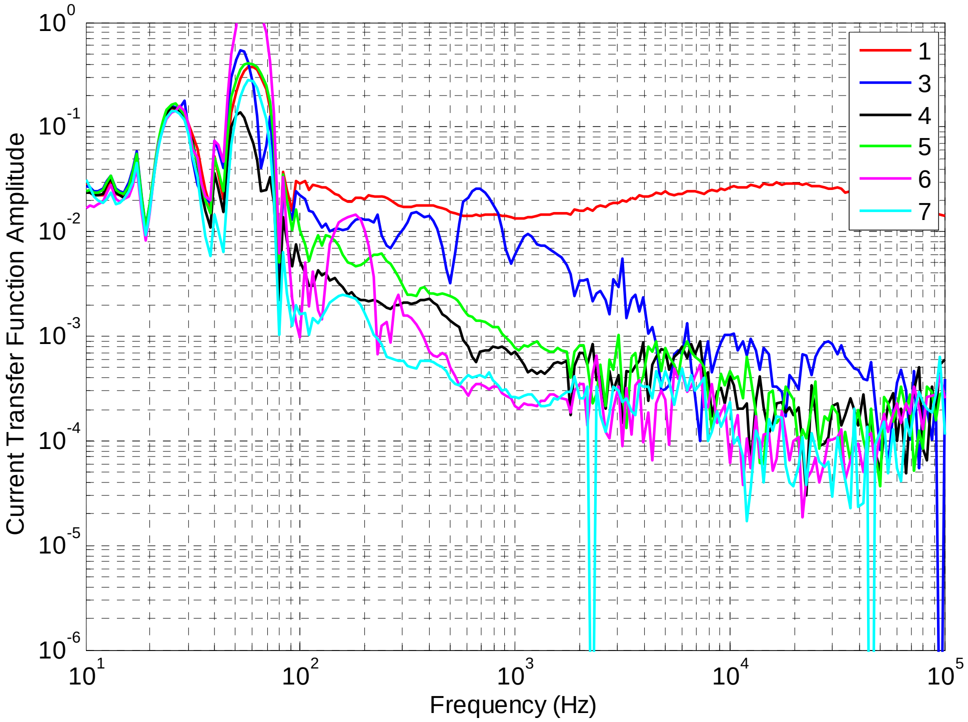

Figure B-4 Direct drive current transfer function of conveyor structure with a local ground.

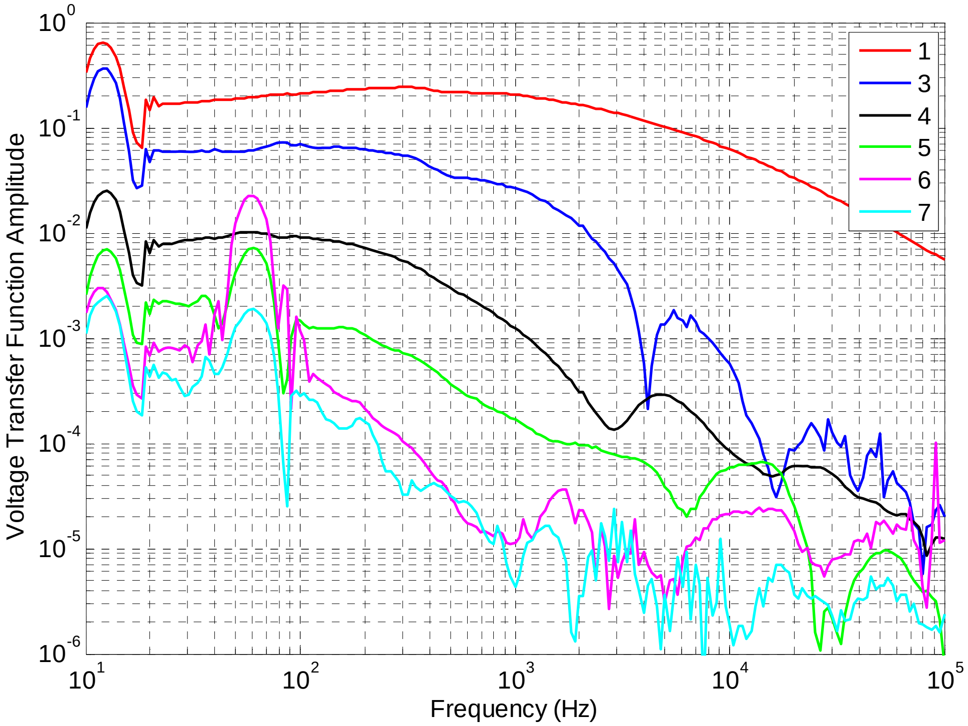

Figure B-5 Direct drive voltage transfer function of conveyor structure with a fence ground.

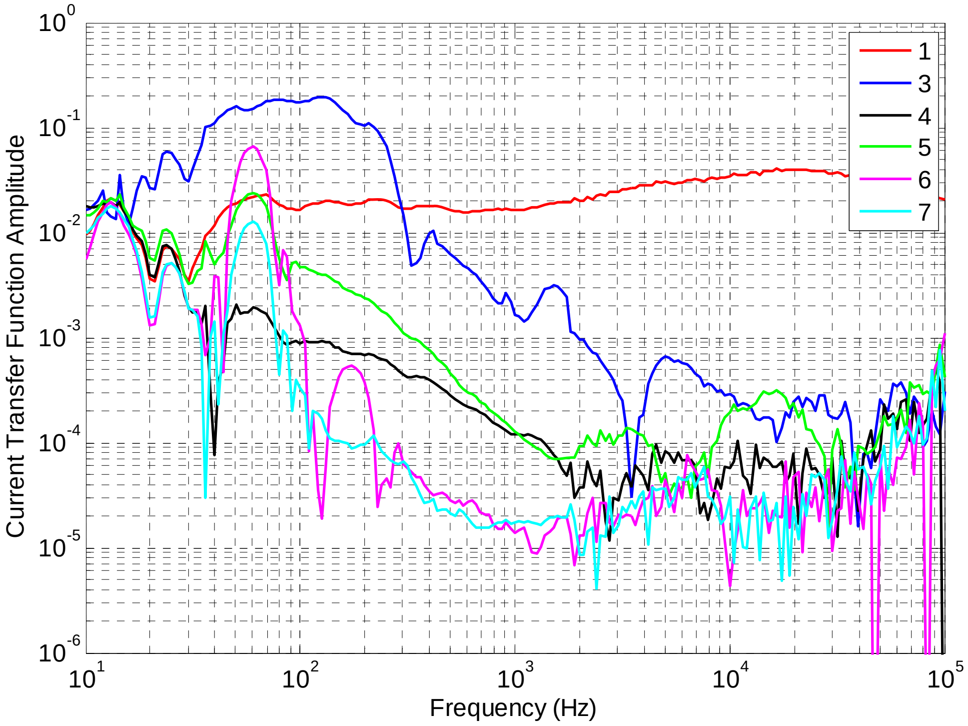

Figure B-6 Direct drive current transfer function of conveyor structure with a fence ground.

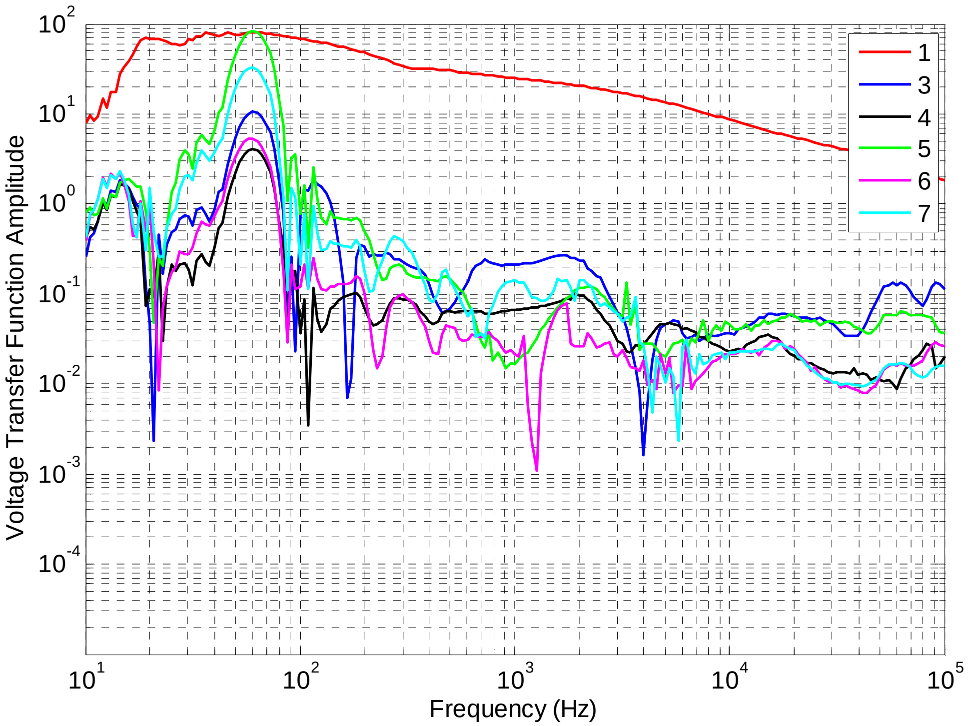

Figure B-7 Direct drive voltage transfer function of rail structure with a local ground.

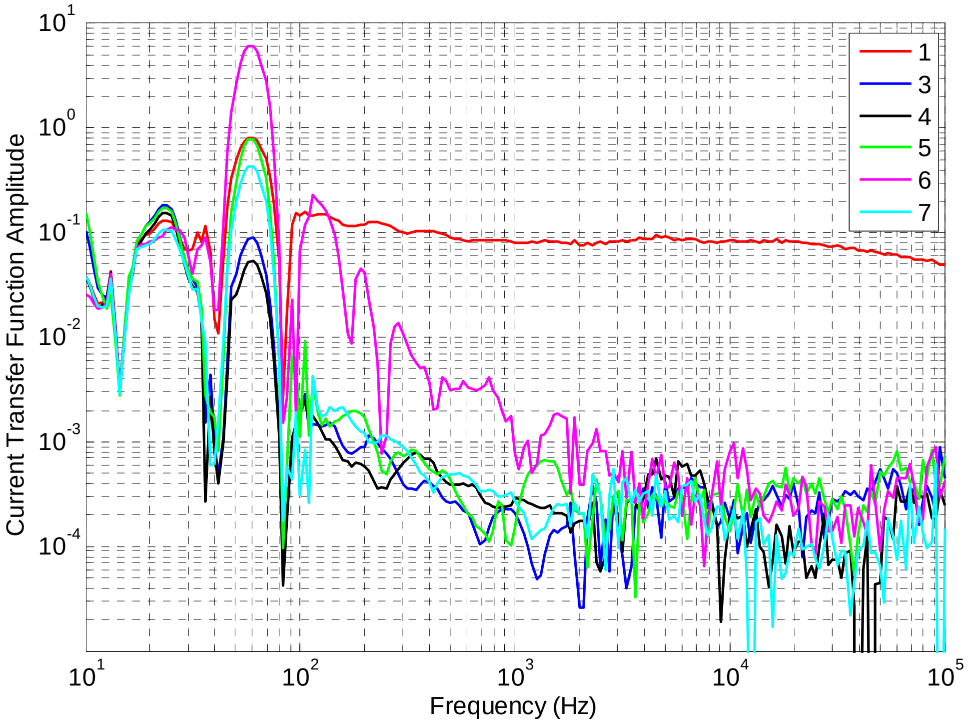

Figure B-8 Direct drive current transfer function of rail structure with a local ground.

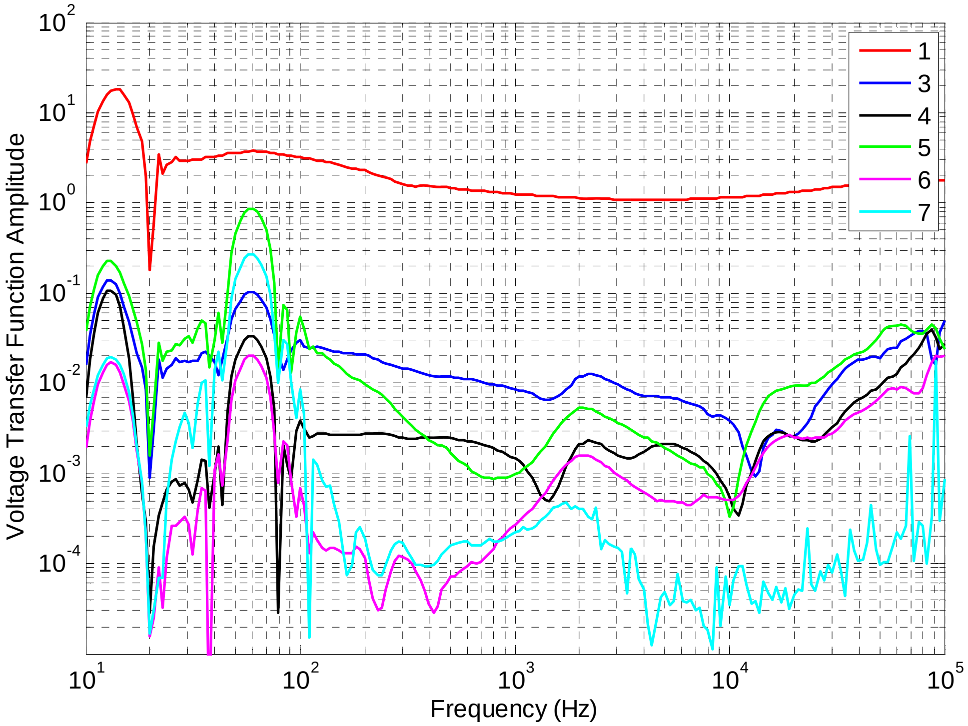

Figure B-9 Direct drive voltage transfer function of rail structure with a fence ground.

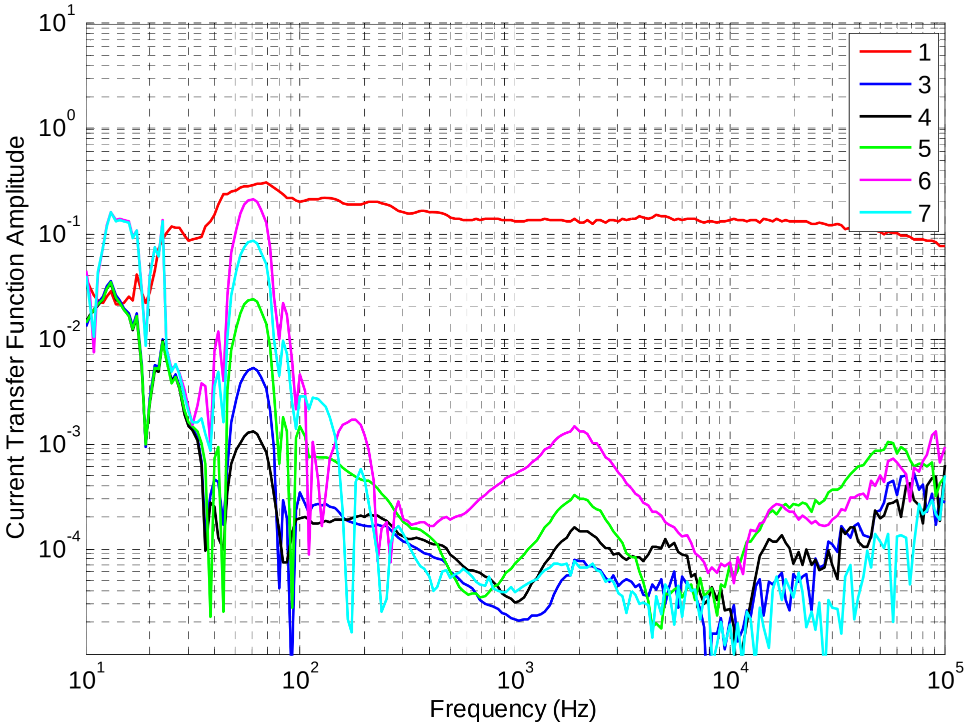

Figure B-10 Direct drive current transfer function of rail structure with a fence ground.

The following transfer functions were measured with the mine grounding system similar to the grounding scheme in place during explosion.

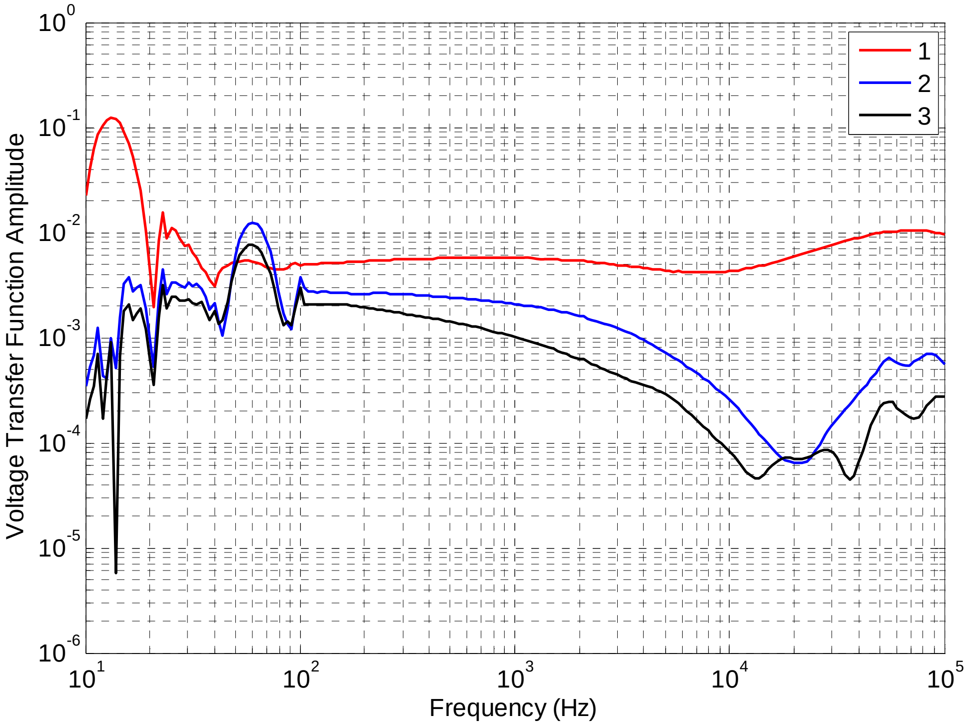

Figure B-11 Direct drive voltage transfer function of power cable shield with a local ground.

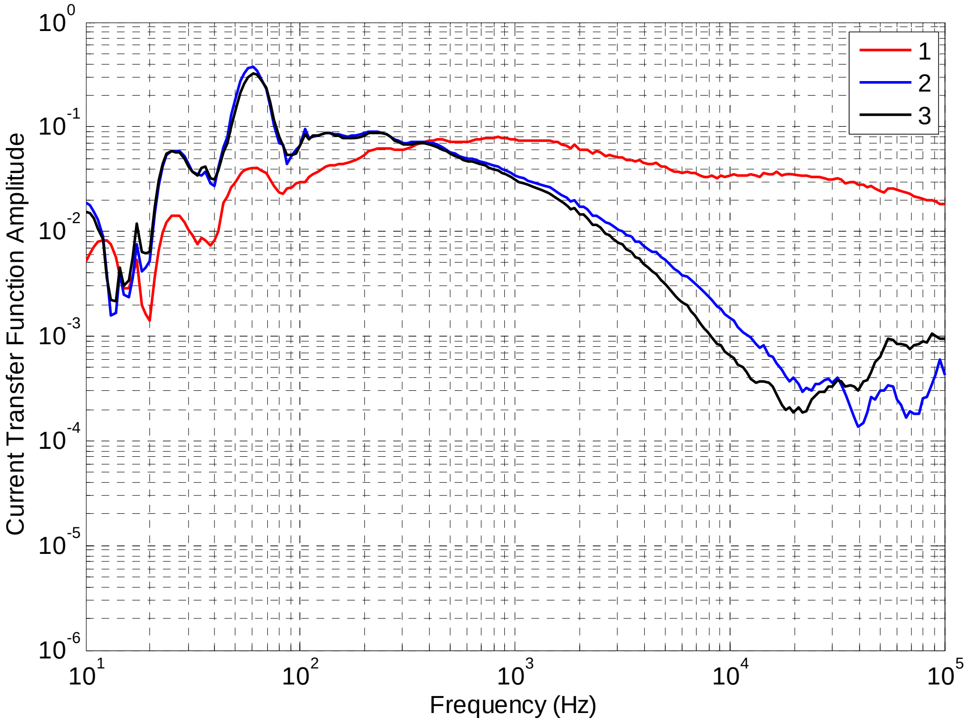

Figure B-12 Direct drive current transfer function of power cable shield with a local ground.

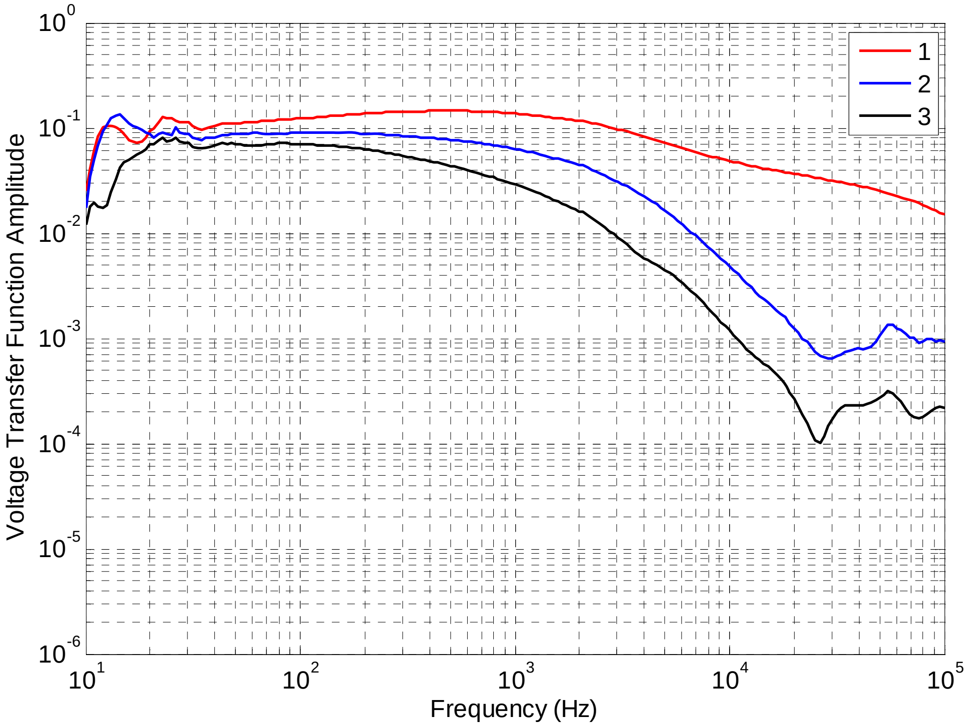

Figure B-13 Direct drive voltage transfer function of power cable shield with a fence ground.

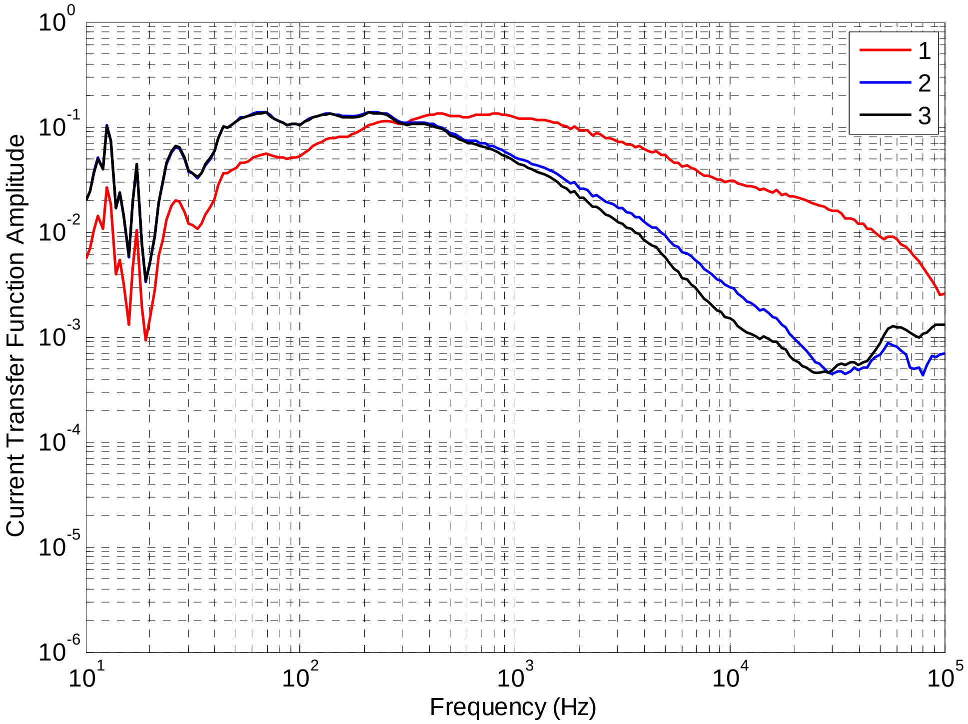

Figure B-14 Direct drive current transfer function of power cable shield with a fence ground.

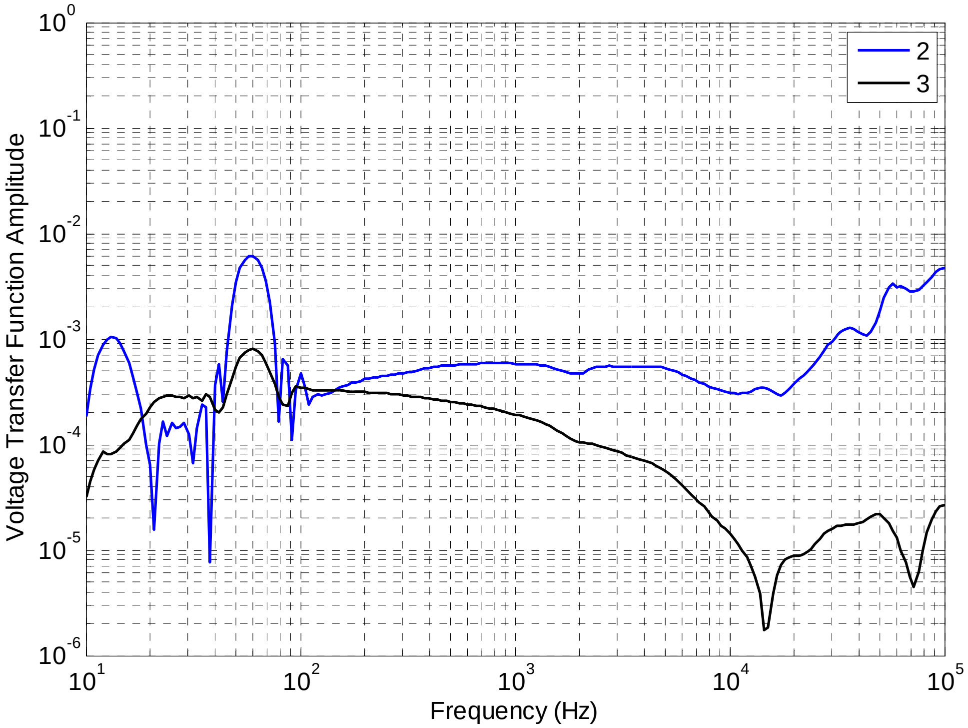

Figure B-15 Direct drive voltage transfer function of rail structure with a local ground.

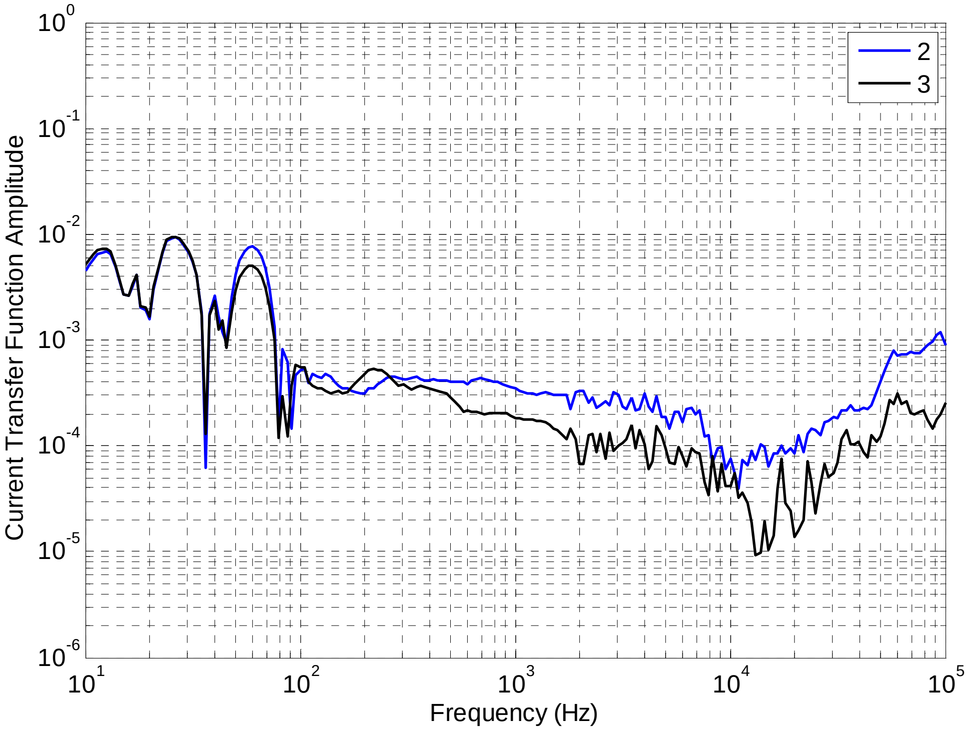

Figure B-16 Direct drive current transfer function of rail structure with a local ground.

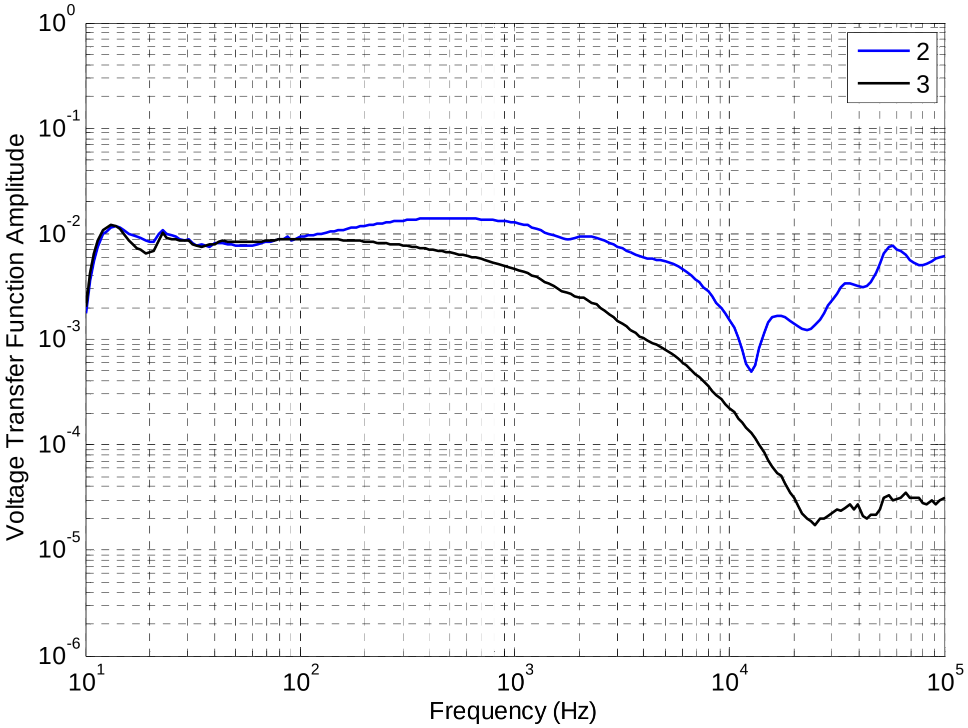

Figure B-17 Direct drive voltage transfer function of rail structure with a fence ground.

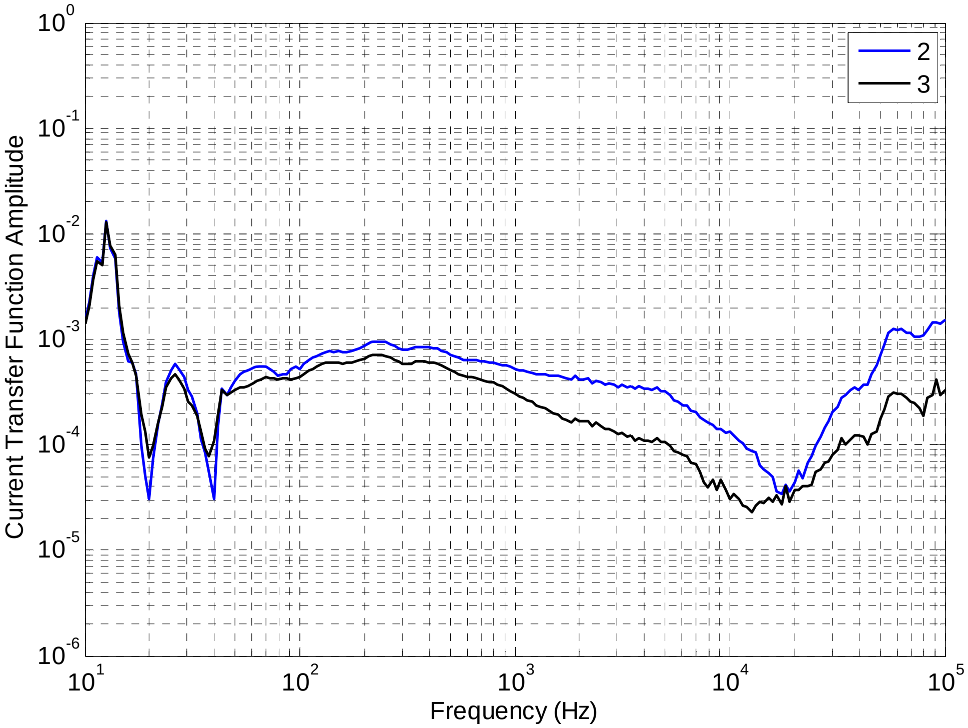

Figure B-18 Direct drive current transfer function of rail structure with a fence ground.

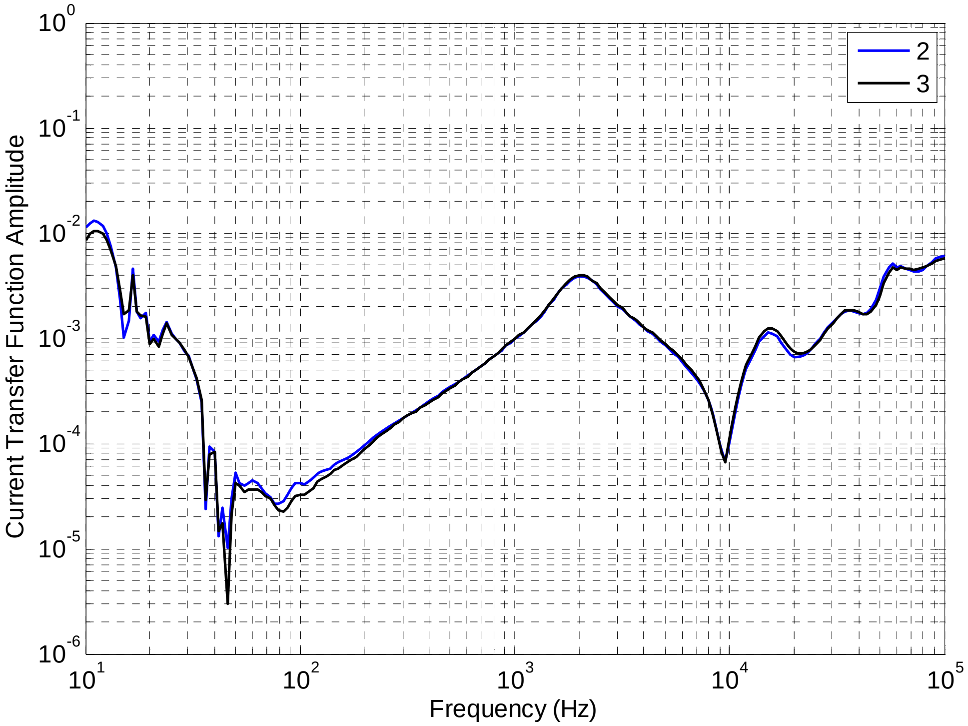

Figure B-19 Direct drive current transfer function of trolley communication line with a local ground.

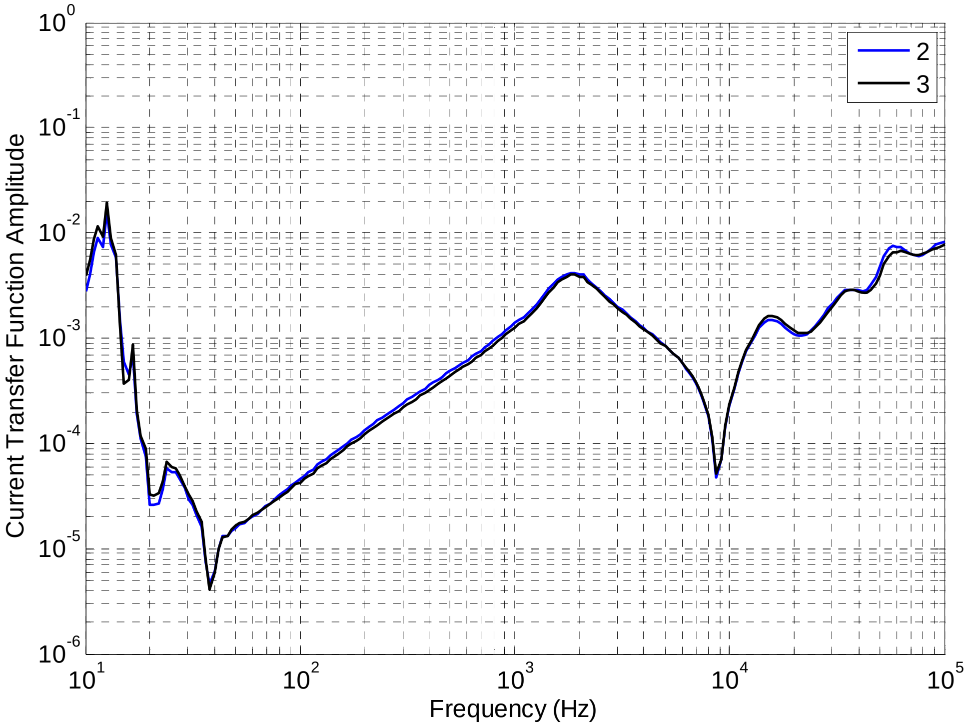

Figure B-20 Direct drive current transfer function of trolley communication line with a fence ground.

Indirect Drive Transfer Function Data: Surface current drive in the P-direction

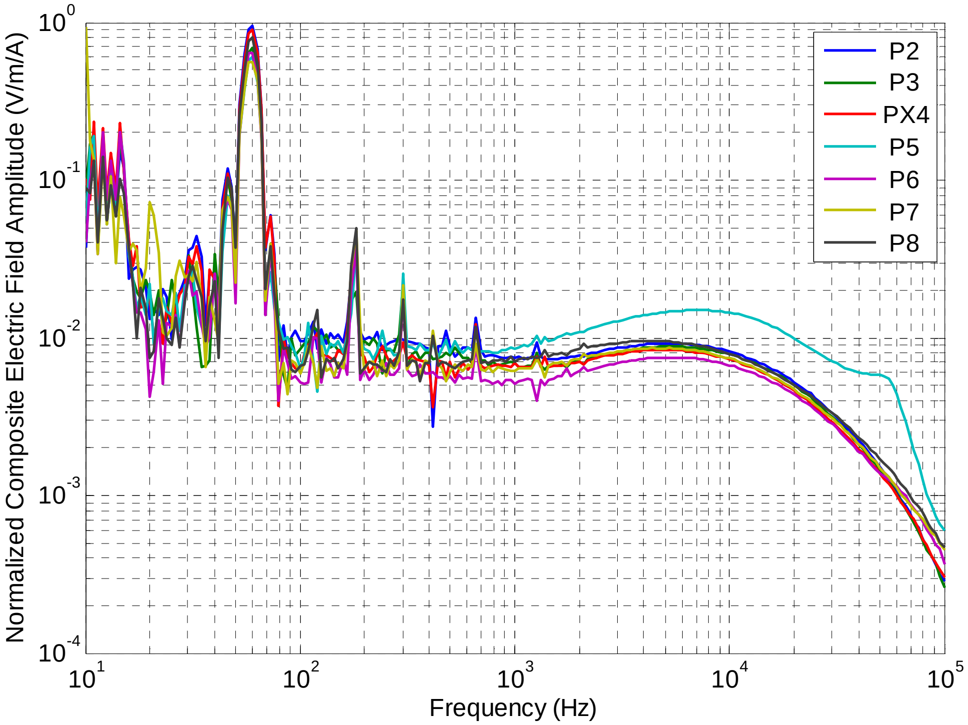

Figure B-21 Normalized composite electric field for P-directed surface current drive at positions from P2 to P8.

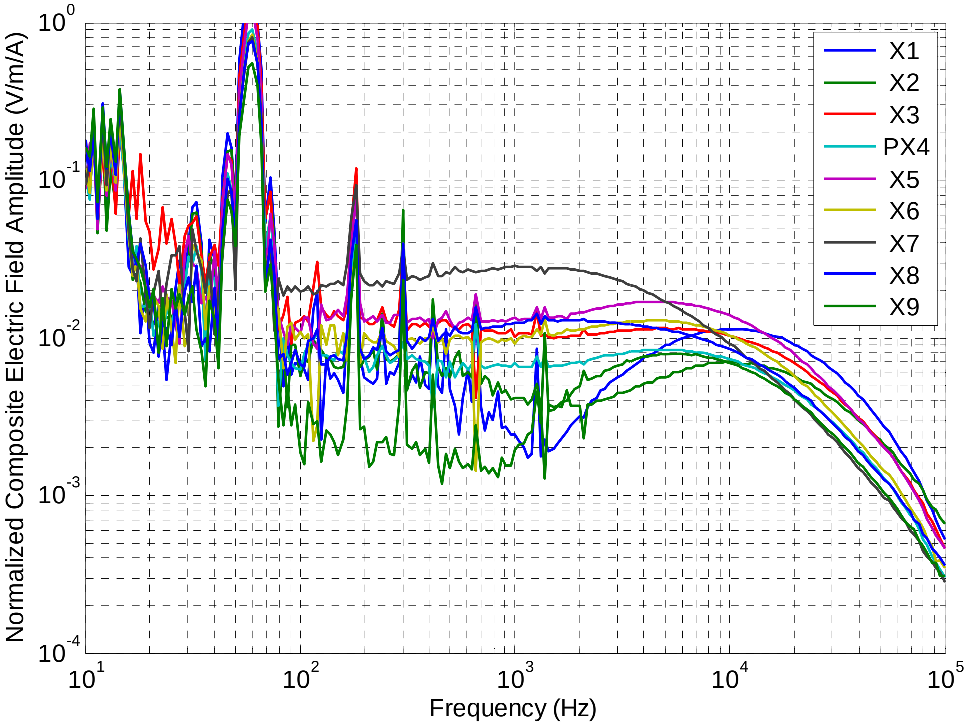

Figure B-22 Normalized composite electric field for P-directed surface current drive at positions from X1 to X9.

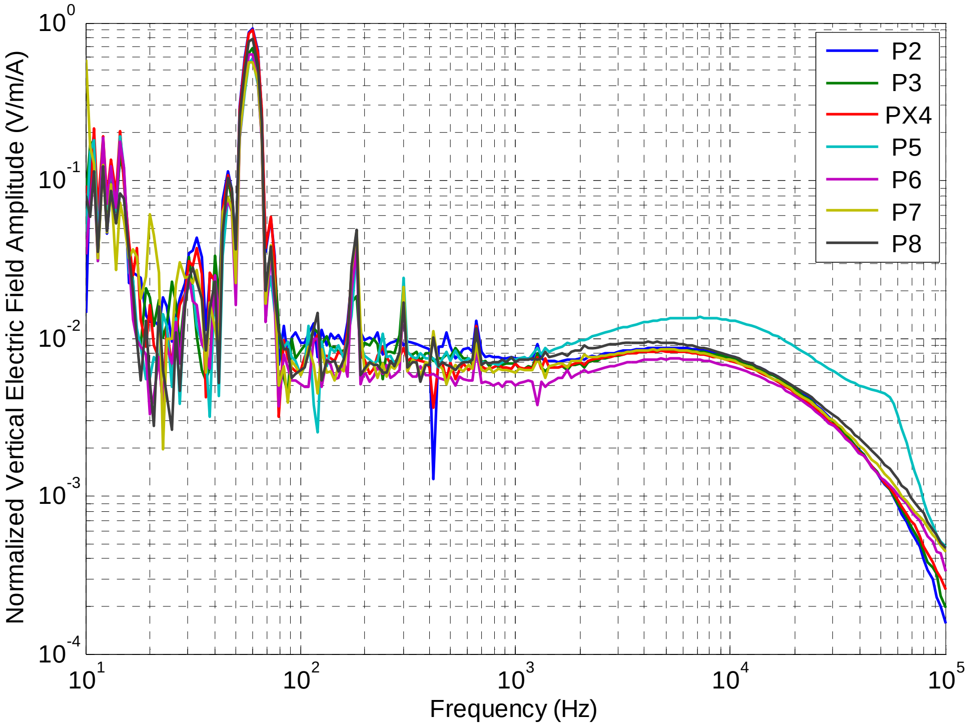

Figure B-23 Normalized vertical electric field for P-directed surface current drive at positions from P2 to P8.

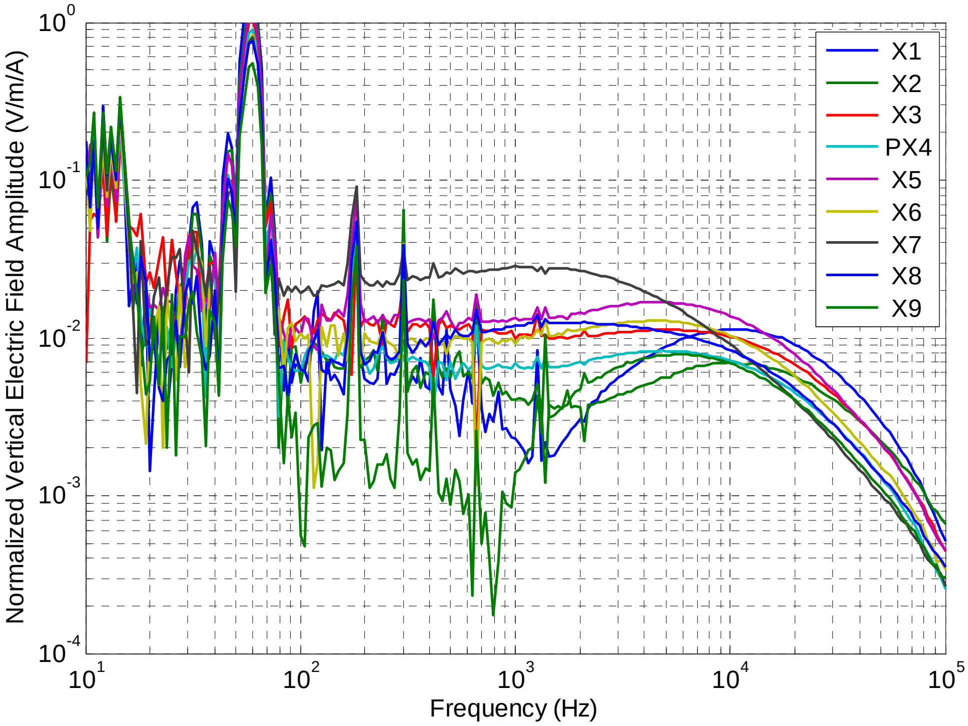

Figure B-24 Normalized vertical electric field for P-directed surface current drive at positions from X1 to X9.

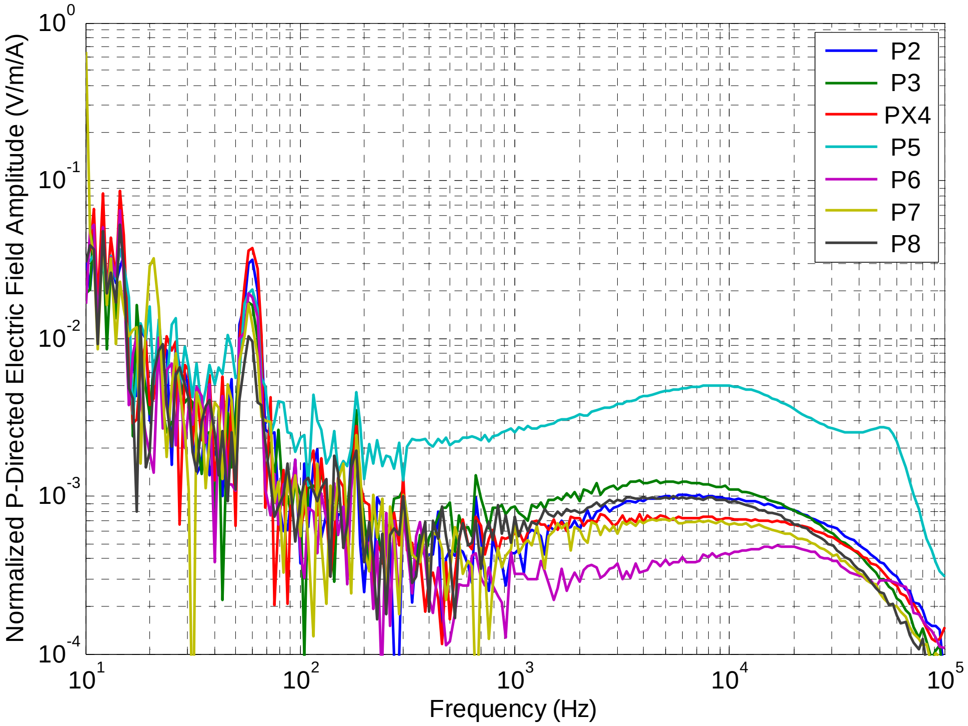

Figure B-25 Normalized P-directed electric field for P-directed surface current drive at positions from P2 to P8.

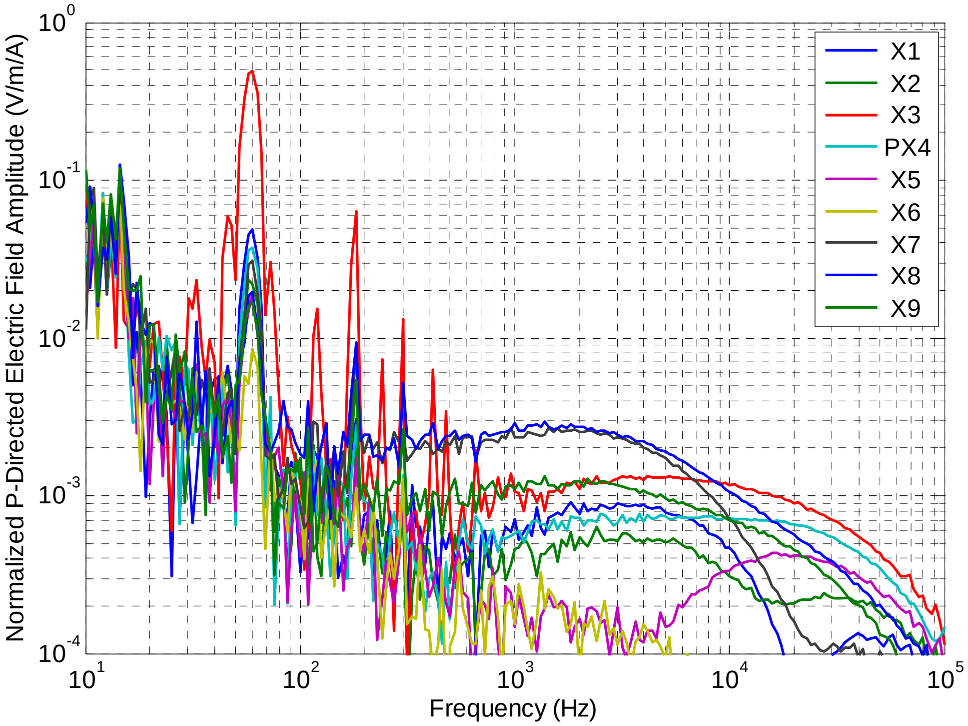

Figure B-26 Normalized P-directed electric field for P-directed surface current drive at positions from X1 to X9.

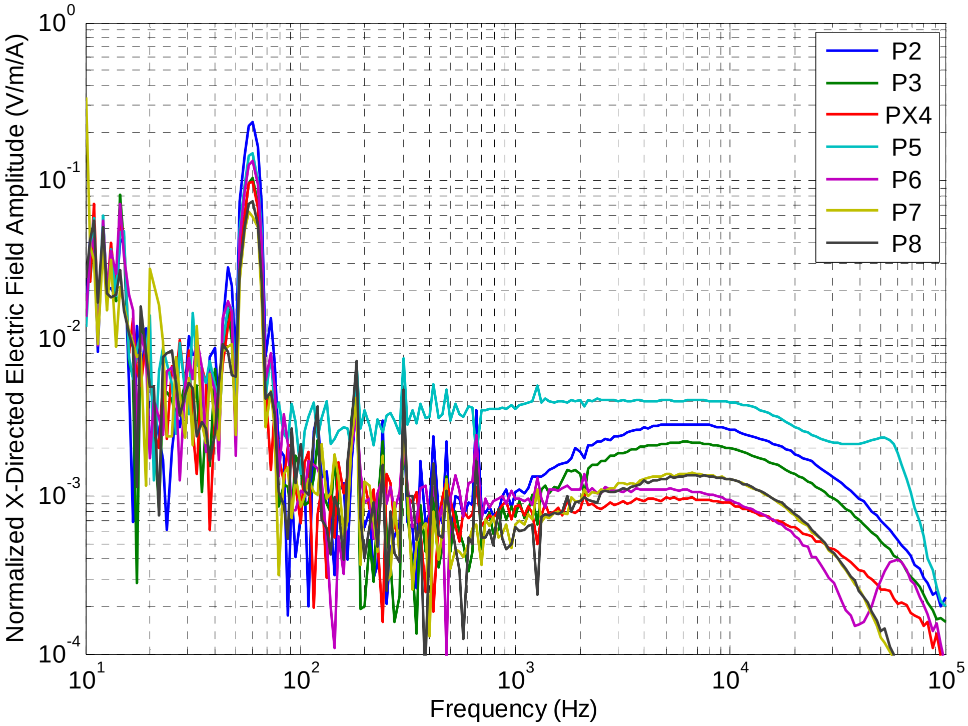

Figure B-27 Normalized X-directed electric field for P-directed surface current drive at positions from P2 to P8.

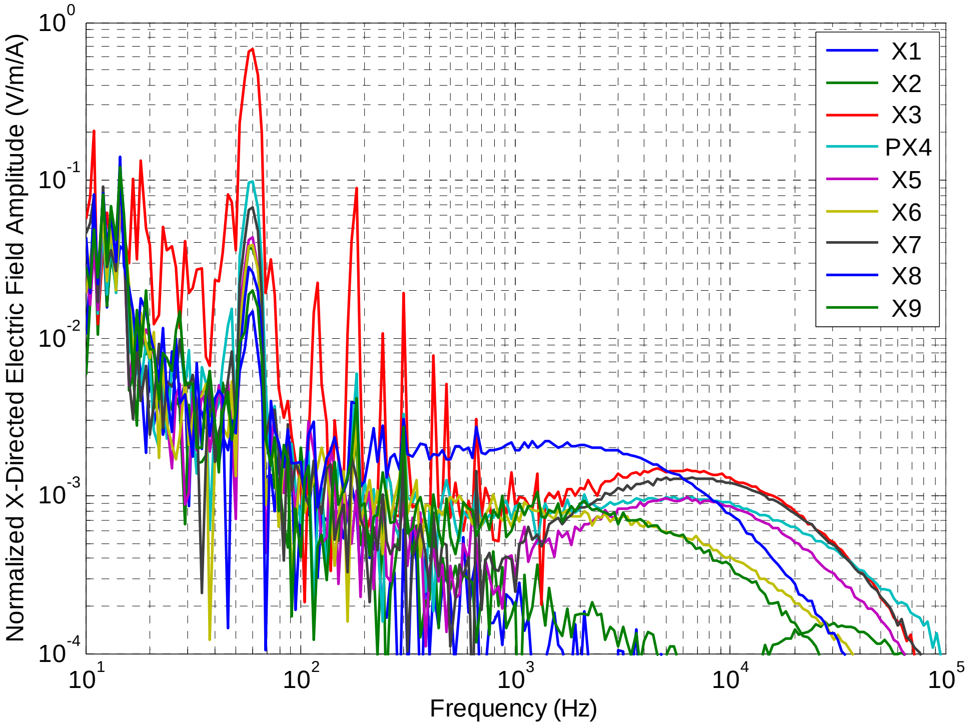

Figure B-28 Normalized P-directed electric field for P-directed surface current drive at positions from X1 to X9.

Indirect Drive Transfer Function Data: Surface current drive in the X-direction

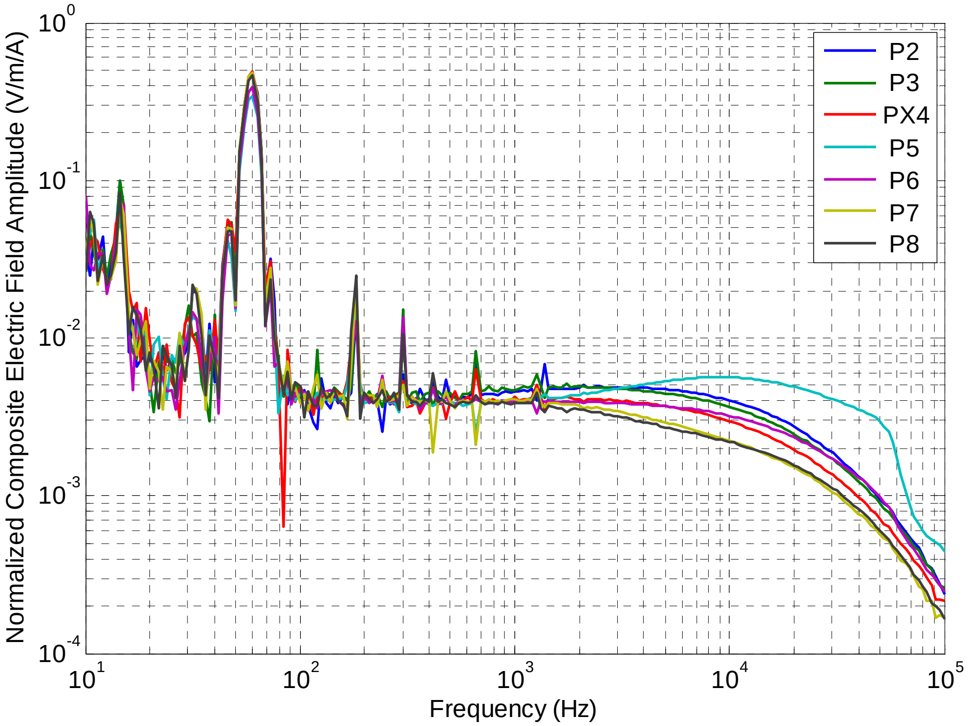

Figure B-29 Normalized composite electric field for X-directed surface current drive at positions from P2 to P8.

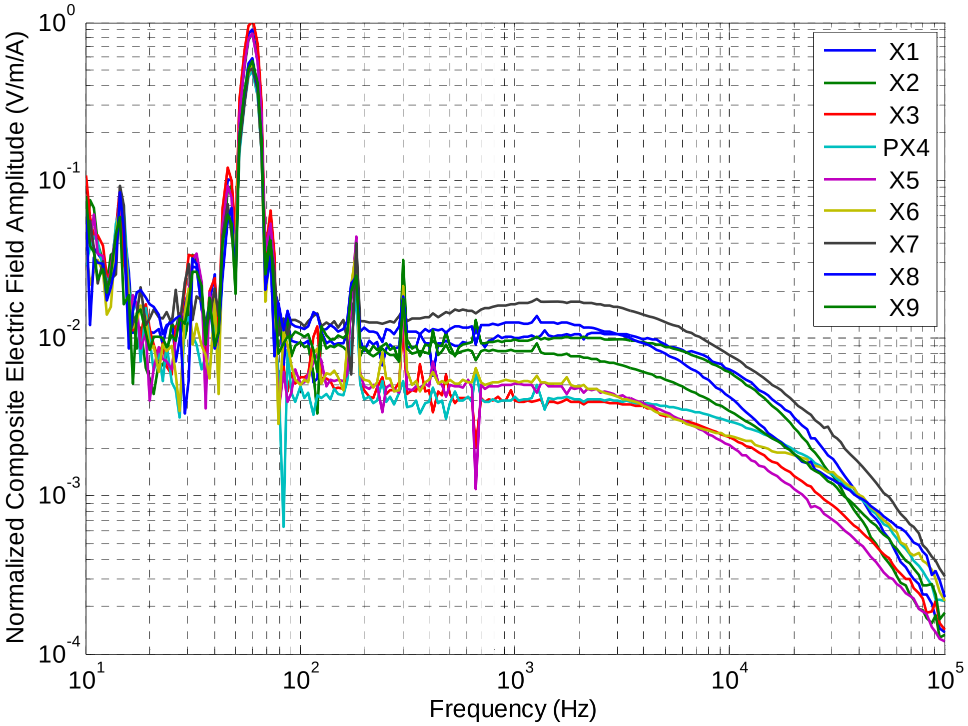

Figure B-30 Normalized composite electric field for X-directed surface current drive at positions from X1 to X9.

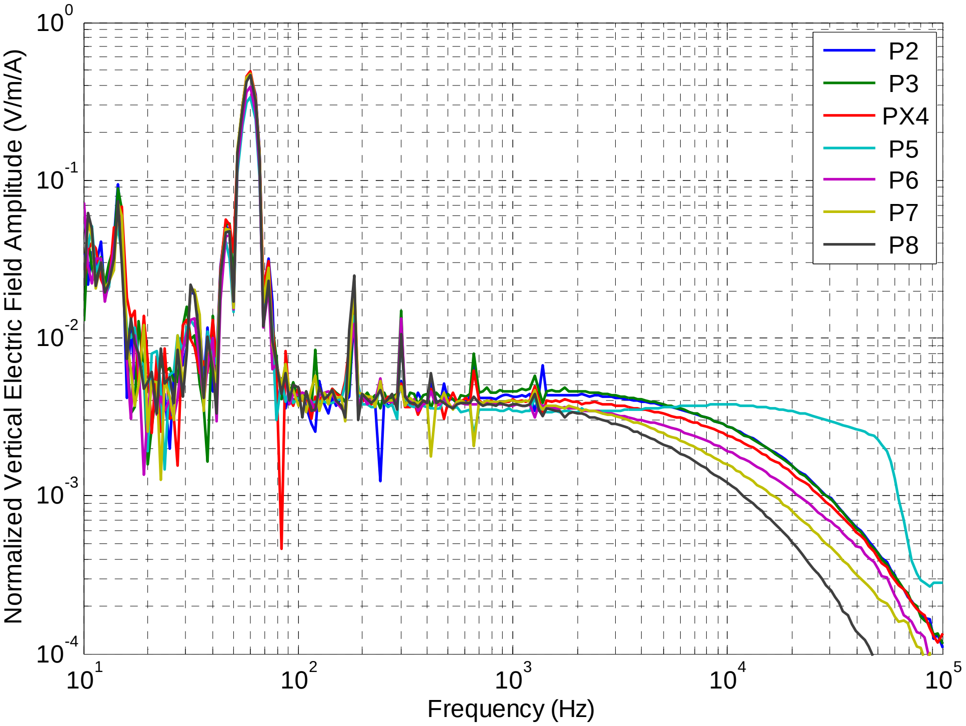

Figure B-31 Normalized vertical electric field for X-directed surface current drive at positions from P2 to P8.

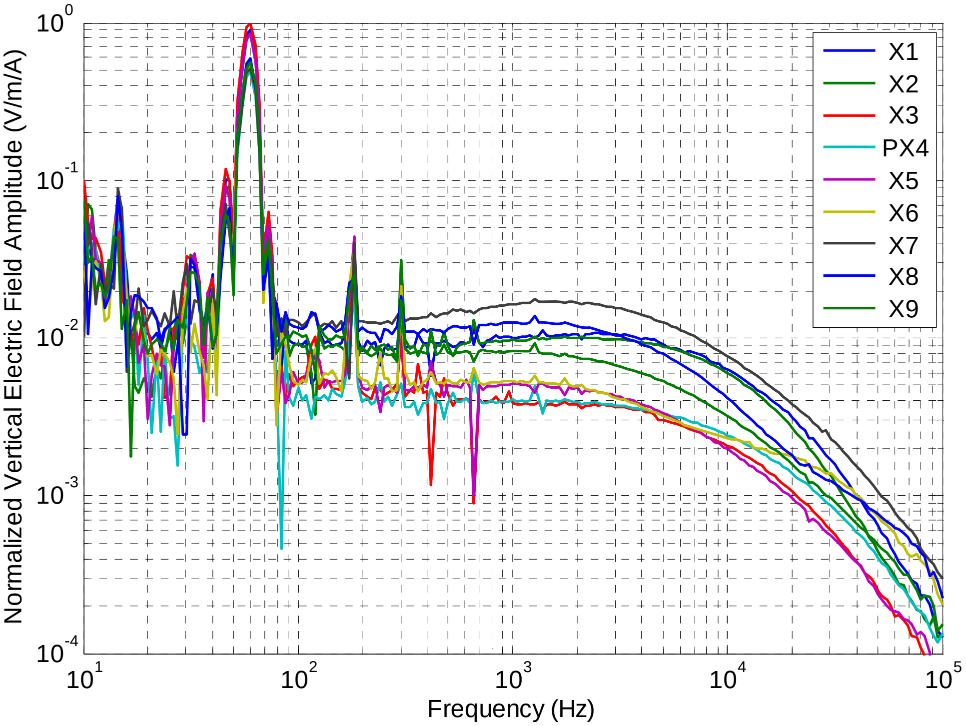

Figure B-32 Normalized vertical electric field for X-directed surface current drive at positions from X1 to X9.

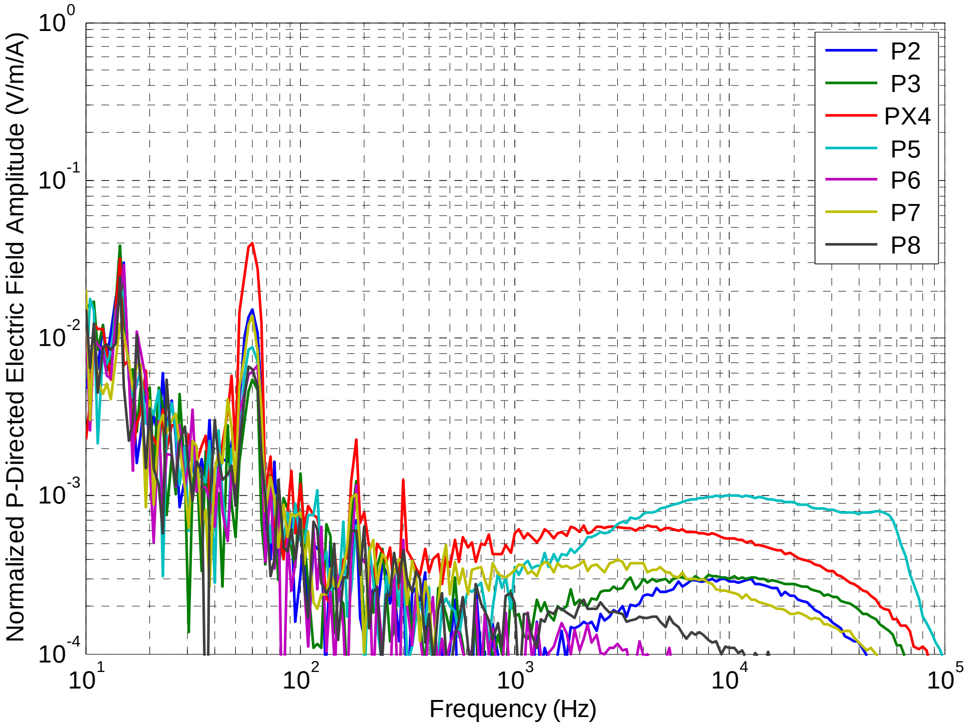

Figure B-33 Normalized P-directed electric field for X-directed surface current drive at positions from P2 to P8.

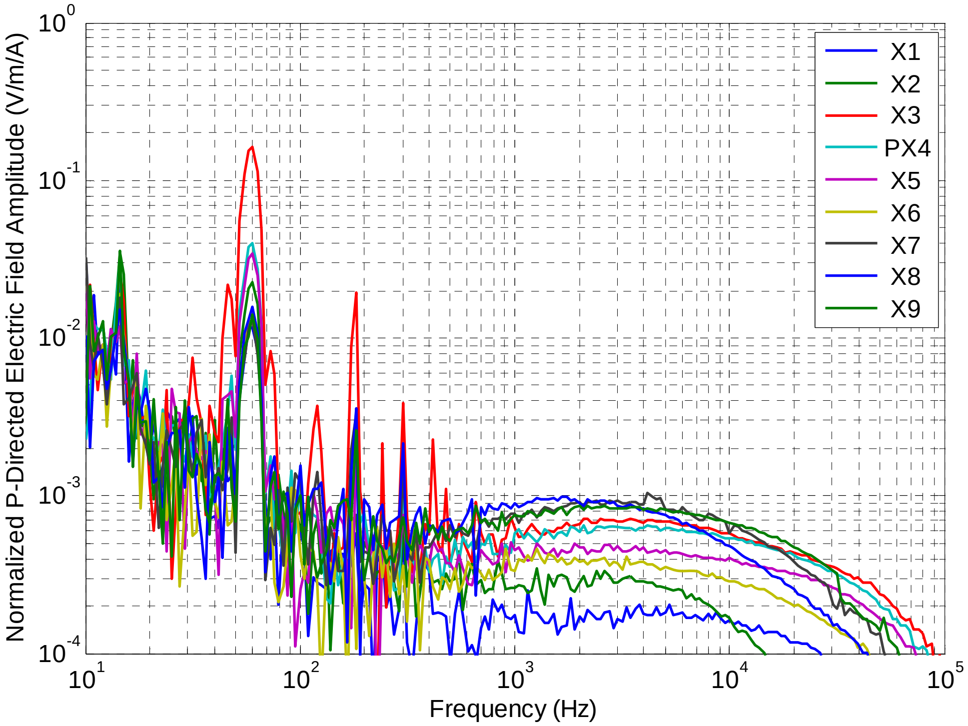

Figure B-34 Normalized P-directed electric field for X-directed surface current drive at positions from X1 to X9.

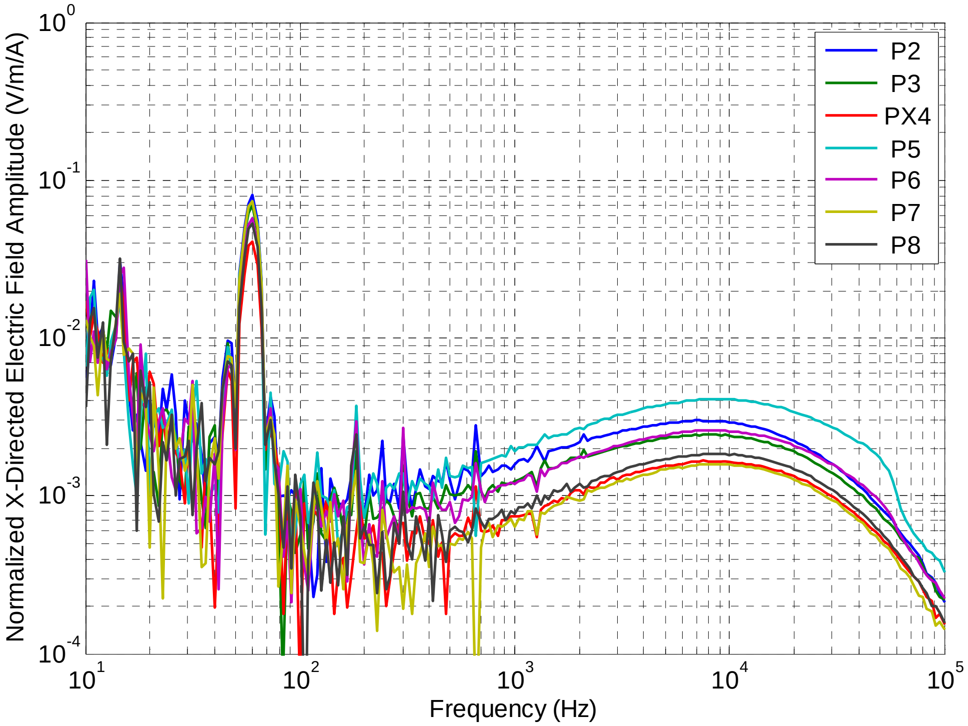

Figure B-35 Normalized X-directed electric field for X-directed surface current drive at positions from P2 to P8.

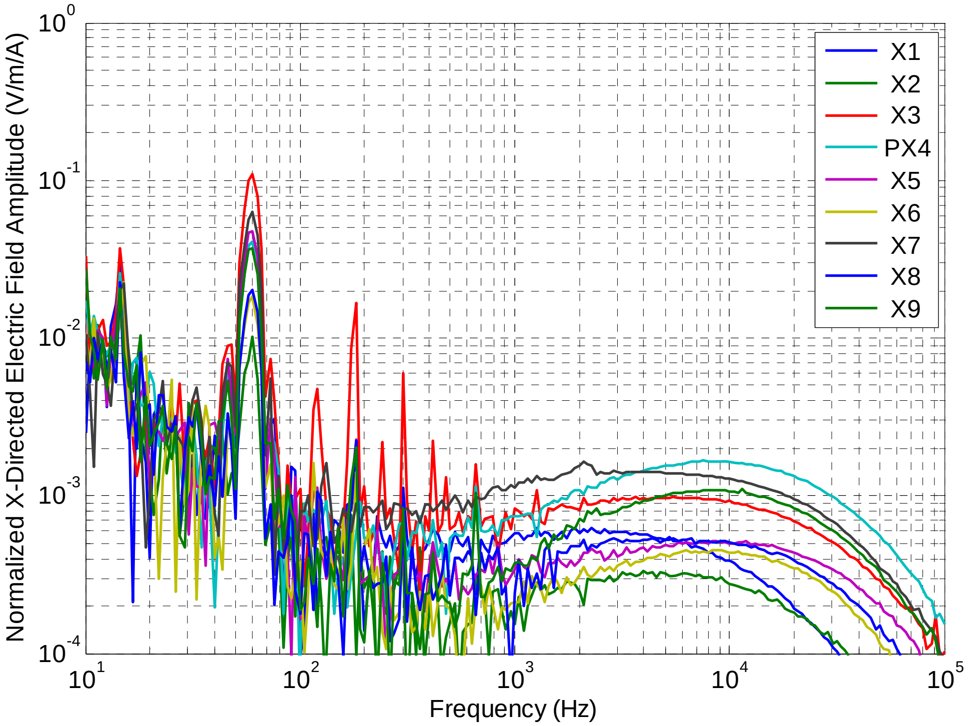

Figure B-36 Normalized X-directed electric field for X-directed surface current drive at positions from X1 to X9.

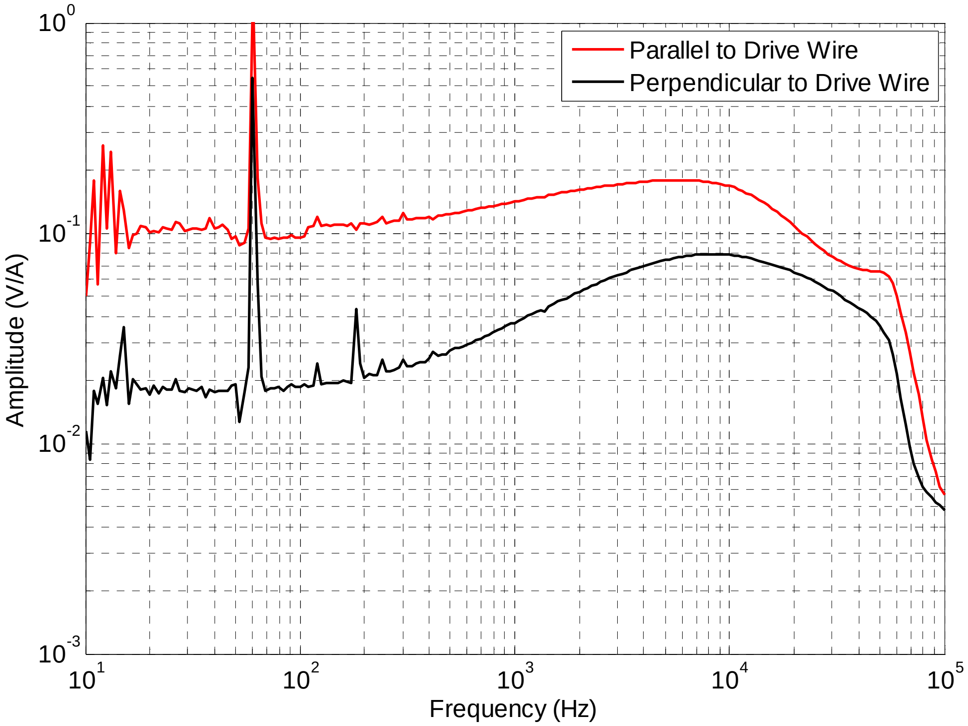

Figure B-37 Induced voltage on pump cable (~300 m long) due to wire current drives on surface.

Appendix C Sample Eiger Files

The following files are example input and output files for a finite length wire at the surface of a conductive half-space. The frequency is set to 10 Hz and a constant current distribution is set on the wire.

horiz_wire_2_reg01.eig (used as input file into Eiger and Moench)

```
------------------------------------------------------------------------------------------
Horizontal wire above a half space
 Created on 12/ 6 2007 at 11: 1 from MattsWire.jfg by Jf ver: 25/10/02
dynamic       3       1  np      11 Pnts      10 IE       0 FE       9 Unk
 1
      1     wire                10       0
 1
  1 bar                  1   2   1   2   1
 1
  1 bar                 ordinary            vector              T F pec_efie            T  1  2
 1
 1 1 2
      1
      1 layered             nonperiodic
      3
( 4.000000E+00, -2.246936E+07) ( 0.100000E+01,  0.000000E+00)
-0.200000E+03 ( 4.000000E+00, -2.246936E+07) ( 0.100000E+01,  0.000000E+00)
 0.000000E+00 ( 0.100000E+01,  0.000000E+00) ( 0.100000E+01,  0.000000E+00)
 0.100000E+03 ( 0.100000E+01,  0.000000E+00) ( 0.100000E+01,  0.000000E+00)
      0       0
 F
     11
      1 -0.250000E+03  0.000000E+00  0.508000E-01       1
      2  0.250000E+03  0.000000E+00  0.508000E-01       1
      3 -0.200000E+03  0.000000E+00  0.508000E-01       1
      4 -0.150000E+03  0.000000E+00  0.508000E-01       1
      5 -0.100000E+03  0.000000E+00  0.508000E-01       1
      6 -0.500000E+02  0.000000E+00  0.508000E-01       1
      7  0.000000E+00  0.000000E+00  0.508000E-01       1
      8  0.500000E+02  0.000000E+00  0.508000E-01       1
      9  0.100000E+03  0.000000E+00  0.508000E-01       1
     10  0.150000E+03  0.000000E+00  0.508000E-01       1
     11  0.200000E+03  0.000000E+00  0.508000E-01       1
     10       0       9
      1 wire                   1       1       1
 0.129410E-02
      1       3
      1
      1
      1       0
      1
( 0.100000E+01, 0.000000E+00)
      2 wire                   1       1       1
```

```
 0.129410E-02
      3        4
      1
      1
      1        1
      2
( 0.100000E+01, 0.000000E+00)
      1
(-0.100000E+01, 0.000000E+00)
      3 wire                  1        1        1
 0.129410E-02
      4        5
      1
      1
      1        1
      3
( 0.100000E+01, 0.000000E+00)
      2
(-0.100000E+01, 0.000000E+00)
      4 wire                  1        1        1
 0.129410E-02
      5        6
      1
      1
      1        1
      4
( 0.100000E+01, 0.000000E+00)
      3
(-0.100000E+01, 0.000000E+00)
      5 wire                  1        1        1
 0.129410E-02
      6        7
      1
      1
      1        1
      5
( 0.100000E+01, 0.000000E+00)
      4
(-0.100000E+01, 0.000000E+00)
      6 wire                  1        1        1
 0.129410E-02
      7        8
      1
      1
      1        1
      6
( 0.100000E+01, 0.000000E+00)
      5
(-0.100000E+01, 0.000000E+00)
      7 wire                  1        1        1
 0.129410E-02
      8        9
      1
      1
      1        1
      7
```

```
( 0.100000E+01, 0.000000E+00)
       6
(-0.100000E+01, 0.000000E+00)
       8 wire                       1       1       1
 0.129410E-02
       9      10
       1
       1
       1       1
       8
( 0.100000E+01, 0.000000E+00)
       7
(-0.100000E+01, 0.000000E+00)
       9 wire                       1       1       1
 0.129410E-02
      10      11
       1
       1
       1       1
       9
( 0.100000E+01, 0.000000E+00)
       8
(-0.100000E+01, 0.000000E+00)
      10 wire                       1       1       1
 0.129410E-02
      11       2
       1
       1
       0       1
       9
(-0.100000E+01, 0.000000E+00)
 0
 1
 0
 0 0 0
 9
 1 1 (1.0,0.0E+0)
 2 2 (1.0,0.0E+0)
 3 3 (1.0,0.0E+0)
 4 4 (1.0,0.0E+0)
 5 5 (1.0,0.0E+0)
 6 6 (1.0,0.0E+0)
 7 7 (1.0,0.0E+0)
 8 8 (1.0,0.0E+0)
 9 9 (1.0,0.0E+0)
 1
 1 0
 1 3
 0.000000E+00  0.000000E+00  0.000000E+00  0.000000E+00  0.000000E+00  0.000000E+00
 1
 1.00000000000000E+01        1
 0
 0
-----------------------------------------------------------------------------------------
end file horiz_wire_2_reg01.eig
-----------------------------------------------------------------------------------------
```

input01 (used as input script into Moench)

```
----------------------------------------------------------------------------------------------------
horiz_wire_2_reg01
horiz_wire_2_reg01
nf   !near field
manually
1 region
0,0,-100
11
-300,0,-100
1
horiz_wire_2_reg01
quit
----------------------------------------------------------------------------------------------------
end file input01
----------------------------------------------------------------------------------------------------
```

horiz_wire_2_reg01.mnh (used as input file into Moench)

```
----------------------------------------------------------------------------------------------------
  Horizontal wire above a half space
  Created on 12/ 6 2007 at 16:57 from MattsWire.jfg by Jf ver
 dynamic       3       1  np      11 Pnts      10 IE       0
      10.000000000
 Results                   9
           1 (1.00000000000000,0.000000000000000E+000)
           2 (1.00000000000000,0.000000000000000E+000)
           3 (1.00000000000000,0.000000000000000E+000)
           4 (1.00000000000000,0.000000000000000E+000)
           5 (1.00000000000000,0.000000000000000E+000)
           6 (1.00000000000000,0.000000000000000E+000)
           7 (1.00000000000000,0.000000000000000E+000)
           8 (1.00000000000000,0.000000000000000E+000)
           9 (1.00000000000000,0.000000000000000E+000)
----------------------------------------------------------------------------------------------------
end file horiz_wire_2_reg01.mnh
----------------------------------------------------------------------------------------------------
```

horiz_wire_2_reg01.nfld0 (output file from Moench)

```
----------------------------------------------------------------------------------------------------
Near field
 Frequency :   10.0000000000000       Hz
 Excitation:           1

 ****************************************************
 Point locations where field is evaluated (x,y,z coordinates)
         11          1
 0.00000E+00    0.00000E+00   -0.10000E+03    0.00000E+00
-0.30000E+02    0.00000E+00   -0.10000E+03    0.00000E+00
-0.60000E+02    0.00000E+00   -0.10000E+03    0.00000E+00
-0.90000E+02    0.00000E+00   -0.10000E+03    0.00000E+00
-0.12000E+03    0.00000E+00   -0.10000E+03    0.00000E+00
-0.15000E+03    0.00000E+00   -0.10000E+03    0.00000E+00
-0.18000E+03    0.00000E+00   -0.10000E+03    0.00000E+00
-0.21000E+03    0.00000E+00   -0.10000E+03    0.00000E+00
-0.24000E+03    0.00000E+00   -0.10000E+03    0.00000E+00
-0.27000E+03    0.00000E+00   -0.10000E+03    0.00000E+00
-0.30000E+03    0.00000E+00   -0.10000E+03    0.00000E+00
 Results
 Scattered E field (x,y,z components)
(-0.38733E-03,-0.14805E-04)   (-0.51593E-23,-0.20063E-21)   (-0.94868E-19, 0.84703E-20)
(-0.39740E-03,-0.14609E-04)   (-0.56512E-23,-0.20094E-21)   ( 0.60492E-04,-0.10495E-05)
(-0.42756E-03,-0.14404E-04)   (-0.60621E-23,-0.18343E-21)   ( 0.13448E-03,-0.16510E-05)
(-0.47595E-03,-0.14084E-04)   (-0.64086E-23,-0.16248E-21)   ( 0.23947E-03,-0.19567E-05)
(-0.53191E-03,-0.13433E-04)   (-0.67795E-23,-0.16539E-21)   ( 0.39980E-03,-0.25164E-05)
(-0.55972E-03,-0.12717E-04)   (-0.71223E-23,-0.16628E-21)   ( 0.63970E-03,-0.33960E-05)
(-0.48283E-03,-0.12038E-04)   (-0.74255E-23,-0.15659E-21)   ( 0.94273E-03,-0.42975E-05)
(-0.23292E-03,-0.11573E-04)   (-0.76636E-23,-0.13458E-21)   ( 0.11830E-02,-0.49502E-05)
( 0.11289E-03,-0.11254E-04)   (-0.74794E-23,-0.59474E-22)   ( 0.11855E-02,-0.49181E-05)
( 0.36012E-03,-0.10653E-04)   (-0.68895E-23, 0.33177E-22)   ( 0.95045E-03,-0.42976E-05)
( 0.43148E-03,-0.98403E-05)   (-0.63013E-23, 0.86272E-22)   ( 0.65326E-03,-0.36323E-05)
 Scattered H field (x,y,z components)
(-0.37496E-19, 0.17635E-21)   ( 0.11483E-02,-0.69101E-05)   (-0.24588E-22,-0.46394E-21)
(-0.42095E-19, 0.21569E-21)   ( 0.11453E-02,-0.68490E-05)   (-0.31247E-22,-0.54823E-21)
(-0.46112E-19, 0.25569E-21)   ( 0.11351E-02,-0.66587E-05)   (-0.38613E-22,-0.62570E-21)
(-0.49633E-19, 0.30024E-21)   ( 0.11130E-02,-0.63112E-05)   (-0.46651E-22,-0.70251E-21)
(-0.52736E-19, 0.34273E-21)   ( 0.10692E-02,-0.57873E-05)   (-0.55349E-22,-0.77599E-21)
(-0.55492E-19, 0.38055E-21)   ( 0.98770E-03,-0.51103E-05)   (-0.64723E-22,-0.86146E-21)
(-0.57945E-19, 0.42396E-21)   ( 0.84836E-03,-0.41565E-05)   (-0.74668E-22,-0.93091E-21)
(-0.60126E-19, 0.46780E-21)   ( 0.64541E-03,-0.30185E-05)   (-0.85234E-22,-0.10031E-20)
(-0.61808E-19, 0.51769E-21)   ( 0.41256E-03,-0.17224E-05)   (-0.96149E-22,-0.10666E-20)
(-0.61635E-19, 0.55502E-21)   ( 0.21050E-03,-0.53252E-06)   (-0.10705E-21,-0.11029E-20)
(-0.58741E-19, 0.58122E-21)   ( 0.72600E-04, 0.46881E-06)   (-0.11748E-21,-0.11268E-20)
 Incident E field (x,y,z components)
( 0.00000E+00, 0.00000E+00)   ( 0.00000E+00, 0.00000E+00)   ( 0.00000E+00, 0.00000E+00)
( 0.00000E+00, 0.00000E+00)   ( 0.00000E+00, 0.00000E+00)   ( 0.00000E+00, 0.00000E+00)
( 0.00000E+00, 0.00000E+00)   ( 0.00000E+00, 0.00000E+00)   ( 0.00000E+00, 0.00000E+00)
( 0.00000E+00, 0.00000E+00)   ( 0.00000E+00, 0.00000E+00)   ( 0.00000E+00, 0.00000E+00)
( 0.00000E+00, 0.00000E+00)   ( 0.00000E+00, 0.00000E+00)   ( 0.00000E+00, 0.00000E+00)
( 0.00000E+00, 0.00000E+00)   ( 0.00000E+00, 0.00000E+00)   ( 0.00000E+00, 0.00000E+00)
( 0.00000E+00, 0.00000E+00)   ( 0.00000E+00, 0.00000E+00)   ( 0.00000E+00, 0.00000E+00)
( 0.00000E+00, 0.00000E+00)   ( 0.00000E+00, 0.00000E+00)   ( 0.00000E+00, 0.00000E+00)
( 0.00000E+00, 0.00000E+00)   ( 0.00000E+00, 0.00000E+00)   ( 0.00000E+00, 0.00000E+00)
( 0.00000E+00, 0.00000E+00)   ( 0.00000E+00, 0.00000E+00)   ( 0.00000E+00, 0.00000E+00)
```

```
( 0.00000E+00, 0.00000E+00)    ( 0.00000E+00, 0.00000E+00)    ( 0.00000E+00, 0.00000E+00)
 Incident H field (x,y,z components)
( 0.00000E+00, 0.00000E+00)    ( 0.00000E+00, 0.00000E+00)    ( 0.00000E+00, 0.00000E+00)
( 0.00000E+00, 0.00000E+00)    ( 0.00000E+00, 0.00000E+00)    ( 0.00000E+00, 0.00000E+00)
( 0.00000E+00, 0.00000E+00)    ( 0.00000E+00, 0.00000E+00)    ( 0.00000E+00, 0.00000E+00)
( 0.00000E+00, 0.00000E+00)    ( 0.00000E+00, 0.00000E+00)    ( 0.00000E+00, 0.00000E+00)
( 0.00000E+00, 0.00000E+00)    ( 0.00000E+00, 0.00000E+00)    ( 0.00000E+00, 0.00000E+00)
( 0.00000E+00, 0.00000E+00)    ( 0.00000E+00, 0.00000E+00)    ( 0.00000E+00, 0.00000E+00)
( 0.00000E+00, 0.00000E+00)    ( 0.00000E+00, 0.00000E+00)    ( 0.00000E+00, 0.00000E+00)
( 0.00000E+00, 0.00000E+00)    ( 0.00000E+00, 0.00000E+00)    ( 0.00000E+00, 0.00000E+00)
( 0.00000E+00, 0.00000E+00)    ( 0.00000E+00, 0.00000E+00)    ( 0.00000E+00, 0.00000E+00)
( 0.00000E+00, 0.00000E+00)    ( 0.00000E+00, 0.00000E+00)    ( 0.00000E+00, 0.00000E+00)
( 0.00000E+00, 0.00000E+00)    ( 0.00000E+00, 0.00000E+00)    ( 0.00000E+00, 0.00000E+00)
 Total E field (x,y,z components)
(-0.38733E-03,-0.14805E-04)    (-0.51593E-23,-0.20063E-21)    (-0.94868E-19, 0.84703E-20)
(-0.39740E-03,-0.14609E-04)    (-0.56512E-23,-0.20094E-21)    ( 0.60492E-04,-0.10495E-05)
(-0.42756E-03,-0.14404E-04)    (-0.60621E-23,-0.18343E-21)    ( 0.13448E-03,-0.16510E-05)
(-0.47595E-03,-0.14084E-04)    (-0.64086E-23,-0.16248E-21)    ( 0.23947E-03,-0.19567E-05)
(-0.53191E-03,-0.13433E-04)    (-0.67795E-23,-0.16539E-21)    ( 0.39980E-03,-0.25164E-05)
(-0.55972E-03,-0.12717E-04)    (-0.71223E-23,-0.16628E-21)    ( 0.63970E-03,-0.33960E-05)
(-0.48283E-03,-0.12038E-04)    (-0.74255E-23,-0.15659E-21)    ( 0.94273E-03,-0.42975E-05)
(-0.23292E-03,-0.11573E-04)    (-0.76636E-23,-0.13458E-21)    ( 0.11830E-02,-0.49502E-05)
( 0.11289E-03,-0.11254E-04)    (-0.74794E-23,-0.59474E-22)    ( 0.11855E-02,-0.49181E-05)
( 0.36012E-03,-0.10653E-04)    (-0.68895E-23, 0.33177E-22)    ( 0.95045E-03,-0.42976E-05)
( 0.43148E-03,-0.98403E-05)    (-0.63013E-23, 0.86272E-22)    ( 0.65326E-03,-0.36323E-05)
 Total H field (x,y,z components)
(-0.37496E-19, 0.17635E-21)    ( 0.11483E-02,-0.69101E-05)    (-0.24588E-22,-0.46394E-21)
(-0.42095E-19, 0.21569E-21)    ( 0.11453E-02,-0.68490E-05)    (-0.31247E-22,-0.54823E-21)
(-0.46112E-19, 0.25569E-21)    ( 0.11351E-02,-0.66587E-05)    (-0.38613E-22,-0.62570E-21)
(-0.49633E-19, 0.30024E-21)    ( 0.11130E-02,-0.63112E-05)    (-0.46651E-22,-0.70251E-21)
(-0.52736E-19, 0.34273E-21)    ( 0.10692E-02,-0.57873E-05)    (-0.55349E-22,-0.77599E-21)
(-0.55492E-19, 0.38055E-21)    ( 0.98770E-03,-0.51103E-05)    (-0.64723E-22,-0.86146E-21)
(-0.57945E-19, 0.42396E-21)    ( 0.84836E-03,-0.41565E-05)    (-0.74668E-22,-0.93091E-21)
(-0.60126E-19, 0.46780E-21)    ( 0.64541E-03,-0.30185E-05)    (-0.85234E-22,-0.10031E-20)
(-0.61808E-19, 0.51769E-21)    ( 0.41256E-03,-0.17224E-05)    (-0.96149E-22,-0.10666E-20)
(-0.61635E-19, 0.55502E-21)    ( 0.21050E-03,-0.53252E-06)    (-0.10705E-21,-0.11029E-20)
(-0.58741E-19, 0.58122E-21)    ( 0.72600E-04, 0.46881E-06)    (-0.11748E-21,-0.11268E-20)
----------------------------------------------------------------------------------------------------
end file horiz_wire_2_reg01.nfld0
----------------------------------------------------------------------------------------------------
```

Appendix D List of Underground Sealed Area Coal Mine Explosions Suspected of Lightning Initiation

1. Mary Lee #1 – August 22, 1993, Walker County, AL
2. Oak Grove Mine – April 5, 1994, Jefferson County, AL
3. Gary 50 – Between June 9 and 16, 1995
4. Oak Grove Mine – January 29, 1996, Jefferson County, AL
5. Oasis Contracting Mine # 1 – May 22, 1996, Boone County, WV
6. Oasis Contracting Mine # 1 – June 15, 1996, Boone County, WV
7. Oak Grove Mine – July 9, 1997, Jefferson County, AL
8. Soldier Canyon Mine – July, 2001, Wellington, UT
9. Pinnacle Mine – September 1, 2003, Wyoming County, WV
10. Pinnacle Mine – August 30, 2005, WV, Wyoming County, WV
11. Sago Mine – January 2, 2006, Tallmansville, WV

Appendix E Memorandum from Dr. Krider

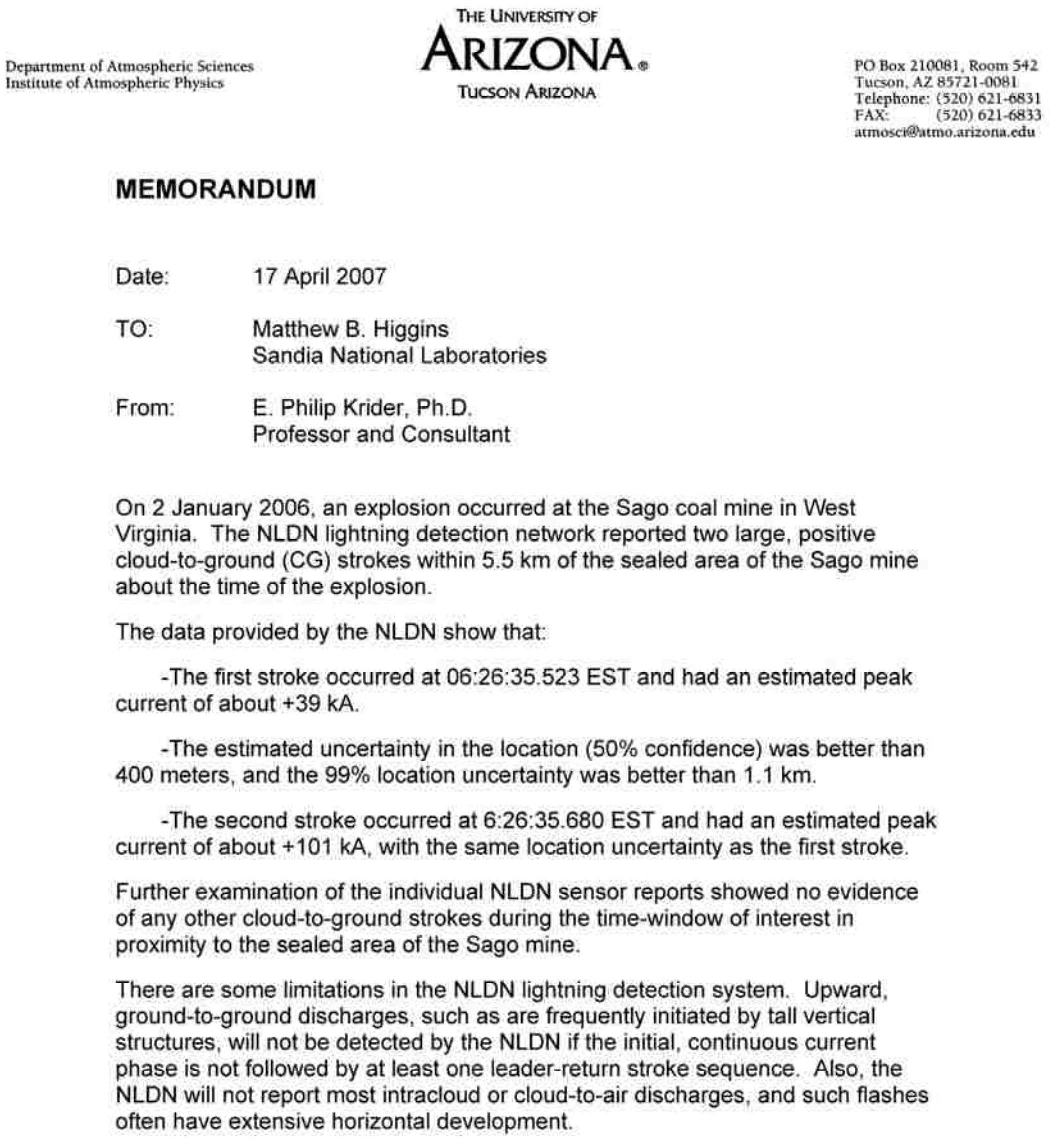

THE UNIVERSITY OF
ARIZONA®
TUCSON ARIZONA

Department of Atmospheric Sciences
Institute of Atmospheric Physics

PO Box 210081, Room 542
Tucson, AZ 85721-0081
Telephone: (520) 621-6831
FAX: (520) 621-6833
atmosci@atmo.arizona.edu

MEMORANDUM

Date: 17 April 2007

TO: Matthew B. Higgins
Sandia National Laboratories

From: E. Philip Krider, Ph.D.
Professor and Consultant

On 2 January 2006, an explosion occurred at the Sago coal mine in West Virginia. The NLDN lightning detection network reported two large, positive cloud-to-ground (CG) strokes within 5.5 km of the sealed area of the Sago mine about the time of the explosion.

The data provided by the NLDN show that:

-The first stroke occurred at 06:26:35.523 EST and had an estimated peak current of about +39 kA.

-The estimated uncertainty in the location (50% confidence) was better than 400 meters, and the 99% location uncertainty was better than 1.1 km.

-The second stroke occurred at 6:26:35.680 EST and had an estimated peak current of about +101 kA, with the same location uncertainty as the first stroke.

Further examination of the individual NLDN sensor reports showed no evidence of any other cloud-to-ground strokes during the time-window of interest in proximity to the sealed area of the Sago mine.

There are some limitations in the NLDN lightning detection system. Upward, ground-to-ground discharges, such as are frequently initiated by tall vertical structures, will not be detected by the NLDN if the initial, continuous current phase is not followed by at least one leader-return stroke sequence. Also, the NLDN will not report most intracloud or cloud-to-air discharges, and such flashes often have extensive horizontal development.